Development of Rosette Nanotubes For HIV-1 Therapy

by

Kumakshi Sharma

A thesis submitted in partial fulfillment of the requirements for the degree of

Master of Science

Department of Chemistry
University of Alberta

Abstract

The development of therapeutics to target dendritic cells (DCs) for the treatment of diseases is of great importance, as these cells are known to play an important role in antigen processing and presentation in the immune system. Herein, we explore the applications of biocompatible, self-assembled rosette nanotubes (RNTs) as a therapeutic agent to deliver a HIV antigen to the DCs. ELDKWA is linear fragment (epitope) present on the ectodomain of HIV-1 envelope glycoprotein 41 complex, which recognizes the galactoceramide receptors on the DC cell surface and lysine (K) acts as a spacer between the peptide ELDKWA and the RNTs. Our strategy is to functionalize the RNTs on the outer surface with the bio-active peptides ELDKWAK, RGDSK and DRGSK. RGD is a cell-adhesion peptide, which may aid in the attachment of the HIV-1 antigen (ELDKWA) to the DC cell surface and DRG is the scrambled version of RGD. The RNTs with the bioactive peptides were co-mixed with fluorescently-labeled RNTs to study the cell uptake of the RNTs.

Preface

This thesis is an original work by Kumakshi Sharma. No part of the thesis has been published in a journal. But the work done in the thesis has been presented at Conferences.

Conference Presentations:

Kumakshi Sharma, Jae-Young Cho and Hicham Fenniri. Self-assembled Rosette Nanotubes for HIV Therapy. CSC May 26-30, 2013, Quebec Convention Centre, Quebec City.

Kumakshi Sharma, Jae-Young Cho, Usha D. Hemraz and Hicham Fenniri. Co-assembly Study of Rosette Nanotubes for HIV Therapy. Alberta Nano Research Symposium, Feb 7, 2014, Edmonton.

Kumakshi Sharma, Jae-Young Cho, Usha D. Hemraz and Hicham Fenniri. Development of Rosette Nanotubes for HIV-1 Therapy. European Society of Pediatric Infectious Diseases, May 6-10, 2014, Dublin.

Acknowledgements

Foremost, I would like to express my deep gratitude to my supervisor, Dr. Hicham Fenniri for allowing me to work on this project and for his continuous support, encouragement and guidance over the years. Without his guidance and persistent help this thesis would not have been possible. I would also like to thank my committee members Dr. Robert Campbell and Dr. Todd Lowry for their continuous support and valuable suggestions. My heartfelt appreciation goes to my previous supervisor Dr. Mavanur R. Suresh in helping me develop the concept of this project.

My sincere thanks to the Department of Chemistry, University of Alberta and National Institute for Nanotechnology (NINT) for helping me in my program and supporting my research. I take this opportunity to recognize the efforts put by Dr. Usha D. Hemraz and Dr. Rachel Beingessner in helping me write the thesis. I really appreciate Dr. Jae-Young Cho for his contribution in the SEM, TEM and AFM imaging in my project. I would like to offer special thanks to Dr. Mike Xia for helping me in the training of analytical instruments.

I would like to acknowledge the confocal imaging facility and the flow cytometry laboratory in Department of Experimental Oncology at the Cross Cancer Institute for helping me in my research project. Without the help and advise of Dr. Xuejun Sun, Geraldine Barron and Jingzhou Huang, it would not have been possible to complete my biology experiments in the given time. I also thank the Bio-facility at NINT to help me continue the biology work.

I would sincerely thank my husband, Dr. Advaita Ganguly for supporting me in every possible way. Of course, I am deeply touched by the immense support of my parents, family and friends (Dr. Jae-Young, Dr. Zhimin Yan, Dr. Weizheng Shen, Uyen Ho, Liang Shuai and Zhaoyi Qin) in the completion of this degree.

Table of Contents

Topic	Page
Chapter 1. Introduction	1
1.1. Vaccines	2
1.1.1. Overview	2
1.1.2. Traditional Vaccines	2
1.2. Components of Immune system	6
1.3. Synthetic peptide-based DC vaccines	7
1.4. Types of delivery systems	9
1.4.1. Nanoparticles	9
1.4.2. Carbon Nanotubes (CNTs)	11
1.4.3. Helical Rosette Nanotubes (RNTs)	14
1.5. Human Immunodeficiency Virus I (HIV-1)	19
1.5.1. HIV-1 Envelope Structure and Function	19
1.5.2. HIV Infection	20
1.5.3. HIV-1 Vaccine Candidates	21
1.6. Objective of the Thesis	23
1.7. References	25
Chapter 2. Synthesis and Self-assembly of Bio-peptides functionalized with Twin G∧C	38
2.1. Introduction	39
2.2. Solid-phase peptide synthesis (SPPS)	42
2.3. Results and Discussion	43
2.3.1. ELDKWAK-TB	43
2.3.2. Synthesis of ELDKWAK-TB	44
2.3.3. Characterization and self-assembly of ELDKWAK-TB	46
2.3.4. RGDSK-TB	47

2.3.5. Synthesis of RGDSK-TB 47
2.3.6. Characterization and self-assembly of RGDSK-TB 49
2.3.7. DRGSK-TB 52
2.3.8. Synthesis of DRGSK-TB 52
2.3.9. Characterization and self-assembly of DRGSK-TB 54
2.4. Conclusion 56
2.5. Experimental Section 57
2.5.1. Materials 57
2.5.2. Synthesis of ELDKWAK-TB 58
2.5.3. Synthesis of RGDSK-TB 61
2.5.4. Synthesis of DRGSK-TB 64
2.5.5. Characterization by Microscopy 68
2.5.6. Sample preparation of ELDKWAK-TB 69
2.5.7. Sample preparation of RGDSK-TB 69
2.5.8. Sample preparation of DRGSK-TB 69
2.9. References 70

Chapter 3. Co-assembly Study of Rosette Nanotubes (RNTs) 74

3.1. Introduction 75
3.2. Results and Discussion 79
3.2.1. Self-assembly of K-TB 79
3.2.2. Co-assembly of K-TB with ELDKWAK-TB (Solution A) 81
3.2.3. Time-dependent study of co-assembly of K-TB with ELDKWAK-TB 83
3.2.4. Circular Dichroism (CD) study of co-assembly of K-TB with ELDKWAK-TB 86
3.2.5. Co-assembly of FITC-TB with TBL (Solution B) 89
3.2.5. Co-mixing of FITC-TB/TBL (1:15) with K-TB/ELDKWAK-TB (9:1) in the ratio 10:1 91
3.3. Conclusion 92

3.4. Experimental design 93
3.4.1. Characterization by microscopy 93
3.4.2. Circular Dichroism (CD) spectroscopy 94
3.4.3. Sample preparation of K-TB 94
3.4.4. Sample preparation of K-TB co-assembled with ELDKWAK-TB (9:1) 94
3.4.5. Time-dependent study of K-TB and K-TB/ELDKWAK-TB (9:1) 94
3.4.6. Sample preparation of FITC-TB co-assembled with TBL (1:15) 95
3.4.7. Sample preparation of co-mixing FITC-TB/TBL (1:15) with K-TB/ELDKWAK-TB (9:1) in the volume ratio (1:10) 95
3.4.8. Sample preparation of co-mixing FITC-TB/TBL (1:15) with K-TB/ELDKWAK-TB (9:1) in the ratio (10:1) 95
3.4.9. Time-dependent study of co-mixing FITC-TB/TBL (1:15) with K-TB/ELDKWAK-TB (9:1) in the volume ratio of 10:1 96
3.5. References 97

Chapter 4. Biological Studies of Rosette Nanotubes for HIV-1 Therapy 99

4.1. Introduction 100
4.2. Results and Discussion 104
4.2.1. Concentration-dependent study of cellular transfection of RNTs 104
4.2.2. Time-dependent study of cellular transfection of RNTs 107
4.2.3. Effect of co-mixing of RGDSK-TB and DRGSK-TB on the cellular uptake of the FITC-labeled K-TB/ELDKWAK-TB RNTs 110
4.2.4. Co-localization study of the cellular uptake FITC-labeled RNTs 113
4.2.5. Enzyme-linked immunosorbent assay (ELISA) for K-TB/ 114

ELDKWAK-TB (9:1) RNTs.
4.3. Conclusion 119
4.4. Materials and Methods 120
4.4.1. Materials 120
4.4.2. Cell culture 120
4.4.3. Sample preparation for confocal imaging and flow cytometry 120
4.4.4. Confocal imaging 121
4.4.5. Concentration-dependent study of cell uptake of RNTs 122
4.4.6. Time-dependent study of cell uptake of RNTs 122
4.4.7. Co-localization study 122
4.4.8. Effect of RGDSK-TB and DRGSK-TB on the cell uptake of RNTs 122
4.4.9. Flow cytometry 123
4.4.10. Time-dependent study of the cell uptake of RNTs 123
4.4.11. Effect of RGDSK-TB and DRGSK-TB on the cell uptake of RNTs 124
4.4.12. Enzyme-linked immunosorbent assay (ELISA) 124
4.4.13. Preparation of the standard curve 125
4.4.14. ELISA for K-TB/ELDKWAK-TB (9:1) RNTs with controls 125
4.5. References 126

Chapter 5. Bibliography 129

List of Tables

Table	Page
Table 1-1: Infectious Diseases and vaccines used to prevent them. [a] Not routinely available, [b] No longer available in U.S; SC = subcutaneous, IM = intramuscular, ID = intradermal, Sys = systemic, Muc = mucosal, MCV = meningococcal conjugate vaccine, MPSV = meningococcal polysaccharide vaccine, IPV = inactivated (killed) polio vaccine, OPV = live attenuated (weakened) oral polio vaccine	5
Table 1-2: Neutralizing epitopes exposed on HIV-1 mature oligomeric envelope. ([1] Strain specific neutralization. [2] Some weakly)	22
Table 3-1: Summary of the ratio of the individual components of the co-mixed RNTs	95
Table 4-1: Summary of the ratio of the individual components of the co-mixed RNTs	105
Table 4-2: Summary of the ratio of the individual components of the co-mixed RNTs	110

List of Figures

Figures	Page
Figure 1-1: Some components of immature and mature dendritic cell functions.	7
Figure 1-2: An Overview of micro- and nanotechnologies for synthetic peptide-based vaccines.	8
Figure 1-3: Dendritic cells (DCs) and nanoparticle (NP) targeting.	11
Figure 1-4: Carbon Nanotubes (CNTs) functionalized with drugs molecules for biomedical applications.	12
Figure 1-5: (A) The hydrogen bonding between the Watson Crick A-A-D sequence of cytosine and the complementary D-D-A of guanine, (B) the hybrid G∧C base pair, (C) the 6-membered macrocycle formed by 18 hydrogen bonds between the hybrid G∧C motifs, and (D) the stacking of the rosettes with lysine functionalized G∧C motifs to form helical rosette nanotube with diameter 3.5 nm.	15
Figure 1-6: The structures of a single G∧C motif functionalized with (A) the amino acid sequence RGDSK, RGDSK-MB and (B) the rosette formed by the 18 hydrogen bonds between the G∧C motifs functionalized with RGDSK. The structures of mono G∧C motif functionalized with (C) a lysine residue, K-MB and (D) the rosette formed by the hydrogen bonding between the six K-MB units. (E). The modeling of the K-MB co-assembled with RGDSK-MB in a ratio 95:5 to form helical RNTs.	16
Figure 1-7: The structures of twin G∧C motif functionalized with (A) the lysine residue, K-TB and (B) the amino acid sequence	17

RGDSK, RGDSK-MB.

Figure 1-8: Structure of HIV-1 envelope glycoprotein and the neutralizing antibodies binding sites. 20

Figure 2-1: Structures of ELDKWAK, RGDSK and DRGSK coupled to twin G∧C bases (ELDKWAK-TB, RGDSK-TB and DRGSK-TB, respectively). 41

Figure 2-2: (A) Twin G∧C monomer with an aminobutyl group (TBL), (B) formation of six-membered rosette and (C) formation of rosette nanotubes (RNTs). 42

Figure 2-3: (A) Structure of HIV-1 linear epitope ELDKWA and (B) twin G∧C motif functionalized with ELDKWA showing the possible steric effects, which can hinder the successful coupling. 43

Figure 2-4: Synthetic scheme for the synthesis of ELDKWAK-TB. 45

Figure 2-5: SEM images of ELDKWAK-TB RNTs in water (0.102 mM, at 0 min). 47

Figure 2-6: Synthetic scheme for the synthesis of RGDSK-TB. 48

Figure 2-7: The predicted mode of self-assembly of RGDSK-TB. 49

Figure 2-8: SEM images of RNTs formed by self-assembly of RGDSK-TB in water (0.113 mM, aged for 1 d). 50

Figure 2-9: SEM images of RGDSK-TB in water (0.113 mM, aged for 4 d). 50

Figure 2-10: TEM images of RNTs formed by self-assembly of RGDSK-TB in water (0.113 mM, aged for 1 d). 51

Figure 2-11: AFM images of RNTs formed by self-assembly of 51

RGDSK-TB in water (0.113 mM, aged for 7 d).

Figure 2-12: Synthetic scheme for the synthesis of DRGSK-TB 53

Figure 2-13: SEM images of RNTs formed by self-assembly of DRGSK-TB in water (0.144 mM, aged for 4 d). 54

Figure 2-14: TEM images of RNTs formed by self-assembly of DRGSK-TB in water (0.144 mM, aged for 4 d). 55

Figure 2-15: AFM images of RNTs formed by self-assembly of DRGSK-TB in water (0.144 mM, aged for 2 d). 55

Figure 3-1: Structures of (A) peptide RGDSK functionalized mono G∧C motif (RGDSK-MB), and (B) lysine, K functionalized mono G∧C motif (K-MB). 75

Figure 3-2: SEM images of formation of aggregates by ELDKWAK-TB RNTs 76

Figure 3-3: Structures of (A) lysine, K functionalized twin G∧C motif (K-TB) and (B) ELDKWAK functionalized with twin G∧C bases (ELDKWAK-TB). 78

Figure 3-4: Structures of (A) FITC functionalized twin G∧C (TB-FITC) and (B) twin G∧C monomer with an aminobutyl group (TBL). 78

Figure 3-5: SEM images of RNTs formed by self-assembly of K-TB in water at 0.039 mM concentration (A and B aged at 1 hour; C and D aged at 24 h). 79

Figure 3-6: TEM images of RNTs formed by self-assembly of K-TB in water (9 μM, aged at 24 h) 80

Figure 3-7: AFM images of RNTs formed by self-assembly of K-TB in water (9 μM, aged at 24 h). 80

Figure 3-8: SEM images of well-dispersed RNTs formed by self-assembly of K-TB in water (0.039 mM, aged at 0 min). 81

Figure 3-9: SEM images of RNTs formed by co-assembly of K-TB with ELDKWAK-TB in a molar ratio 9:1 in water (0.037 mM, aged for 3 d). 82

Figure 3-10: TEM images of RNTs formed by co-assembly of K-TB with ELDKWAK-TB in a molar ratio 9:1 in water (0.037 mM, aged for 3 d). 82

Figure 3-11: AFM images of RNTs formed by co-assembly of K-TB with ELDKWAK-TB in a molar ratio 9:1 in water (0.037 mM, aged for 3 d). 83

Figure 3-12: SEM images of RNTs formed by self-assembly of K-TB (A) at 0.05 mg/ml, ELDKWAK-TB (B) at 0.02 mg/ml and co-assembly of K-TB with ELDKWAK-TB in a molar ratio 9:1(C) aged at 0 min. 84

Figure 3-13: SEM images of K-TB (0.039 mM) and K-TB co-assembled with ELDKWAK-TB in a molar ratio 9:1 (0.037 mM) at different time intervals. 85

Figure 3-14: CD spectra of (A) self-assembly of K-TB, and (B) co-assembly of K-TB with ELDKWAK-TB in a molar ratio 9:1 (50 μM, aged at 0 min). 86

Figure 3-15: CD spectra of time study of self-assembly of (A) K-TB, (B) ELDKWAK-TB, and (C) co-assembly of K-TB with ELDKWAK-TB (9:1), at a concentration of 50 μM. 87

Figure 3-16: CD spectra of time study of self-assembly of K-TB and ELDKWAK-TB, and co-assembly of K-TB with ELDKWAK-TB (9:1), at a concentration of 50 μM, at 253 nm (A) and 300 nm (B). 87

Figure 3-17: SEM images of FITC-TB co-assembled with TBL in the molar ratio 1:15 (A and B at concentration 0.025 mg/ml and 0.0125, and C and D at concentration 0.0125 mg/ml; aged for 30 d). 89

Figure 3-18: TEM images of FITC-TB co-assembled with TBL in the molar ratio 1:15 (0.025 mg/ml, aged for 30 d). 90

Figure 3-19: AFM images of FITC-TB co-assembled with TBL in the molar ratio 1:15 (0.025 mg/ml, aged for 30 d). 90

Figure 3-20: SEM images of (A and C) FITC-TB/TBL (1:15) (B and D) co-mixing of FITC-TB/TBL (1:15) with K-TB/ELDKWAK-TB (9:1) in a ratio of 10:1 (0.05 mg/ml). 91

Figure 4-1: SEM images of RNTs formed in water by (A) self-assembly of ELDKWAK-TB (B) self-assembly of K-TB (C) co-assembly of K-TB with ELDKWAK-TB in the molar ratio 9:1 (D) co-mixing of FITC-TB/TBL (1:15) with K-TB/ELDKWAK-TB (9:1) in the weight ratio of 1:10. 103

Figure 4-2: Confocal imaging of cellular uptake of RNTs at different concentrations (0.25, 0.5 and 1 μg/ml) in the JAWS II cells. Blue: nuclei (DAPI), green: FITC-labeled RNTs. 105

Figure 4-3: 3D confocal images of JAWS II cells transfected with FITC-labeled RNTs for 24 hours. Scale bar = 7 μm. 106

Figure 4-4: Confocal imaging of cellular uptake of RNTs at different times (3, 6, 12, 24, 36, 48 hours at 1 μg/ml concentration 108

of RNTs) in the JAWS II cells. Blue: nuclei (DAPI), green: FITC-labeled RNTs.

Figure 4-5: Histogram plots of measuring the cellular uptake of RNTs at different times (3, 12, 24, 36, 48 hours at 1 μM concentration of RNTs) in the JAWS II cells. 109

Figure 4-6: Confocal images of the effect of RGDSK-TB and DRGSK-TB on the cellular uptake of FITC-labeled K-TB/ELDKWAK-TB (Solution A) RNTs in the JAWS II cells. Blue: nuclei (DAPI), green: FITC-labeled RNTs. 111

Figure 4-7: Histogram plots of effect of addition of RGDSK-TB and DRGSK-TB RNTs on the cellular uptake of FITC-labeled K-TB/ELDKWAK-TB RNTs (in the ratio 1:10 and 10:1) in the JAWS II cells. 112

Figure 4-8: Confocal images of co-localization of FITC-labeled RNTs in the JAWS II cells. Blue: nuclei (DAPI), green: FITC-labeled RNTs, red: acidic components (LysoTracker Red), orange: FITC-labeled RNTs co-localized in acidic components of the cell. 113

Figure 4-8: ELISA with absorbance at 450 nm versus concentration of K-TB/ELDKWAK-TB (Solution A) RNTs. 115

Figure 4-9: ELISA measuring the absorbance at 450 nm with respect to the concentration of Solution A (K-TB/ELDKWAK-TB) RNTs and the controls (TBL and peptide ELDKWA). 116

Figure 4-10: ELISA measuring the absorbance at 450 nm with respect to the concentration of Solution A RNTs and the controls (peptide ELDKWA and peptide ELDKWA co-mixed with Solution A RNTs in the volume ratio of 1:1). 117

List of Abbreviations

Ab	Antibody
AFM	Atomic Force Microscopy
AMEM	Alpha minimum essential medium
APCs	Antigen presenting cells
CBN	Carbon black nanoparticles
CD	Circular dichroism
CD4bs	CD4 binding site
CNTs	Carbon nanotubes
CTL	Cytolytic T-lymphocyte
DCs	Dendritic cells
1,2-DCE	1,2-dichloroethane
DCM	Dichloromethane
DIC	Diisopropylcarbodiimide
DIEA	*N*-ethyl-*N*-isopropylpropan-2-amine
DMF	*N,N*-dimethylformamide
EAMP-II	Endothelial monocyte-activating polypeptide-II
ELISA	Enzyme-linked immunosorbent assay
Env	Envelope
Et_2O	Ether
FBS	Fetal bovine serum
GalCer	Galactosyl ceramide
G∧C	Guanine-Cytosine
gp	Glycoprotein
GM-CSF	Granulocyte macrophage colony-stimulating factor
HBTU	2-(1H-benzotriazol-1-yl)-1,1,3,3-tetramethyluronium hexafluorophosphate
Hib	Haemophilus influenzae type b
HIV-1	Human immunodeficiency virus type-1
HOPG	Highly ordered pyrolytic graphite

ID	Intradermal
IM	Intramuscular
IL-8	Interleukin-8
IPV	Inactivated (killed) polio vaccine
mAb	Monoclonal antibody
MeOH	Methanol
MCV	Meningococcal conjugate vaccine
MHC	Major histocompatibility complex
MPSV	Meningococcal polysaccharide vaccine
MWNTs	Multiwalled carbon nanotubes
NPs	Nanoparticles
OPV	Oral polio vaccine
PEG-PLGA	methoxypolyethylene glycol and poly (lactide-coglycolic acid)
OB	Osteoblast
QDs	Quantum Dots
RIA	Radioactive immunoassay
RNTs	Rosette nanotubes
SC	Subcutaneous
SEM	Scanning Electron Microscopy
siRNA-PEI NPs	Polyetheylenimmine-small interfering nanocomplex
SPPS	Solid-phase peptide synthesis
Sys	Systemic
SWNTs	Single-walled carbon nanotubes
TCLA	T cell-line adapted
TCR	T-cell receptor
TEM	Transmission Electron Microscopy
TFA	Trifluoroacetic acid
TLR	Toll-like receptors
TIS	Triisopropyl silane
Ti	Titanium

TM	Transmembrane
TMB	3,3’,5,5’-tetramethylbenzidine
TNF-α	Tumor-necrosis factor-α
VLPs	Virus-like particles

Chapter 1

Introduction

1.1 Vaccines

1.1.1 Overview

For the past 200 years vaccines have been developed for a number of infectious diseases such as smallpox, diphtheria, tetanus, poliomyelitis, tuberculosis, measles, mumps, rubella, H. influenza type B, etc.[1] Despite this great achievement, there are many other diseases including *H. pylori*, hepatitis C, the Ebola virus, and human immunodeficiency virus (HIV), that still require a vaccine to be developed.[1] This need is further substantiated by the World Health Organization, which stated in 2004, 3 out of every 10 dead people were infected with a communicable disease.[2] The focus of this thesis is to develop a therapeutics to prevent the infection by human immunodeficiency virus type-1 (HIV-1).

There are some critical factors have that need to be taken into consideration when developing a vaccine. For example, an effective vaccine must have the ability to illicit an immune response by leading to the generation of antibodies specific to the antigen.[3] The cost, dose, number and route of administration of the vaccine also need to be considered.[4] For example, vaccines can be injected through a systemic route, such as intramuscular or subcutaneous.[5] These vaccines elicit a strong immune response by antibody production, but result in a low mucosal immunity.[6] This type of strategy works well against diseases where the pathogens traverse the epithelial barrier to enter the host, but are ineffective in the case of HIV for instance, where protection is needed at various levels of infection.[7] In contrast to the systemic route, the oral and intranasal route of vaccine administration leads to the development of epithelial antibodies and generate a cell mediated immune response.[6]

1.1.2. Traditional Vaccines

Traditionally, live attenuated organisms, killed whole organisms or toxoids (inactivated toxins) have been used in vaccine development.[8,9] This is because they replicate a natural infection thereby eliciting a humoral and cell-mediated

immune response.[10] In the case of live vaccines, these have been developed for diseases such as small pox, polio, measles, mumps, rubella, varicella and the adenovirus. Although these vaccines benefit from requiring only one booster dose, there are serious drawbacks such as inefficient attenuation, the potential to replicate and the risk of reverting back to their wild virulent form, which can lead to a fatal diseased state.[8-10] Killed or whole organism vaccines against influenza, hepatitis A and toxoid vaccines against diphtheria and tetanus, on the other hand, need to be given in multiple doses as they induce a weak immune response. [8,9]

More recently, recombinant DNA technology has been used to develop DNA, subunit vaccines and conjugate vaccines. In general, DNA vaccines are considered to be safe, tolerant and have the potential to illicit antibody, CTL (cytotoxic T-lymphocytes) and T-cell immune responses.[3] In this type of vaccine an antigenic gene is inserted into a bacterial plasmid that is incorporated into a viral or a bacterial vector. When the plasmid enters the nucleus of the cell, it undergoes transcription and upon the production of proteins in the cytoplasm, an immune response is generated.[11] In the case of the subunit vaccines, only a part of the pathogen is used such as a peptide or a protein. These vaccines are comparatively safer than the attenuated vaccines since they cannot revert to their wild form, but require extensive purified quantities from recombinant technologies.[9,12] Subunit protein vaccines also face the risk of degradation by protease activity and can induce a weak immune response. Hence they need delivery mechanisms to protect them from degradation.[13,14] This type of vaccine has been used to eradicate Haemophilus influenzae type b (Hib) meningitis from young infants.

Advances in vaccine development have led to the use of adjuvants and delivery mechanisms, to target the particular type of immune response and increase the intensity of the immune response.[15,16] Aluminum salts, for example, have been extensively used as adjuvants in vaccines in the U.S[17] as they show a high antibody titre with only one immunization.[18] Because of the particulate nature of aluminum salts, they can easily undergo phagocytosis by macrophages and

dendritic cells,[19,20] leading to enhanced absorption of the antigen, its recognition and presentation.[18] However aluminum salts also have the disadvantage of being inconsistent in eliciting humoral immunity[18] and are unstable to freezing and thawing.[17] Table 1-1 describes the vaccines that have been developed till date against various infections and their routes of administration.

Infection and Vaccine	**Type of Vaccine**	**Recommended Administration**	**Resulting Efficacy**
Anthrax[a]	Inactivated organism	SC	Sys
Cholera	Toxin B subunit + inactivated organism	Oral	Muc
Cholera	Live attenuated	Oral	Muc
Diptheria	Toxoid	IM	Sys
Hepatitis A	Inactivated organism	IM	Sys
Hepatitis B	Inactivated organism/ subunit	IM	Sys
Hemophilus influenza type B	Conjugate	SC	Sys
Human papillomavirus	Protein subunit	IM	
Influenza	Inactivated non-infectious virus	SC or IM	Sys
Influenza	Live attenuated	Nasal	Muc
Japanese encephalitis	Inactivated mouse-brain derived	SC	Sys
Lyme disease[b]	Protein subunit	IM	Sys
Measles	Live virus	SC	Sys
Meningococcal	Purified bacterial capsular	IM (MCV)	Sys

	polysaccharide		
Mumps	Live attenuated virus	SC	Sys
Pertussis	Whole cell or acellular	IM	Sys
Streptococcus pneumonia	Polysaccharide	IM or SC	Sys
Poliomyelitis (IPV)	Inactivated organism	IM or SC	Sys
Poliomyelitis (OPV)	Live attenuated organism	Oral	Muc
Rabies	Cell-culture or embryonated eggs	IM or ID	Sys
Rotavirus	Live attenuated	Oral	Muc
Rubella	Live attenuated	SC	Sys
Small pox	Live virus	Percutaneous	Sys
Tetanus	Toxoid	IM	Sys
Typhoid fever	Live attenuated mutant	Oral	Muc*
Typhoid fever	Vi polysaccharide	Deep SC or IM	Sys
Tuberculosis	Live organism	ID	Sys
Varicella (chicken pox)	Live attenuated	SC	Sys
Yellow fever	Live virus	SC	Sys

Table 1-1: Infectious Diseases and vaccines used to prevent them. [a] Not routinely available, [b] No longer available in U.S; SC = subcutaneous, IM = intramuscular, ID = intradermal, Sys = systemic, Muc = mucosal, MCV = meningococcal conjugate vaccine, MPSV = meningococcal polysaccharide vaccine, IPV = inactivated (killed) polio vaccine, OPV = live attenuated (weakened) oral polio vaccine. (Reprinted from Elsevier publications. Chadwick S, Kriegel C, Amiji M. Nanotechnology solutions for mucosal immunization. Adv. Drug. Deliv. Rev. 2010. 18;62(4-5):394-407. Copyright © 2010.)

1.2. Components of Immune system

Immune responses are classified either as innate or adaptive, depending on the type, speed and the specificity of the reaction. Innate immunity is known to provide a general and immediate defense by the components of the immune system such as neutrophils, monocytes, macrophages and cytokines, when a foreign body crosses the first line of defense (e.g. physical and microbiological barrier).[21] In contrast to this, with the adaptive immune response, a precise, antigen-specific response mediated by the T-lymphocytes and B-lymphocytes, results, which may take long to develop but leads to a memory for subsequent responses.[22,23] The adaptive immune responses occur on the surface of antigen-presenting cells (APCs) that present the antigens coupled with the major histocompatibility complex (MHC) to the T cells recognized by the T-cell receptor (TCR) complexes. Macrophages, dendritic cells (DCs) and B cells are the 3 types of APCs in the immune system, which communicate with the innate immune response via the cytokines.[24]

Dendritic cells discovered first by Ralph Steinman, are known to be the origin of hematopoietic cells, which control the immune system.[25] DCs are APCs, which stimulate the antigen specific T-cells to differentiate into its subsets and hence, play a role in initiating the adaptive immune responses. DCs are also known for their ability to silence T-cells. Thus DCs govern both 'immunogenicity' and tolerance.[26] DCs are involved in priming and stimulating both T-cells and B-cells, thereby playing a crucial role in innate and adaptive immunity.[27] Experiments have shown that DCs even in their not fully matured form, have the ability to stimulate T-cell tolerance *in vivo.* It is therefore possible to target the immature DCs to the populations of specific antigens without isolating them.[28-30] Fully matured DCs with encapsulated antigens are transferred to the secondary T-lymphoid organs, which then initiate T-cell mediated immunity by MHC and co-stimulatory molecule signaling.[32] Figure 1-1 illustrates the various receptors,

factors and the functions of the DCs that can be exploited via various strategies to develop an immunotherapy or a vaccine against a particular disease or infection.

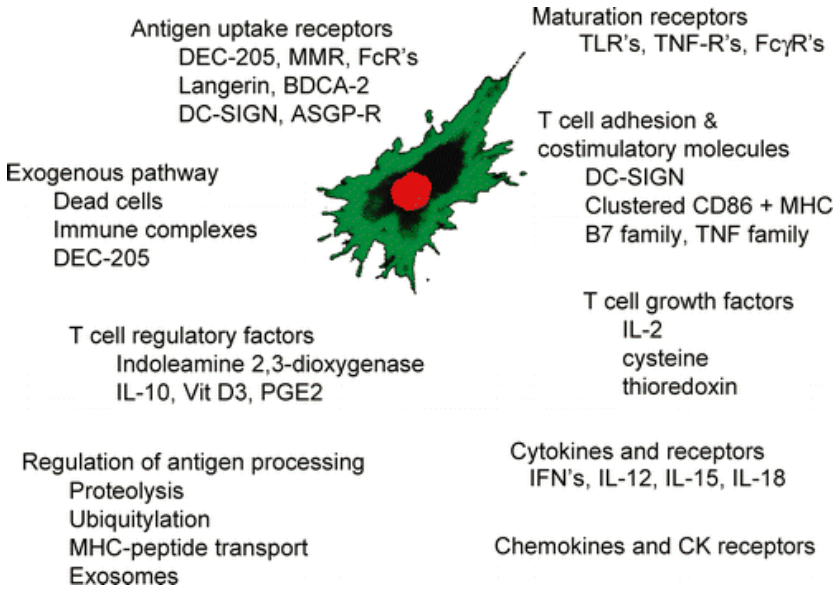

Figure 1-1: Some components of immature and mature dendritic cell functions.[32] (Reprinted by permission from Annual Reviews. Steinman RM, Hawiger D, and Nussenzweig MC. 2003. Tolerogenic Dendritic cells. *Annual Review of Immunology*. Vol. 21: 685- 711. Copyright © 2003.)

1.3. Synthetic peptide-based DC vaccines

Subunit peptide-based vaccines have low immunogenicity due to the limitations of being degraded by the protease activity and the bioavailability to cross the cellular membranes.[33,34,13] Therefore, the synthesis of peptides that are the epitopes for a particular disease and development of the adequate adjuvant for the delivery system can open up the gates for obtaining clinically potent vaccines.[35]

In order to develop an effective vaccine against infectious pathogens like HIV and malaria, both the humoral and cellular responses need to be stimulated.[36] Cytolytic T-lymphocyte (CTL) immune responses also need to be activated to prevent the infection from pathogens and tumors. CTL responses can be mediated

by CD8 T-cells, helper Th1 cells and natural killer cells.[37] As illustrated in Figure 1-2, immature DCs capture the antigens (peptides in micro- and nanoparticles), then mature into APCs and migrate to the lymph nodes where they present the peptides/antigens to the T-lymphoyctes.[37,38] However, DCs can also present the peptides to the T-cells via MHC class I or II molecules. Thus, exogenous antigens need to be cross-presented to the class I molecule to generate $CD8^+$ T-cells and produce CTL responses.[36] Usually, CTL immune responses do not occur in many peptide-based vaccines, as they get cross-presented to the MHC class II molecules. This would lead to the development of only humoral or antibody-dependent immune response and not CTL responses.[39]

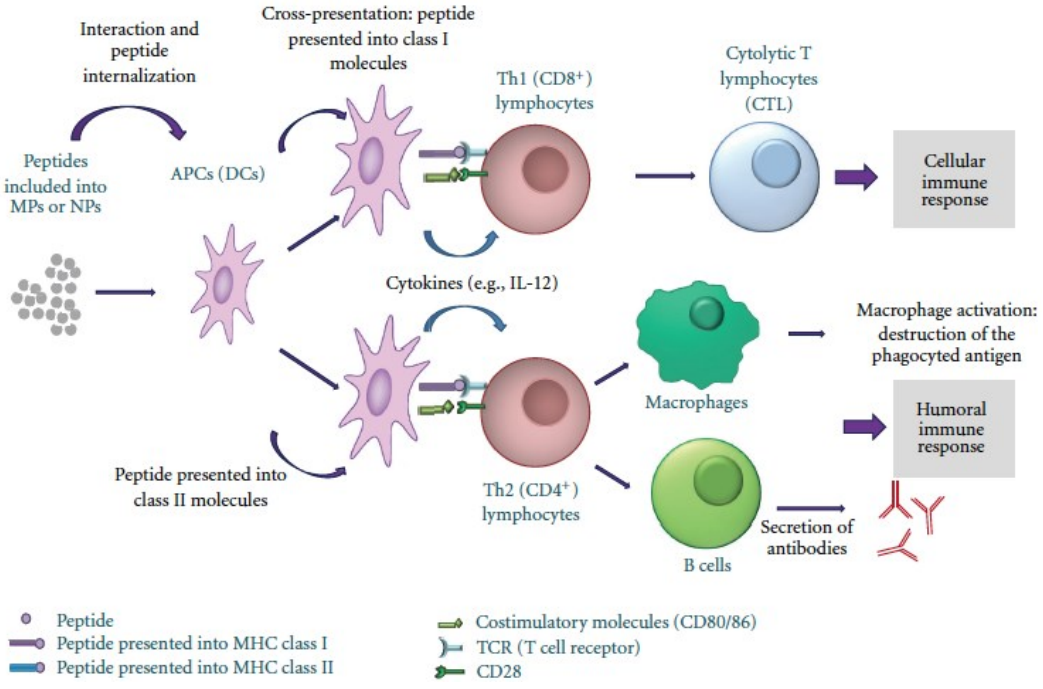

Figure 1-2: An Overview of micro- and nanotechnologies for synthetic peptide-based vaccines. (Reprinted by permission from Hindawi Publishing Corporation. Salvador A, Igartua M, Hernández RM, Pedraz JL. An Overview on the Field of Micro- and Nanotechnologies for Synthetic Peptide-Based Vaccines. 2011. *J. Drug Deliv*. 2011:181646. Copyright © 2011.)

The cross-presentation of antigens delivered by the micro- or nanoparticles to the MHC class II molecules occurs only when they escape into the cytosolic and

endoplasmic reticular space.[36] The particulate nature of the micro- and nanoparticles[36], their slow degradation can promote the interaction between the cells and the antigens[4], thereby activating the innate immunity.[40]

The aim of our thesis is to develop a synthetic peptide based nano-vaccine against HIV-1. The various delivery systems, nanoparticles and nanomaterials that act as antigen carriers are described in the subsequent sections.

1.4. Types of Delivery Systems

1.4.1. Nanoparticles

Nanoparticles (NPs) have been effectively utilized as vaccine adjuvants since they can modulate humoral and cell-mediated immunity.[41] In particular, NPs with different sizes, shapes and compositions (see below), have been designed to act as vehicles for DC targeting for a number of infectious diseases and cancer. In general this has been accomplished by conjugating antigens (such as peptides, antibodies, drugs, polysaccharides) to the NPs that are recognized by cell surface receptors, leading to an uptake via endocytosis (Figure 1-3). Alternatively, NPs have also been used to encapsulate antigens, in order to protect them from degradation by protease activity. In this case, they are taken up by the cell through phagocytosis or pinocytosis. Finally, NPs have also been labeled with magnetic particles or quantum dots to allow for their migration to be tracked. [42,43]

In regards to the different types of NPs that have utilized to effectively target DCs, leading to DC maturation without having a cytotoxic effect, these have included: (a) dendrimers, (b) polymeric NPs, (c) endosomes, (d) magnetic NPs and (e) quantum dots.

Dendrimers: These are polymeric in nature with branched molecules that can be engineered on the nanoscale and self-assemble in a hierarchical manner. Dendrimers are monodisperse macromolecules, which have a controlled size and molecular mass during synthesis. This leads to an improvement in the physical and chemical properties (like lower viscosity, higher miscibility) as compared to

linear polymers. A novel dendrimer conjugated to mannose has been known to have a strong binding affinity for mannose-binding receptors on the DCs, which upon encapsulation by the DCs, is isolated into the lysosomes.[44]

Polymeric NPs: NPs have been engineered to contain molecules that can activate Toll-like receptors (TLRs) on the DCs[45] e.g. polyetheylenimmine-small interfering nanocomplex (siRNA-PEI NPs) are recognized by TLRs specific to tumor DCs.[46]

Endosomes: These are an example of an antigen carrier that can trap NPs conjugated to polymer nucleic acids by receptor-mediated endocytosis to protect them from lysosomal degradation.[47,48] For example, methoxypolyethylene glycol and poly (lactide-coglycolic acid) (PEG-PLGA) NPs entrap a recombinant hepatitis B antigen that gives it the ability to interact with the anti-HBs antibody.[49]

Magnetic NPs: These tend to internalize in the DCs and localize in the lysosomes and do not have an effect on endocytosis with the particle size ranging from 10-200 nm.[50] DCs can also be targeted by large sized styrene NPs (500-2000 nm) that traffic to the lymph nodes unlike the small sized NPs that easily drain themselves to the lymph nodes.[51]

Quantum Dots (QDs): These are semiconductor nanocrystals that possess bright and photostable fluorescence,[52] which can be coated with polymers on their surface, conjugated with biomolecular moieties and encapsulated in the biological system such as DCs, for *in vitro* and *in vivo* imaging and modulation of DCs to stimulate an antigen-specific immune response.[52-55]

NPs act as an antigen carrier and an adjuvant that targets the APCs such as DCs. This lead to stimulation of T-cell and antibody immune response, thereby making an effective vaccine strategy. Specific antigens like the recombinant hepatitis B surface antigen or the p24 HIV-1 protein have been encapsulated by the NPs to form effective delivery systems to target DCs.[57] However, it has been reported that NPs can result in allergic reaction upon the formation of allergen-NP complex.[58] For example, OVA-treated rats were reported to have lung inflammation with the exposure to the silica-NPs, as compared to the control rats.[59, 60]

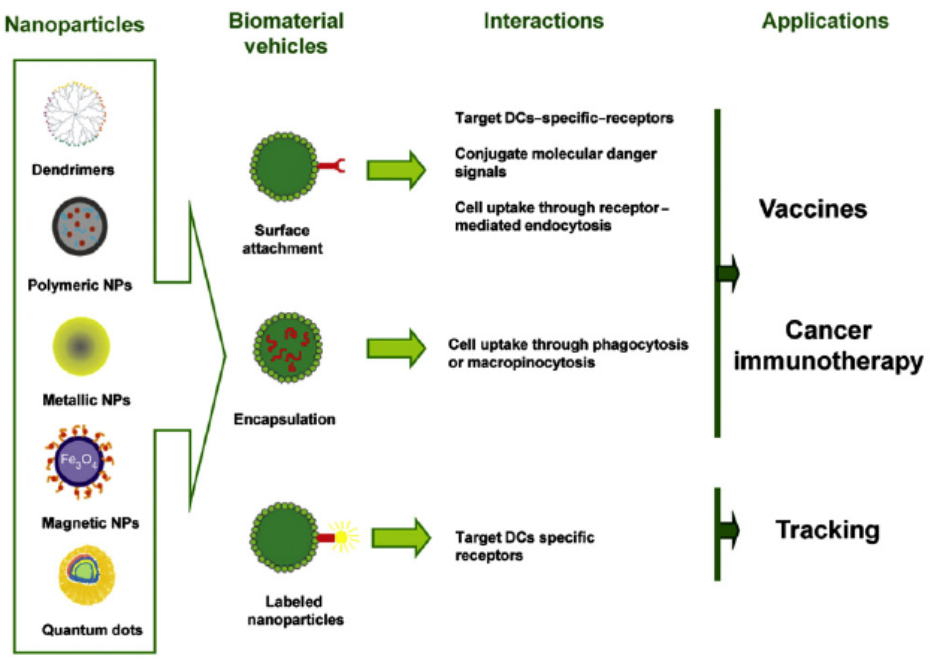

Figure 1-3: Dendritic cells (DCs) and nanoparticle (NP) targeting.[56] (Reprinted by permission from Elsevier Publications. Klippstein R, Pozo D. Nanotechnology-based manipulation of dendritic cells for enhanced immunotherapy strategies. Nanomedicine. 2010. 6(4): 523-9. Copyright © 2010.)

Other nanomaterials such as, carbon black nanoparticles (CBN)[60], single-walled carbon nanotubes (SWCNT)[61], have also been studied as an adjuvant.

1.4.2. Carbon Nanotubes (CNTs)

Carbon nanotubes (CNTs) are organized cylindrical fibers, consisting of a hexagonal carbon lattice, which have carbons arranged in sp^2-bonded structures.[62] CNTs are of two types: multiwalled carbon nanotubes (MWNTs) and single-walled carbon nanotubes (SWNTs). MWNTs were discovered first and are similar to graphite fibers[63], except that they are highly structurally arranged in comparison to the graphite fibres.[65] The central hollow region in the MWNTs are surrounding by the concentric cylindrical layers, with an interlayer distance of

0.34 nm that is close to that of graphite.[66] However SWNTs, are similar to the fullerene fibers, with a single-layer cylinder and a uniform diameter.[67,68]

Functionalized CNTs have been developed for biomedical applications such as cell internalization, gene delivery, and intracellular trafficking.[69] Figure 1-4 shows the structure of the CNTs functionalized with drug molecules, for drug delivery.

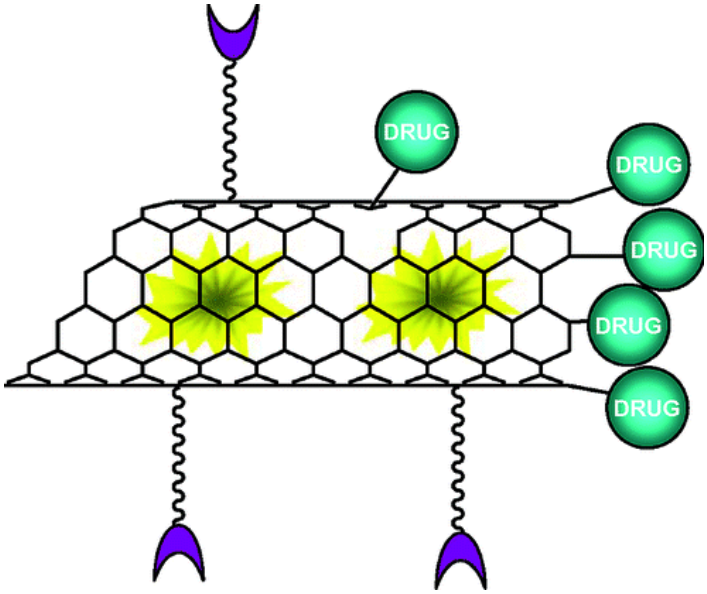

Figure 1-4: Carbon Nanotubes (CNTs) functionalized with drugs molecules for biomedical applications.[70] (Reprinted by permission from ACS Publications. Prato M, Kostarelos K, and Bianco A. Functionalized carbon nanotubes in drug design and delivery. Acc. Chem. Res. 2008. 41(1):60-8). Copyright © 2008).

A CNT-based vaccine against tumor was developed *in vitro* to target the DCs. In this vaccine construct, varying amounts of protein antigens against the tumor were loaded into the CNTs by covalent attachment. This CNT-tumor protein complex result in the stimulation of the immune response and, activate and generate the lymphocytes (T-killer cells) that would attack and destroy the tumor cells.[71] CNTs also result in the phagocytosis of the DCs inside the tumor tissue that releases the antigenic proteins and generate more of the antigens to the DCs. This in turn, increased the immunogenicity of the proteins significantly.[72] For example, a MWNT-tumor lysate protein complex has been reported to show an efficient

immune response in a mouse model H22 of liver cancer, immunized with a MWNT-tumor protein vaccine.

Along with proteins, other biological macromolecules such as DNA molecules and nucleic acids, that cannot enter the cells due to selective permeability of the cell membrane,[73] have been adsorbed onto the CNT outer wall by hydrophobic and electrostatic attractions.[74,75] This has resulted in the macromolecules retaining and in-fact enhancing their biological activity, due to the non-specific interactions with the CNT.[76,77] The CNTs loaded with the macromolecules have been encapsulated into the cells via receptor-mediated endocytosis,[78] or have been diffused into the cells via the phospholipid bilayer through an active process.[79] It has also been reported the SWNTs can act as antigen carriers for the weakly immunogenic 19 amino acid peptide WT1-Peptide 427, a Wilm's tumor antigen. The antigen presenting DCs internalized the SWNTs vaccine construct to induce the CD4 T-cell immune response.[80]

Even though CNTs have a great potential as a tumor antigen nanocarrier, they also have some toxic effects that can be a concern in the development of a safe vaccine. *In vitro* studies have revealed that toxic effects of CNTs include reduced cell viability, cell cycle disruption, apoptosis induction, and generation of oxidative stress and inflammatory responses.[81-83] However, the *in vivo* effects of CNT administration have shown that they can cross the blood-brain barrier to enter the central nervous system in mice[84], resulting in oxidative stress and peroxide-stimulated inflammation that leads to neuronal apoptosis.[85,86]

1.4.3. Helical Rosette Nanotubes (RNTs)

RNTs are a unique class of biologically inspired nanomaterials, formed by the DNA building blocks, guanine (G) and cytosine (C).[88] Mark Mascal and Andrew Marsh, first independently reported the synthesis of the DNA-base (G∧C) hybrid.[88,89] The Watson-Crick acceptor-acceptor-donor (A-A-D) sequence of cytosine is at an angle of 120° to the complementary donor-donor-acceptor (D-D-A) sequence of guanine in the G∧C base pair as shown in Figure 1-5. The hydrogen bonding between the donor and the acceptor sequences results in the formation of the hexagon-shaped macrocycle as seen in Figure 1-5C.[87-89]

Fenniri *et al*., demonstrated that these 6-membered supramacrocycles (rosettes) sustained by 18 hydrogen bonds, further self-assemble in water under physiological conditions in a hierarchical manner, owing to electrostatic, hydrophobic and stacking interactions.[87] The stacking of individual rosettes upon one another leads to the formation of the RNTs having a 1.1 nm inner channel diameter.[90,93] The surface of the nanotubes can be modified by covalently attaching a functional group or a sequence to the G∧C base, resulting in the variation of the outer diameter.[91] Variable temperature studies have shown that rise in temperature leads to increased self-assembly as it involves non-covalent interactions that are enthalpy-driven. The rise in temperature also contributes to the hydrophobic effect that releases the ordered water molecules to the bulk solvent, causing the rosettes in the solute to self-associate, thereby making the self-assembly process entropically-driven.[92]

A tricyclic[93] and tetracyclic[94] variant of the bicyclic G∧C base, designated as xG∧C[93] and xxG∧C[94] respectively, has also been designed by Borzsonyi *et al*. The hydrogen bonding between the six xG∧C and xxG∧C base unit forms the rosettes that self-assemble into RNTs with inner diameter of 1.4 nm[93] and 1.7 nm[94] respectively, as compared to 1.1 nm in case of the G∧C base RNTs. The new RNT constructs with an increased inner diameter can be used to functionalize the inner channel of the RNTs. [93,94]

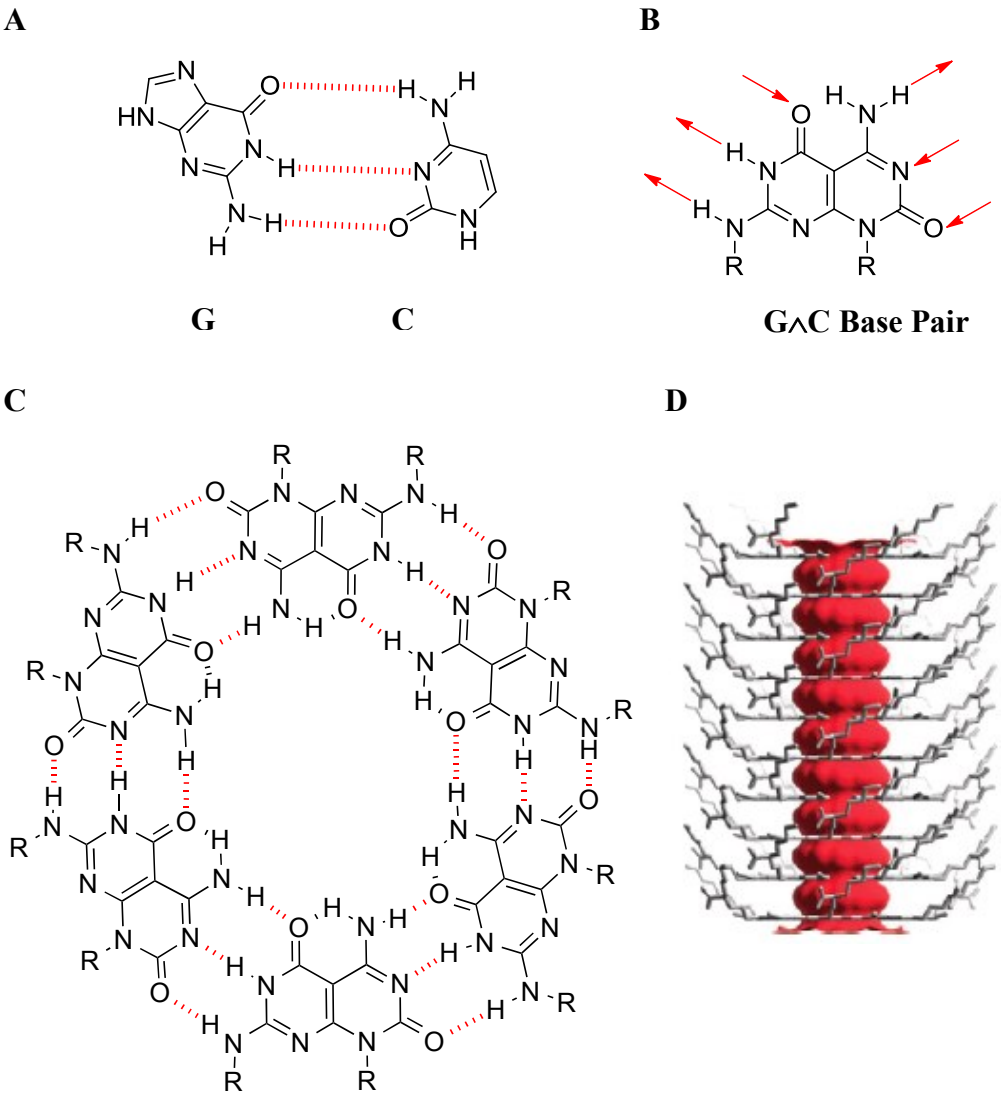

Figure 1-5: (A) The hydrogen bonding between the Watson Crick A-A-D sequence of cytosine and the complementary D-D-A of guanine, (B) the hybrid G∧C base pair, (C) the 6-membered macrocycle formed by 18 hydrogen bonds between the hybrid G∧C motifs, and (D) the stacking of the rosettes with lysine functionalized G∧C motifs to form helical rosette nanotube with diameter 3.5 nm.

The physical and chemical properties of the RNTs have been modified by covalently functionalizing the single G∧C base (MB) with a variety of groups such as, lysine (K-MB) or the amino acid sequence, RGDSK (arginine-glycine-aspartic acid-serine-lysine) as shown in Figure 1-6.[91] Two uniquely functionalized

G∧C motifs can also be co-assembled. For example, K-MB was co-assembled with RGDSK-MB in a molar ratio of 95:5 in water to form RNTs (Figure 1-6).[110]

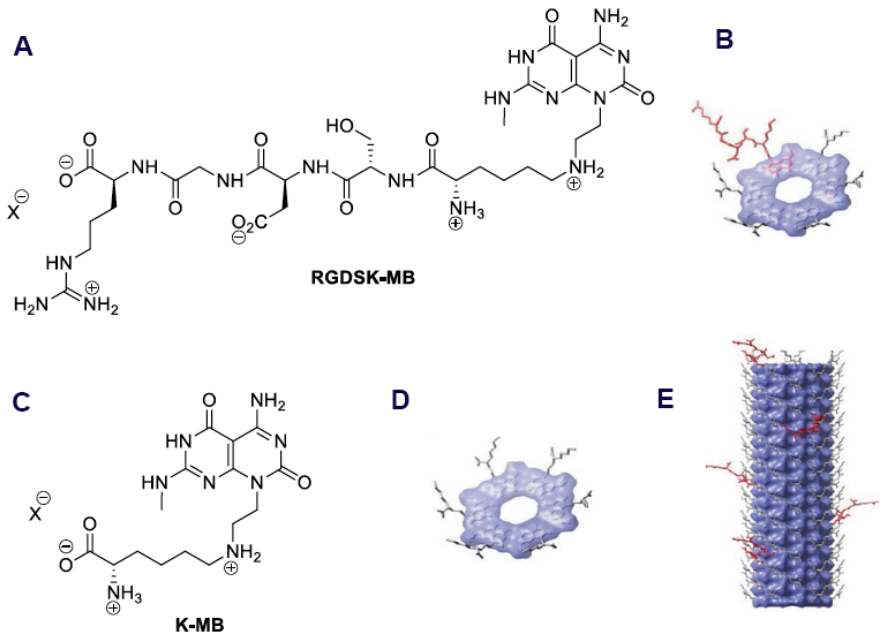

Figure 1-6: The structures of a single G∧C motif functionalized with (A) the amino acid sequence RGDSK, RGDSK-MB and (B) the rosette formed by the 18 hydrogen bonds between the G∧C motifs functionalized with RGDSK. The structures of mono G∧C motif functionalized with (C) a lysine residue, K-MB and (D) the rosette formed by the hydrogen bonding between the six K-MB units. (E). The modeling of the K-MB co-assembled with RGDSK-MB in a ratio 95:5 to form helical RNTs.

A twin G∧C base system has also been synthesized, which is thermodynamically more favorable than the mono base system. The twin base system formed the hexameric rosette by 36 hydrogen bonds between the twin G∧C motifs instead of 18 in the mono base system. The greater number of hydrogen bonds and increased the amphiphilic character during organization results in enhanced thermal stability of the twin RNTs. Another factor that contributes to the stability of twin G∧C base system includes the reduced steric hindrance and electrostatic repulsion on the surface of the RNTs due to decreased functional density and net charge,

respectively.[91] The twin G∧C motif can also be functionalized with an amino acid residue, lysine or a peptide sequence, RGDSK as shown in Figure 1-7.

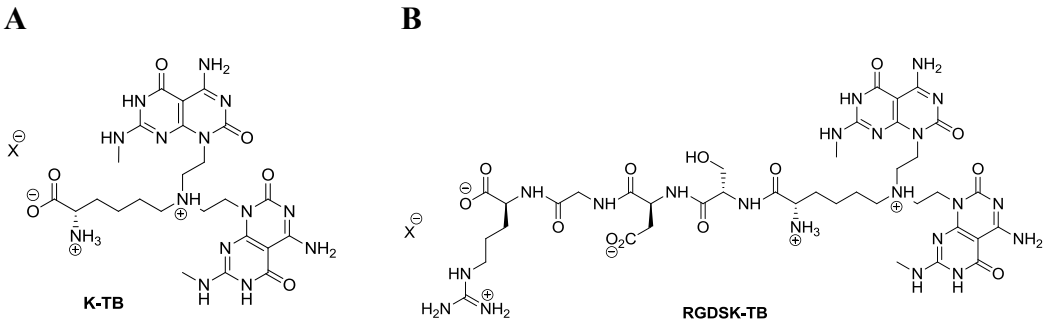

Figure 1-7: The structures of twin G∧C motif functionalized with (A) the lysine residue, K-TB and (B) the amino acid sequence RGDSK, RGDSK-TB.

The RNTs have been exploited for various biomedical applications. It has been established for example, that RNTs with a lysine side-chain (K-MB), lead to enhanced osteoblast (OB) adhesion when coated onto the titanium (Ti) surface.[95] The surface properties due to the chemical tunability of the RNTs, their self-assembly property, the ability to be adsorbed on the Ti surface, and their encapsulation into the cells after interactions on the cell surface, makes the K-MB RNT system a novel candidate for the osteogenic Ti implant.[97] It has been reported that the single G∧C functionalized lysine-RNTs mimics the lysine-rich bovine bone morphogenic proteins that promotes OB adhesion, their proliferation and differentiation in osteoblast-like MC3T3-E1 cells.[96] It has also been found that nanocomposites comprised of RNTs and hydroxyapatite in poly(2-hydroxyethyl methacrylate) hydrogels have much better OB adhesion as compared to hydroxyapatite alone *in vitro*.[97] RNTs have also been functionalized by three bio-peptides, peptide-(A); SNVILKKYRN, peptide-(B); KPSSAPTQLN and peptide-(C); KAISVLYFDDS, which are the core peptides of the bone morphogenic protein-7 (BMP-7). These peptides have shown adhesion to the Ti surface and resulting in the increased OB function.[98]

Journeay *et al.* investigated the effects of K-MB RNT system on the human macrophage cell line U937. Macrophages play a vital role in recognizing the foreign particles in the lung environment and stimulating the immune responses.[99] The expression of tumor-necrosis factor-α (TNF-α), EAMP-II and interleukin-8 (IL-8) were assessed to account for the inflammatory responses in macrophages.[100-102] While TNF-α is responsible for initiation of the pro-inflammatory lung responses,[101,102] EAMP-II and IL-8 are the chemo-attractants respectively for monocytes and neutrophils.[103-106] It was found that RNTs formed by the self-assembly of lysine-mono G∧C base did not induce inflammatory responses in the cell line U937.[99]

Lung inflammatory responses have also been investigated by the *in vivo* study on the C57BL/6 mice by Suri *et al*. [108] The RNTs formed by the self-assembly of lysine-twin G∧C base, when administered through intranasal route into the mice did not show considerable lung inflammation. Journeay *et al.* reported that the biological design of the RNTs show low acute pulmonary toxicity *in vivo* and are toxicologically favorable for biomedical applications.[109] It has been reported that RGD-tagged RNTs can lead to activation of cell signal pathways (P38 mitogen-activated protein kinase) that in turn result in the generation of cytokines like TNF-α *in vitro*. Similar pathways can also be activated by the binding of RGD sequences on the RNTs to the αvβ3 integrin on the cell surface.[107] This was achieved by co-assembling the lysine-mono G∧C base with the RGDSK-mono G∧C base in a molar ratio of 90:10. [108] Another study investigated and confirmed that K-RNTs and RGDSK-RNTs (monobase system) when co-assembled in a molar ratio of 95:5, inhibited the MAPK signaling pathway and chemotaxis without causing apoptosis in neutrophils via the αvβ3 integrin pathway.[111]

Given the potential of the RNTs in the biomedical applications and their low toxicity, the aim of our current research was to extend the applications of RNTs in developing them as the potent antigen carrier for the HIV-1.

1.5. Human Immunodeficiency Virus Type-1 (HIV-1)

In 2010 it was estimated that there were between 1.5 and 1.8 million deaths caused by human immunodeficiency virus (HIV).[112,113] These statistics indicate the global impact of HIV and the need to control the spread of HIV-1 infection by developing a vaccine against it.

1.5.1. HIV-1 Envelope Structure and Function

The attachment of the HIV-1 virus and its entry into the target cell are the early steps in the HIV infection. The HIV-1 mature envelope glycoprotein (gp) complex play a role in this process. This complex has a heterodimer of a transmembrane (TM) subunit gp41, which is noncovalently bound to a surface subunit gp120. Together these form a trimeric configuration. Five variable regions (V1-V5) and five conserved regions (C1-C5) of gp120 have been determined.[114,115] The structure of gp120 constitutes two major domains, an inner and outer domain and one mini-domain known as the bridging sheet.[116] The interface of these three domains has a depression, which forms the CD4 binding site (CD4bs).[117] The gp120 subunit of the virus interacts with the cellular receptor CD4 on the target cell, leading to the attachment of the virus on the cell surface and hence beginning of the HIV infection. The CD4 binding induces the conformational changes, which are necessary for the interactions of gp120 with its co-receptors.[114,117,118] The CD4 is flexible enough to expose the co-receptor binding site of gp120, coming closer to the co-receptor for further interaction and hence the target cell and the viral membranes come in close proximity. Conformational changes as a result of co-receptor binding destabilize the gp120-gp41 interactions. This leads to transformation of gp-41 into a "prehairpin" intermediate, hence inserting the fusion peptide of gp41 into the membrane of the target cell and causing gp120 subunits to dissociate. Due to further conformational changes, gp41 transforms into the "hairpin" structure, causing viral and target cell membranes to fuse. This presents the nucleocaspid with the

viral genome into the host cell.[120] Figure 1-8 illustrates the schematic structure of the HIV-1 envelope protein.

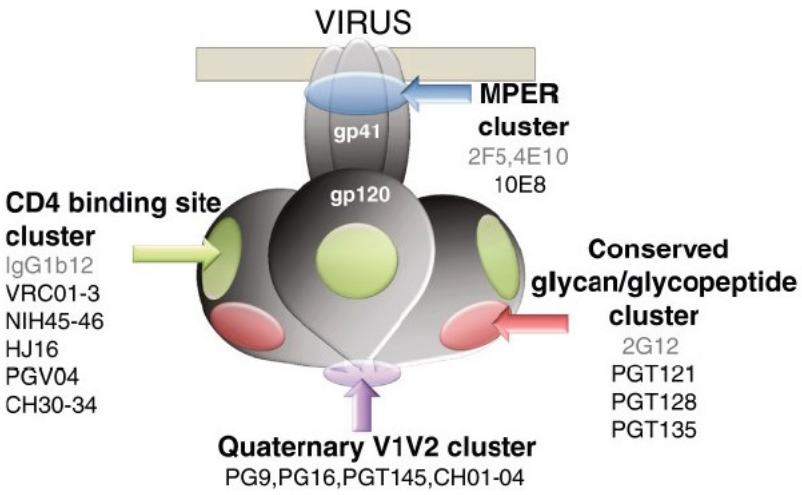

Figure 1-8: Structure of HIV-1 envelope glycoprotein and the neutralizing antibodies binding sites. (Reprinted by permission from BioMed Central Ltd. Schiffner T, Sattentau QJ and Dorrell L. Development of prophylactic vaccines against HIV-1. *Retrovirology*. 2013. 17;10: 72. Copyright © 2013).

1.5.2. HIV Infection

HIV is transmitted through various modes. Following the sexual transmission, the mucous layer in the columnar epithelium in the endocervix and the mucosal sites in the stratified squamous epithelium in the ectocervix, inner foreskin, rectum, vaginal mucosa and glans forms the natural barriers for the HIV viral invasion. Once HIV crosses these natural barriers, they cause infection by either of the two mechanisms: (a) endocytosis of the DCs, or (b) infection of DCs, macrophages, or CD4+ directly. This leads to transportation of the virus to the local lymph nodes, following the presentation of the virus to the cells, and amplification and spread of the infection. HIV-1 viral envelope has three glycoprotein (gp) 160 molecules, each comprising of a gp120 present on the surface of the envelope and a transmembrane protein gp41. The CCR5 binding site on the surface of gp120, CD4bs on the envelope and the proximal external region at the base of the gp41

are the essential targeting sites for the neutralizing antibodies to come and react on the envelope.[120] Figure 1-8 shows the envelope structure of HIV-1 and the various targeting sites for the neutralizing antibodies.

1.5.3. HIV-1 Vaccine Candidates

In general, a potent and effective vaccine against HIV should be capable of developing and inducing strong, adequate, constant humoral and cell-mediated immune responses.[120] Previous research into the development of a suitable HIV vaccine was focused on a prophylactic vaccine to induce an antibody response against the HIV-1 envelope protein. Unfortunately, the two recombinant vaccines developed against HIV-1 envelope glycoprotein (gp) 120 that were in Phase III trials could only generate strain specific antibody response and hence were unable to control the HIV-1 infection.[121]

HIV-1 neutralization sensitivity is an important factor to take into account while studying the vaccine candidates for HIV. T cell-line adapted (TCLA) viruses are known to be highly sensitive to neutralization which has misrepresented the HIV-1 vaccine for many years.[122] The surface of the envelope reveals the neutralizing epitopes on gp120, which gets exhibited in the oligomeric configuration and get displayed towards the target cell. Table 1-2 shows the neutralizing epitopes on the HIV-1 mature oligomeric envelope.[123-125]

The objective of this research is to functionalize the RNTs with a short bioactive peptide that is an epitope on the gp41 of the HIV-1 envelope. ELDKWA (glutamic acid-leucine-aspartic acid-lysine-tryptophan-alanine) is the linear sequence present on the membrane proximal external region (MPER in Figure 1-8) part of the ectodomain (residues 662-667).[126] ELDKWA is the epitope on gp41 of the HIV-1 glycoprotein complex which is unveiled on the native oligomeric conformation. 2F5 is the monoclonal antibody (mAb) specific for gp41 that recognizes the epitope ELDKWA and exhibits the neutralizing activity.[126-130]

Epitopes	Antibodies	Neutralization of	
		TCLA strains	Primary Isolates
gp 120			
V3	Loop2, 19b, 447/52D	Yes	No
CD4bs	F105, 21h, 15e	Yes	No
CD4bs/V2	b12	Yes	Yes
CD4i	17b, 48d	Yes	No
V2	C108G	Yes	No[1]
	L15, 697D	No	No[2]
Base of V3 and V4 loop	2G12	Yes	Yes
gp 41			
ELDKWA (residues 667-672)	2F5	Yes	Yes

Table 1-2: Neutralizing epitopes exposed on HIV-1 mature oligomeric envelope. ([1] Strain specific neutralization. [2] Some weakly).

1.6. Objective of the Thesis

In this thesis, we endeavor to develop a nanoscale delivery system to carry the antigen for HIV-1, by functionalizing the biocompatible, self-assembled RNTs with the epitope on gp41 of the HIV-1 to target the DCs. The attachment of HIV-1 to the target cell and its transcytosis is the initial step in the HIV infection. The TM protein gp41 acts as a HIV-1 fusion protein. Sequences 667-672 (ELDKWA) on the gp41 of HIV- 1 are involved in the Galactosyl ceramide (GalCer) binding to the epithelial cells or immature DCs.[131]

In the second chapter of the thesis, we discuss the synthesis of three bioactive peptides, ELDKWAK, a gp41 epitope, RGDSK, a cell adhesion peptide[132] and DRGSK, the scrambled version of RGDSK by Fmoc protected solid-phase peptide synthesis (SPPS). Following the synthesis, these peptides are functionalized with twin G∧C motif via reductive amination on the solid support. In the above sequences, while ELDKWA is the epitope, lysine (K) was added that act as a spacer between the peptide and the twin G∧C motif. Similarly, RGD is the cell adhesion peptide, serine-lysine (SK) was added after RGD and DRG, to act as the spacer between the amino acid sequence and the twin G∧C base pairs. The final products, ELDKWAK, RGDSK and DRGSK functionalized with twin G∧C motifs, designated as ELDKWAK-TB, RGDSK-TB and DRGSK-TB, respectively, were characterized and their self-assembly under aqueous conditions was investigated.

In chapter 3, we investigate the co-assembly of K-TB with ELDKWAK-TB in a 9:1 molar ratio in order to form a stable RNT system. Also in this chapter, we discuss the fluorescein isothiocyante (FITC) labeled RNTs that are formed by the co-assembly of the FITC-functionalized twin G∧C base (FITC-TB) and the twin-base linker (TBL) in a molar ratio 1:15 in water. These fluorescent RNTs are used to study the cell uptake of the K-TB/ELDKWAK-TB RNTs.

In chapter 4, we study the uptake of K-TB/ELDKWAK-TB (9:1) RNTs by the DCs, by co-mixing them with FITC-TB/TBL (1:15) in different ratios. The cell uptake of the RNTs was confirmed visually by the confocal microscopy and quantitatively by the fluorescence measurements via flow cytometry. Further in this chapter, an enzyme-linked immunosorbent assay (ELISA) was developed to investigate the binding of the K-TB/ELDKWAK-TB (9:1) RNTs to the human HIV-1 gp41 mAb, 2F5 that is specific for the epitope ELDKWA.

Overall, these *in vitro* studies confirm that the twin G∧C base RNT system functionalized with the gp41 epitope ELDKWA, (K-TB/ELDKWAK-TB) is an efficient delivery system for carrying the HIV-1 antigen to the DCs.

1.7. References:

1. Ogra PL, Faden H, Welliver RC, Vaccination strategies for mucosal immune responses. *Clin. Microbiol. Rev*. **2001**. 14: 430–445.
2. World Health Organization. The global burden of disease: 2004 update, Geneva, Switzerland, **2008**.
3. Srivastava I, Singh M. DNA vaccines: focus on increasing potency and efficacy. *Int. J. Pharm. Med*. **2005**. 19: 15–28.
4. Perrie Y, Mohammed AR, Kirby DJ, McNeil SE, Bramwell VW. Vaccine adjuvant systems: enhancing the efficacy of sub-unit protein antigens. *International Journal of Pharmaceutics*. **2008**. 364 (2): 272–280.
5. Russell-Jones GJ. Oral vaccine delivery. *J. Control. Release*. **2000**. 65: 49–54.
6. Wang J, Thorson L, Stokes RW, Santosuosso M, Huygen K, Zganiacz A, Hitt M, Xing Z. Single mucosal, but not parenteral, immunization with recombinant adenoviral-based vaccine provides potent protection from pulmonary tuberculosis. *J. Immunol*. **2004**. 173: 6357–6365.
7. Neutra MR, Kozlowski PA. Mucosal vaccines: the promise and the challenge. *Nat. Rev. Immunol*. **2006**. 6: 148–158.
8. Plotkin SL, Plotkin SA. A short history of vaccination, in: S.A. Plotkin, W.A. Orenstein (Eds.). *Vaccines*, WB Saunders Company, Philadelphia. **2004**. 1–15.
9. National Institute of Allergy and Infectious Diseases, Understanding vaccines: what they are and how they work. http://www.niaid.nih.gov/ publications/vaccine/pdf/undvacc.pdf.
10. Webster DE, Gahan ME, Strugnell RA, Wesselingh SL. Advances in oral vaccine delivery options: what is on the horizon? *Am. J. Drug Deliv*. **2003**. 1: 227–240.
11. Donnelly JJ, Wahren B, Liu MA. DNA vaccines: progress and challenges. *J. Immunol*. **2005**. 175: 633–639.
12. Walsh G. Biopharmaceuticals: Biochemistry and Biotechnology, John Wiley, New York, **1998**.

13. Azad N, Rojanasakul Y. Nanobiotechnology in drug delivery. *Am. J. Drug Deliv*. **2006**. 4: 79–88.
14. Kaminski RW, Turbyfill KR, Oaks EV. Mucosal adjuvant properties of the Shigella invasin complex. *Infect. Immun*. **2006**. 74: 2856–2866.
15. O'Hagan DT. Microparticles as vaccine delivery systems, in: V.E.J.C Schijns, D.T. O'Hagan (Eds.). Immunopotentiators in Modern Vaccines Academic Press, Burlington, MA. **2006**. 123–147.
16. Copland MJ, Rades T, Davies NM, Baird MA. Lipid based particulate formulations for the delivery of antigen. *Immunol. Cel Biol*. **2005**. 83: 97–105.
17. Rabinovich NR, McInnes P, Klein DL, Hall BF. Vaccine technologies: view to the future. *Science*. **1994**. 265: 1401–1404.
18. Simon JK, Edelman R. Clinical evaluation of adjuvants, in: Schijns VEJC, O'Hagan DT (Eds.), *Immunopotentiators in Modern Vaccines*, Academic Press, Burlington, MA. **2006**. 319–342.
19. Gupta RK, Rost BE, Relyveld E, Siber GR. Adjuvant properties of aluminum and calcium compounds, in: M.F. Powell, M.J. Newman (Eds.). *Vaccine Design: the Subunit and Adjuvant Approach*, Plenum Press, New York. **1995**. 229–248.
20. Eldridge JH, Staas JK, Meulbroek JA, Tice TR, Gilley RM. Biodegradable and biocompatible poly(DL-lactide-co-glycolide)microspheres as an adjuvant for staphylococcal enterotoxin B toxoid which enhances the level of toxin-neutralizing antibodies. *Infect. Immun*. **1991**. 59: 2978–2986.
21. Metchnikoff E. Sur la lutta des cellules de l'organismes centre l'invasion des microbes. *Annales. Inst. Pasteur Paris*. **1887**. 1: 321.
22. Delves PJ, Roitt IM. The immune system. Part 1. *N. Engl. J. Med*. **2000**. 343: 3–49.
23. Delves PJ, Roitt IM. The immune system. Part 2. *N. Engl. J. Med.* **2000**. 343: 108–17.

24. Guermonprez P, Valladeau J, Zitvogel L, Thery C, Amigorena S. Antigen presentation and T cell stimulation by dendritic cells. *Annu. Rev. Immunol*. **2002**. 20: 621-67.
25. Steinman RM, Cohn ZA. Identification of a novel cell type in peripheral lymphoid organs of mice. I.Morphology,quantitation, tissue distribution. *J. Exp. Med*. **1973**. 137: 1142–62.
26. Bancherau J. Steinman RM. Dendritic cells and control of immunity. *Nature*. **1998**. 392: 245-52.
27. Tacken PJ, de Vries IJ, Torensma R, Figdor CG. Dendritic-cell Immunotherapy: from ex vivo loading to in vivo targeting. *Nat. Rev. Immunol*. **2007**. 7 (10): 790-802.
28. Hawiger D, Inaba K, Dorsett Y, Guo K, Mahnke K, *et al*. Dendritic cells induce peripheral T cell unresponsiveness under steady state conditions *in vivo*. *J. Exp. Med.* **2001**. 194:769–80.
29. Bonifaz L, Bonnyay D, Mahnke K, Rivera M, Nussenzweig MC, Steinman RM. Efficient targeting of protein antigens to the dendritic cell receptor DEC-205 in the steady state leads to antigen presentation on MHC class I products and peripheral $CD8^+$ T cell tolerance. *J. Exp. Med.* **2002**. 196:1627–38
30. Liu K, Iyoda T, Saternus M, Kimura Y, Inaba K, Steinman RM. Immune tolerance following delivery of dying cells to dendritic cells in situ. *J. Exp. Med.* **2002**. 196:1091–7
31. Lombardi G, Vasquez Y, Lombardi G, Vasquez Y. Dendritic cells. *Handb. Exp. Pharmacol*. **2009**. 188:v-ix.
32. Steinman RM, Hawiger D, and Nussenzweig MC. Tolerogenic Dendritic cells. Annual Review of Immunology. **2003**. 21: 685- 711.
33. Bramwell VW, Eyles JE, and Alpar HO. Particulate delivery systems for biodefense subunit vaccines. *Advanced Drug Delivery Reviews*. **2005**. 57 (9): 1247–1265.
34. Chadwick S, Kriegel C, and Amiji M. Nanotechnology solutions for mucosal immunization. *Advanced Drug Delivery Reviews*. **2010**. 62 (4-5): 394–407.

35. O'Hagan DT, De Gregorio E. The path to a successful vaccine adjuvant-the long and winding road. *Drug Discovery Today*. **2009**. 14 (11-12): 541–551.
36. Look M, Bandyopadhyay A, Blum JS, Fahmy TM. Application diseases in the developing world. *Advanced Drug Delivery Reviews.* **2010**. 62 (4-5): 378–393.
37. Steinman R. Dendritic cells and vaccines. Baylor University Medical Center Proceedings. **2008**. 21 (1): 3–8.
38. Blanco P, Palucka AK, Pascual V, Banchereau J. Dendritic cells and cytokines in human inflammatory and autoimmune diseases. *Cytokine and Growth Factor Reviews*. **2008**. 19 (1): 41–52.
39. McCullough KC, Summerfield A. Targeting the porcine immune system-particulate vaccines in the 21st century. *Developmental and Comparative Immunology*. **2009**. 33 (3): 394–409.
40. De Gregorio E, D'Oro U, Wack A. Immunology of TLR-independent vaccine adjuvants. *Current Opinion in Immunology*. **2009**. 21 (3): 339–345.
41. Banchereau J, Palucka AK. Dendritic cells as therapeutic vaccines against cancer. *Nat. Rev. Immunol*. **2005**. 5:296-306.
42. Reddy ST, Swartz MA, Hubbell JA. Targeting dendritic cells with biomaterials: developing the next generation of vaccines. *Trends Immunol*. 2006. 27:573-9.
43. Allen TM, Cullis PR. Drug delivery systems: entering the mainstream. *Science*. **2004**. 303:1818-22.
44. Sheng KC, Kalkanidis M, Pouniotis DS, Esparon S, Tang CK, Apostolopoulos V, et al. Delivery of antigen using a novel mannosylated dendrimer potentiates immunogenicity *in vitro* and *in vivo*. Eur. J. Immuno. **2008**. 38:424-36.
45. Kumar H, Kawai T, Akira S. Toll-like receptors and innate immunity. *Biochem. Biophys. Res. Commun*. **2009**. 388:621-5.
46. Cubillos-Ruiz JR, Engle X, Scarlett UK, Martinez D, Barber A, Elgueta R, *et al*. Polyethylenimine-based siRNA nanocomplexes reprogram tumor-

associated dendritic cells via TLR5 to elicit therapeutic antitumor immunity. *J. Clin. Invest*. **2009**. 119:2231-44.

47. Reischl D, Zimmer A. Drug delivery of siRNA therapeutics: potentials and limits of nanosystems. *Nanomedicine*. **2009**. 5:8-20.
48. Aline F, Brand D, Pierre J, Roingeard P, Severine M, Verrier B, et al. Dendritic cells loaded with HIV-1 p24 proteins adsorbed on surfactant free anionic PLA nanoparticles induce enhanced cellular immune responses against HIV-1 after vaccination. *Vaccine*. **2009**. 27:5284-91.
49. Bharali DJ, Pradhan V, Elkin G, Qi W, Hutson A, Mousa SA, et al. Novel nanoparticles for the delivery of recombinant hepatitis B vaccine. *Nanomedicine*. **2008**. 4:311-7.
50. Goya GF, Marcos-Campos I, Fernandez-Pacheco R, Saez B, Godino J, Asin L, et al. Dendritic cell uptake of iron-based magnetic nanoparticles. *Cell Biol. Int*. **2008**. 32:1001-5.
51. Manolova V, Flace A, Bauer M, Schwarz K, Saudan P, Bachmann MF. Nanoparticles target distinct dendritic cell populations according to their size. *Eur. J. Immunol*. **2008**. 38:1404-13.
52. Jaiswal JK, Simon SM. Optical monitoring of single cells using quantum dots. *Methods Mol. Biol*. **2007**. 374: 93–104.
53. Cambi A, Lidke DS, Arndt-Jovin DJ, Figdor CG, Jovin TM. Ligandconjugated quantum dots monitor antigen uptake and processing by dendritic cells. *Nano Lett*. **2007**. 7: 970–977.
54. Lidke DS, Nagy P, Jovin TM, Arndt-Jovin DJ. Biotin-ligand complexes with streptavidin quantum dots for in vivo cell labeling of membrane receptors. *Methods Mol. Biol*. **2007**. 374: 69–79.
55. Smith AM, Dave S, Nie S, True L, Gao X (2006) Multicolor quantum dots for molecular diagnostics of cancer. *Expert Rev. Mol. Diagn*. 2006. 6: 231–244.
56. Klippstein R, Pozo D. Nanotechnology-based manipulation of dendritic cells for enhanced immunotherapy strategies. *Nanomedicine*. **2010**. 6(4):523-9.

57. Wang X, Uto T, Akagi T, Akashi M, Baba M. Poly(gamma-glutamic acid) nanoparticles as an efficient antigen delivery and adjuvant system: potential for an AIDS vaccine. *J. Med. Virol.* 2008. 80:11-9.
58. Madl AK, Pinkerton KE. Health effects of inhaled engineered and incidental nanoparticles. *Crit. Rev. Toxicol*. **2009**. 39: 629–658.
59. Han B, Guo J, Abrahaley T, Qin L, Wang L, Zheng Y, Li B, Liu D, Yao H, Yang J, Li C, Xi Z, Yang X. *PLoS One*. Adverse effect of nano-silicon dioxide on lung function of rats with or without ovalbumin immunization. **2011**. 6: e17236.
60. Brandenberger C, Rowley NL, Jackson-Humbles DN, Zhang Q, Lewandowski RP, Wagner JG, Chen W, Kaminski NE, Baker GL, Worden RM, Harkema JR. Engineered silica nanoparticles act as adjuvants to enhance allergic airway disease in mice. *Part*. *Fibre Toxicol*. **2013**. 10: 26.
61. Inoue K, Takano H, Yanagisawa R, Hirano S, Sakurai M, Shimada A, Yoshikawa T. Effects of airway exposure to nanoparticles on lung inflammation induced by bacterial endotoxin in mice. *Environ. Health Perspect*. **2006**. 114: 1325–1330.
62. Inoue K, Yanagisawa R, Koike E, Nishikawa M, Takano H. Repeated pulmonary exposure to single-walled carbon nanotubes exacerbates allergic inflammation of the airway: possible role of oxidative stress. *Free Radical Biol. Med*. **2010**. 48: 924–934.
63. Dresselhaus MS, Dresselhaus G, Eklund PC. Science of Fullerenes and Carbon Nanotubes (Academic, New York). **1996**.
64. Dresselhaus MS, Dresselhaus G, Sugihara K, Spain IL, Goldberg HA. Graphite Fibers and Filaments. Springer-Verlag: New York. **1988**.
65. Bethune DS, Kiang CH, de Vries MS, Gorman G, Savoy R, Vazquez J, Beyers R. Cobalt-catalysed growth of carbon nanotubes with single-atomic-layer walls. *Nature*. **1993**. 363: 605.
66. Iijima, S. Helical microtubules of graphitic carbon. *Nature* (London). **1991**. 354: 56–58.
67. Iijima S, Ichihashi T. Single-shell carbon nanotubes of 1-nm diameter.

Nature. **1993**. 363: 603-605.

68. Tasis D, Tagmatarchis N, Bianco A, Prato M. Chemistry of carbon nanotubes. *Chem. Rev.* **2006**. 106: 1105–1136.
69. Meng J, Meng J, Duan J, et al. Carbon nanotubes conjugated to tumor lysate protein enhance the efficacy of an antitumor immunotherapy. *Small*. **2008**. 4(9): 1364–1370.
70. Prato M, Kostarelos K, and Bianco A. Functionalized carbon nanotubes in drug design and delivery. *Acc. Chem. Res.* **2008**. 41(1): 60-8.
71. Shen H, Ackerman AL, Cody V, et al. Enhanced and prolonged cross-presentation following endosomal escape of exogenous antigens encapsulated in biodegradable nanoparticles. *Immunology*. **2006**. 117(1): 78–88.
72. Lindblad EB. Aluminium adjuvants – in retrospect and prospect. *Vaccine*. **2004**. 22(27–28): 3658–3668.
73. Wadhwa PD, Zielske SP, Roth JC, Ballas CB, Bowman JE, Gerson SL. Cancer gene therapy: scientific basis. *Annu. Rev. Med*. **2002**. 53: 437–452.
74. Madani SY, Tan A, Dwek M, Seifalian AM. Functionalization of single-walled carbon nanotubes and their binding to cancer cells. Int J *Nanomedicine*. **2012**. 7: 905–914.
75. Jovanovic´ SP, Markovic´ ZM, Kleut DN, et al. A novel method for the functionalization of gamma-irradiated single wall carbon nanotubes with DNA. *Nanotechnology*. **2009**. 20(44): 445602.
76. Gomez-Gualdrón DA, Burgos JC, Yu J, Balbuena PB. Carbon nanotubes: engineering biomedical applications. *Prog. Mol. Biol. Transl. Sci*. **2011**. 104: 175–245.
77. Sánchez-Pomales G, Santiago-Rodríguez L, Cabrera CR. DNA-functionalized carbon nanotubes for biosensing applications. *J. Nanosci. Nanotechnol.* **2009**. 9(4): 2175–2188.
78. Kam NW, Liu Z, Dai H. Carbon nanotubes as intracellular transporters for proteins and DNA: an investigation of the uptake mechanism and pathway. *Angew Chem. Int. Ed. Engl*. **2006**. 45(4): 577–581.

79. Pantarotto D, Briand JP, Prato M, Bianco A. Translocation of bioactive peptides across cell membranes by carbon nanotubes. *Chem. Commun*. (Camb). **2004**. 1: 16–17.
80. Villa CH, Dao T, Ahearn I, et al. Single-walled carbon nanotubes deliver peptide antigen into dendritic cells and enhance IgG responses to tumor-associated antigens. *ACS Nano*. **2011**. 5(7): 5300–5311.
81. Manna SK, Sarkar S, Barr J, et al. Single-walled carbon nanotube induces oxidative stress and activates nuclear transcription factor-kappaB in human keratinocytes. *Nano Lett*. **2005**. 5(9): 1676–1684.
82. Ravichandran P, Baluchamy S, Sadanandan B, et al. Multiwalled carbon nanotubes activate NF-kappaB and AP-1 signaling pathways to induce apoptosis in rat lung epithelial cells. *Apoptosis*. **2010**. 15(12): 1507–1516.
83. Cui D, Tian F, Ozkan CS, Wang M, Gao H. Effect of single wall carbon nanotubes on human HEK293 cells. *Toxicol. Lett.* 2005. 155(1): 73–85.
84. Wang H, Wang J, Deng X, et al. Biodistribution of carbon single-wall carbon nanotubes in mice. *J. Nanosci. Nanotechnol*. **2004**. 4(8): 1019–1024.
85. Lam CW, James JT, McCluskey R, Arepalli S, Hunter RL. A review of carbon nanotube toxicity and assessment of potential occupational and environmental health risks. *Crit. Rev. Toxicol*. **2006**. 36(3): 189–217.
86. Nel A, Xia T, Mädler L, Li N. Toxic potential of materials at the nanolevel. *Science*. **2006**. 311(5761): 622–627.
87. Fenniri H, Mathivanan P, Vidale KL, et al. Helical rosette nanotubes: design, self-assembly, and characterization. *J. Am. Chem. Soc*. **2001**. 123(16): 3854–3855.
88. Mascal M, Hext NM, Warmuth R, Moore MH, and Turkenburg JP. Programming a Hydrogen-Bonding Code for the Specific Generation of a Supermacrocycle. *Angew. Chem. Int. Ed. Engl*. **1996**. 108(19), 2203-2206.
89. Marsh A, Silvestri M, and Lehn J-M. Self-complementary hydrogen bonding heterocycles designed for the enforced self-assembly into supramolecular macrocycles. *Chem. Commun*. **1996**. 1527-1528.

90. Fenniri H, Deng BL, Ribbe AE. Helical rosette nanotubes with tunable chiroptical properties. *J. Am. Chem. Soc*. **2002**. 124(37):11064–11072.
91. Moralez JG, Raez J, Yamazaki T, Motkuri RK, Kovalenko A, Fenniri H. Helical rosette nanotubes with tunable stability and hierarchy. J Am Chem Soc. 2005;127(23):8307–8309.
92. Fenniri H, Deng BL, Ribbe AE, Hallenga K, Jacob J, Thiyagarajan P. Entropically driven self-assembly of multichannel rosette nanotubes. *Proc. Natl. Acad. Sci. U S A*. **2002**. 99(2):6487–6492.
93. Borzsonyi G, Johnson RS, Myles AJ, Cho JY, Yamazaki T, Beingessner RL, Kovalenko A, Fenniri H. Rosette nanotubes with 1.4 nm inner diameter from a tricyclic variant of the Lehn-Mascal G∧C base. *Chem. Commun. (Camb)*. **2010**. 46(35): 6527-9.
94. Borzsonyi G, Alsbaiee A, Beingessner RL, Fenniri H. Synthesis of a tetracyclic G∧C scaffold for the assembly of rosette nanotubes with 1.7 nm inner diameter. *J. Org. Chem*. **2010**. 75(21): 7233-9.
95. Chun AL, Moralez JG, Webster TJ, Fenniri H. Helical rosette nanotubes: a more effective orthopaedic implant material. *Nanotechnology*. **2004**. 15: S234–S239.
96. Zhou HY, Ohnuma Y, Takita H, Fujisawa R, Mizuno M, Kuboki Y. Effects of a bone lysine-rich 18 kDa protein on osteoblast-like MC3T3-E1 cells. *Biochem. Biophys. Res. Commun.* **1992**. 186(3): 1288-93.
97. Zhang L, Rodriguez J, Raez J, Myles AJ, Fenniri H, Webster TJ. Biologically inspired rosette nanotubes and nanocrystalline hydroxyapatite hydrogel nanocomposites as improved bone substitutes. *Nanotechnology*. **2009**. 20(17): 175101.
98. Chen Y, Webster TJ. Increased osteoblast functions in the presence of BMP-7 short peptides for nanostructured biomaterial applications. *J. Biomed. Mater. Res. A*. **2009**. 91(1): 296-304.
99. Journeay WS, Suri SS, Moralez JG, Fenniri H, Singh B. Macrophage Inflammatory Response to Self-Assembling Rosette Nanotubes. *Small*. **2009**. 5(12): 1446-52.

100. Rich EA, Panuska JR, Wallis RS, Wolf CB, Leonard ML, Ellner JJ. Dyscoordinate expression of tumor necrosis factor-alpha by human blood monocytes and alveolar macrophages. *Am. Rev. Respir. Dis*. **1989**. 139: 1010–1016.

101. Driscoll KE. TNF-α and MIP-2: role in particle-induced inflammation and regulation by oxidative stress. *Toxicol. Lett*. **2000**. 112–113: 177–183.

102. Driscoll KE, Carter JM, Hassenbein DG, Howard B. Cytokines and particle-induced inflammatory cell recruitment. *Environ. Health Perspect.* **1997**. 105: 1159–1164.

103. Journeay WS, Janardhan KS, Singh B. Expression and function of endothelial monocyte-activating polypeptide-II in acute lung inflammation. *Inflamm. Res*. **2007**. 56: 175–181.

104. Kao J, Houck K, Fan Y, Haehnel I, Libutti SK, Kayton ML, Grikscheit T, Chabot J, Nowygrod R, Greenberg S, Kuang WJ, Leung DW, Hayward JR, Kisiel W, Heath M, Brett J, Stern DM. Characterization of a novel tumor-derived cytokine. Endothelial-monocyte activating polypeptide II. *J. Biol. Chem*. **1994**. 269: 25106–25119.

105. Kao J, Ryan J, Brett J, Chen J, Shen H, Fan Y, Godman G, Familletti PC, F. Wang, Pan YCE, Stern D, Clauss M. Endothelial monocyte-activating polypeptide II. A novel tumor-derived polypeptide that activates host-response mechanisms. *J. Biol. Chem*. **1992**. 267: 20239–20247.

106. Goodman RB, Pugin J, Lee JS, Matthay MA. Cytokine-mediated inflammation in acute lung injury. *Cytokine & Growth Factor Rev*. **2003**. 14: 523–535.

107. Kobayashi Y. Neutrophil infiltration and chemokines. *Crit. Rev*. *Immunol*. **2006**. 26: 307–316.

108. Suri SS, Mills S, Aulakh GK, Rakotondradany F, Fenniri H, Singh B. RGD-tagged helical rosette nanotubes aggravate acute lipopolysaccharide-induced lung inflammation. *Int. J. Nanomedicine*. **2011**. 6: 3113-23.

109. Journeay WS, Suri SS, Moralez JG, Fenniri H, Singh B. Rosette nanotubes show low acute pulmonary toxicity in vivo. *Int. J. Nanomedicine*. **2008**. 3(3): 373–383.

110. Suri SS, Rakotondradany F, Myles AJ, Fenniri H, Singh B. The role of RGD-tagged helical rosette nanotubes in the induction of inflammation and apoptosis in human lung adenocarcinoma cells through the P38 MAPK pathway. *Biomaterials*. **2009**. 30(17): 3084–3090.

111. Le MH, Suri SS, Rakotondradany F, Fenniri H, Singh B. Rosette nanotubes inhibit bovine neutrophil chemotaxis. *Vet. Res*. **2010**. 41(5): 75.

112. Lozano R, Naghavi M, Foreman K, et al. Global and regional mortality from 235 causes of death for 20 age groups in 1990 and 2010: a systematic analysis for the Global Burden of Disease Study 2010. *Lancet*. **2012.** 380: 2095–128.

113. UNAIDS. UNAIDS report on the global AIDS epidemic 2012. http://www.unaids.org/en/media/unaids/contentassets/documents/epidemiology/2012/gr2012/20121120_ UNAIDS_Global_Report_2012_en.pdf (accessed March 6, 2013).

114. Thali M, Moore JP, Furman C, Charles M, Ho DD, Robinson J, Sodroski J. Characterization of conserved human immunodeficiency virus type 1 gp120 neutralization epitopes exposed upon gp120- CD4 binding. *J. Virol.* **1993**. 67: 3978–3988.

115. Chan DC, Kim PS. HIV entry and its inhibition. *Cell.* **1998**. 93:681–684.

116. Kwong PD, Wyatt R, Robinson J, Sweet RW, Sodroski J, Hendrickson WA. Structure of an HIV gp120 envelope glycoprotein in complex with the CD4 receptor and a neutralizing human antibody. *Nature.* **1998**. 393: 648–659.

117. Parren PWHI, Moore JP, Burton DR, Sattentau QJ. The neutralizing antibody response to HIV-1: viral evasion and escape from humoral immunity. *AIDS.* **1999**. (suppl A): S137-S162

118. Sattentau QJ, Moore JP. Conformational changes induced in the human immunodeficiency virus envelope glycoprotein by soluble CD4 binding. *J. Exp. Med*. **1991**. 174:407–415.

119. Sattentau QJ, Moore JP, Vignaux F, Traincard F, Poignard P. Conformational changes induced in the envelope glycoproteins of the human and simian immunodeficiency viruses by soluble receptor binding. *J. Virol.* **1993**. 67: 7383–7393.

120. Munier CM, Andersen CR, Kelleher AD. HIV vaccines: progress to date. *Drugs*. **2011**. 5;71(4): 387-414

121. Cohen J. AIDS vaccine trial produces disappointment and confusion. *Science*. **2003**. 299: 1290–1291.

122. Cohen J. Jitters jeopardize AIDS vaccine trials. *Science.* **1993**. 262:980–981.

123. Burton DR, Pyati J, Koduri R, Sharp SJ, Thornton GB, Parren PWHI, Sawyer LS, Hendry RM, Dunlop N, Nara PL. Efficient neutralization of primary isolates of HIV-1 by a recombinant human monoclonal antibody. *Science.* **1994**. 266: 1024–1027.

124. Roben P, Moore JP, Thali M, Sodroski J, Barbas CF, Burton DR. Recognition properties of a panel of human recombinant Fab fragments to the CD4 binding site of gp120 that show differing abilities to neutralize human immunodeficiency virus type 1. *J. Virol.* **1994**. 68:4821–4828.

125. Mo H, Stamatatos L, Ip JE, Barbas CF, Parren PW, Burton DR, Moore JP, Ho DD. Human immunodeficiency virus type mutants that escape neutralization by human monoclonal antibody IgG1b12. *J. Virol.* **1997**. 71: 6869–6874.

126. Muster T, Steindl F, Purtscher M, Trkola A, Klima A, Himmler G, Ruker F, Katinger H. A conserved neutralizing epitope on gp41 of human immunodeficiency virus type 1. *J. Virol.* **1993**. 67:6642–6647.

127. Muster T, Guinea R, Trkola A, Purtscher M, Klima A, Steindl F, Palese P, Katinger H. Cross-neutralizing activity against divergent human

immunodeficiency virus type 1 isolates induced by the gp41 sequence ELDKWAS. *J. Virol.* **1994**. 68: 4031–4034.

128. Sattentau QJ, Moore JP. Human immunodeficiency virus type neutralization is determined by epitope exposure on the gp120 oligomer. *J. Exp. Med.* **1995**. 182: 185–196.

129. Conley AJ, Kessler JA, Boots LJ, Tung JS, Arnold BA, Keller PM, Shaw AR, Emini EA. Neutralization of divergent human immunodeficiency virus type 1 variants and primary isolates by IAM-41-2F5, an anti-gp41 human monoclonal antibody. *Proc. Natl. Acad. Sci U. S. A.* **1994**. 91: 3348–3352.

130. Burton DR. A vaccine for HIV type 1: the antibody perspective. *Proc. Natl. Acad. Sci U. S. A.* **1997**. 94: 10018–10023.

131. Alfsen A, Bomsel M. HIV-1 gp41 envelope residues 650-685 exposed on native virus act as a lectin to bind epithelial cell galactosyl ceramide. *J. Biol. Chem*. **2002**. 277: 25649-25659.

132. D'Souza SE, Ginsberg MH, Plow EF. Arginyl-glycyl-aspartic acid (RGD): a cell adhesion motif. *Trends Biochem. Sci*. **1991**. 16(7): 246-50.

Chapter 2

Synthesis and Self-assembly of Bio-peptides functionalized with Twin G∧C

2.1. Introduction

A number of peptides have been known for their physiological and biochemical roles in various aspects of life. Apart from their contribution in hormones and in receptor-mediator signal transduction modulators, peptides also play a vital role in cell-cell communication, immunological processes and neurotransmission in central and peripheral nervous system.[1-3] Peptides have also been involved in cardiovascular system and several metabolic processes. The development of therapeutics for various diseases has been based on bioactive peptides. While peptide-based drugs administrated through oral, intravenous or subcutaneous route are often ineffective due to proteolytic degradation, their nasal administration can however, be effective. The chemical modification of a peptide sequence can lead to an increase in its activity and stability inside a biological system, thereby improving its sensitivity to recognize and bind to its receptors.[4]

Due to the limitations in the isolation of peptides from natural sources, synthetic peptide chemistry has gained importance in life science and medical research. For instance, synthetic peptides can act as antigens or antigenic determinant to generate antibodies against them in an animal model.[5,6] Synthetic peptides have also been prepared to study the enzymatic or signalling pathways in the cell by acting as enzyme substrates or enzyme inhibitors.[7] Effective agonists and antagonists of endogenous peptides can be developed by structural modification of the bioactive peptides. The evolution in the synthesis of peptide analogues with varying sequences resulted in the study of structure-activity relationships.[7,8] While in the beginning of twentieth century, Theodor Curtius and Emil Fischer laid the foundation for the first peptide synthesis, the chemical peptide synthesis became popular for research purposes only in the last four decades[4] due to the increased sensitivity of analytical methods and development of isolation and purification techniques. The peptide hormone oxytocin was first chemically synthesized by the Nobel laureate V. du Vigneaud[9] and an analogue of oxytocin was prepared by replacing the glutamine moiety at position four with threonine. The modified

peptide exhibited an improvement in biological activity compared to the naturally occurring peptide hormone.[4]

Since the beginning of the era of peptide chemistry, large-scale synthesis has been mainly carried out in the conventional solution-phase. Although, the traditional solution-phase peptide synthesis resulted in highly pure final products, it was labor-intensive and a major focus had to be placed on choosing the right solvent and protecting groups for optimal yields.[10] Peptide synthesis became extremely popular for research with the advent of peptide synthesis on a solid support, also known as solid-phase peptide synthesis (SPPS), which was developed by Nobel prize winner Robert Bruce Merrifield in 1963.[11]

Rosette nanotubes (RNTs) are self-assembled nanostructures, comprised of hybrid DNA analogues guanine-cytosine (G∧C) motifs. Since RNTs can mimic the biological molecules and their functionality (DNA), they have been considered to be biocompatible and cytocompatible.[12,13] The G∧C motifs have previously been functionalized with several bioactive peptides (like KRSR, RGDSK) that can readily self-assemble in an aqueous environment to form RNTs and have been utilized for their biological applications.[14,15]

This chapter will focus on the synthesis of three RNTs derivatives, functionalized with the biologically active peptides, namely ELDKWAK, RGDSK and DRGSK. The peptide sequence glutamic acid-leucine-aspartic acid-lysine-tryptophan-alanine (ELDKWA) is the linear epitope present on the glycoprotein (gp) 41 of the HIV-1 envelope.[16] The sequence RGD (arginine-glycine-aspartic acid) mediates intercellular adhesion by aiding the binding to the integrin receptors on the cell surface.[4] The peptide DRG (aspartic acid-arginine-glycine) is the scrambled version of the RGD sequence and was synthesized for the control studies. Fmoc-based SPPS was used to synthesize the peptides and couple them to twin a G∧C motif (Figure 2-1). The twin G∧C base pairs form a hexameric structure known as rosette, held together by 36 hydrogen bonds as shown in

Figure 2-2. The rosettes can self-assemble in water or organic solvents to form rosette nanotubes (RNTs).[17]

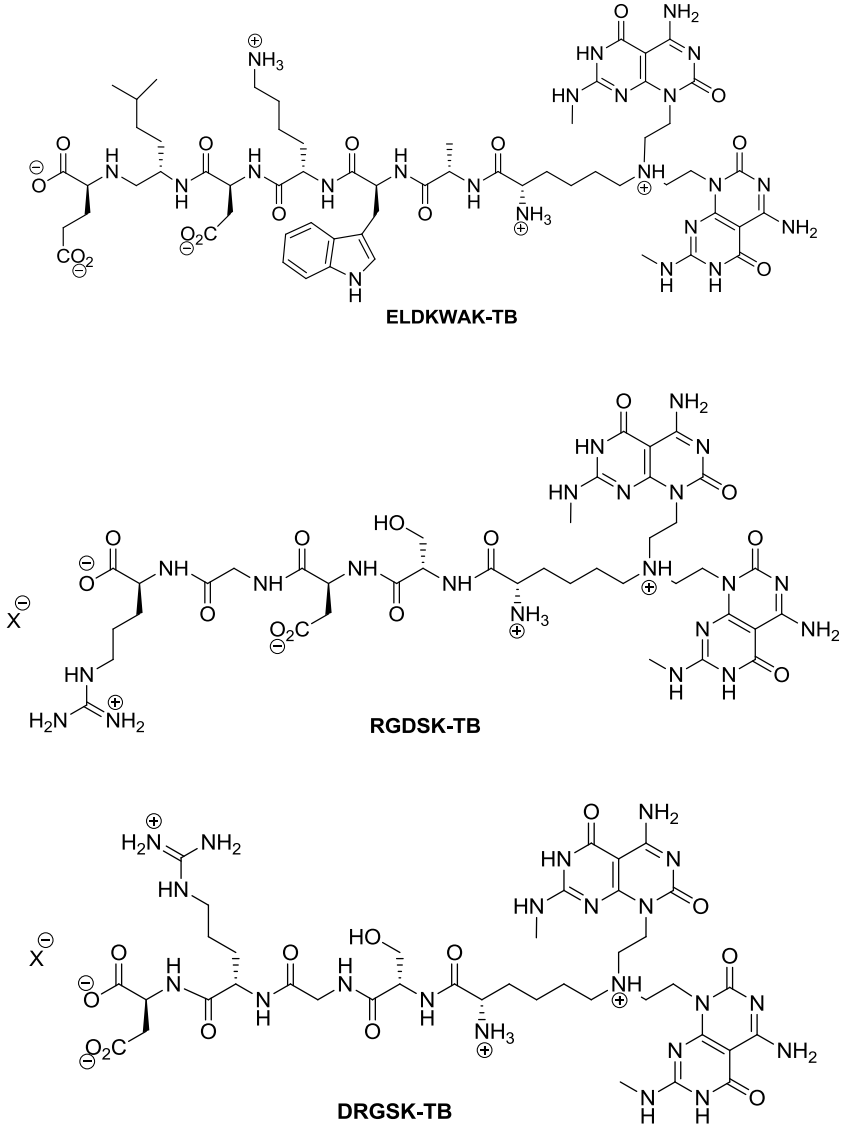

Figure 2-1: Structures of ELDKWAK, RGDSK and DRGSK coupled to twin G∧C bases (ELDKWAK-TB, RGDSK-TB and DRGSK-TB, respectively).

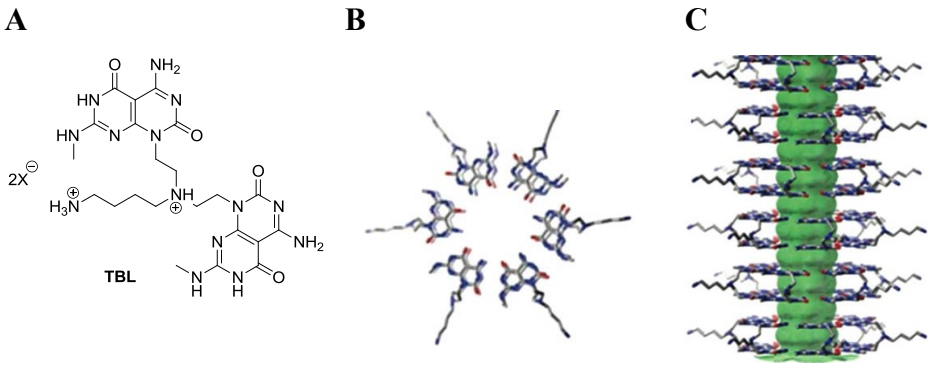

Figure 2-2: (A) Twin G∧C monomer with an aminobutyl group (TBL), (B) formation of six-membered rosette and (C) formation of rosette nanotubes (RNTs).[17]

2.2. Solid-phase peptide synthesis (SPPS)

The target molecules were synthesized using the standard Fmoc-based SPPS. The first amino acid protected with Fmoc at the N-terminus and side chains protected with *t*-Bu group was coupled to the solid phase, Wang resin by undergoing an overnight esterification reaction. The resins were washed after each step with *N,N*-dimethylformamide (DMF), methanol (MeOH) and dichloromethane (DCM). The free hydroxyl groups were capped with a mixture of acetic anhydride and pyridine and the degree of substitution of the hydroxyl groups on the Wang resin by the first amino acid was quantified using UV-Vis spectroscopic analysis at 301 nm. The Fmoc group on the N-terminus was deprotected under basic conditions and the subsequent Fmoc protected amino acids were coupled in a similar fashion. The completion of the coupling reaction was confirmed by the Kaiser test.[18] After the completion of the elongation of the peptide, the Boc-protected G∧C base aldehyde was coupled to the last amino acid via reductive amination. Trifluoroacetic acid (TFA) was used to remove all the protecting groups and release the desired peptide functionalized twin G∧C building blocks from the resin.

2.3. Results and Discussion

2.3.1. ELDKWAK-TB

The development of a therapeutic drug and vaccine to prevent infection and transmittance of HIV-1 has been a major quest for the past three decades. A lot of research has been done on the subunit recombinant gp 120 as the immunogen for HIV-1; but it had some limitations of not being virus neutralizing after vaccination with gp 120 or being in low titres and the antibody response was stimulated only after infection with HIV-1.[19] As such, a new strategy of epitope-vaccine based on the principle neutralizing determinants have been suggested by many scientists to fight HIV-1 infection.[20-22]

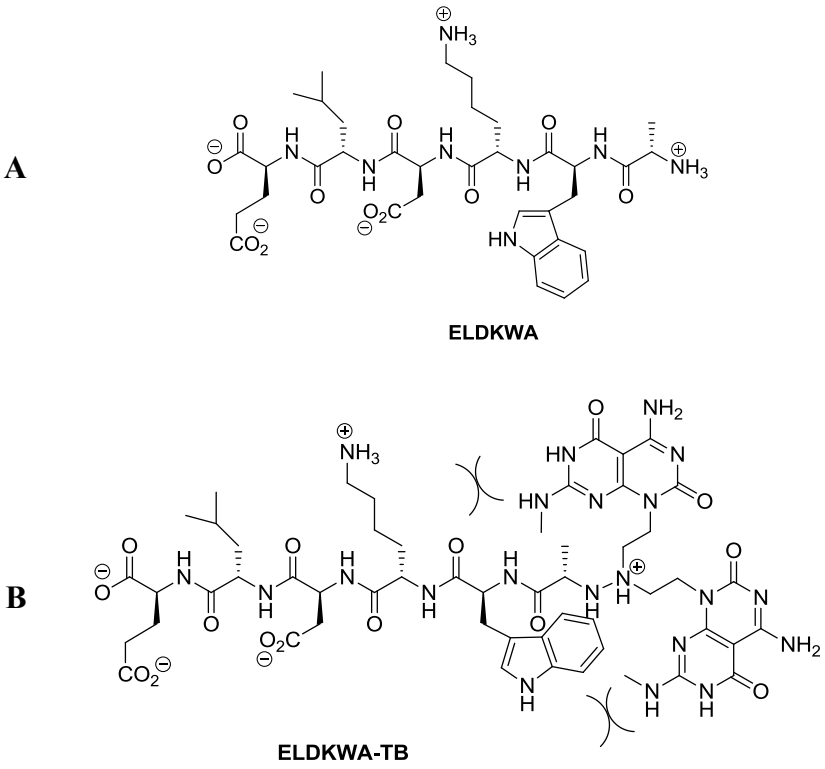

Figure 2-3: (A) Structure of HIV-1 linear epitope ELDKWA and (B) twin G∧C motif functionalized with ELDKWA showing the possible steric effects, which can hinder the successful coupling.

In this chapter, we developed RNTs as a new nanocarrier for the HIV-1 antigen by functionalizing the RNTs with the peptide ELDKWA (sequences 662-667) that is an epitope present on the ectodomain of gp 41 of HIV-1 envelope.[23]

An initial attempt was made to synthesize a twin G∧C monomer functionalized with HIV-1 epitope ELDKWA, by coupling the resin bound peptide to a G∧C base aldehyde via a reductive amination reaction of the amino group of alanine with the aldehyde functional group of the G∧C. However, this coupling reaction was not successful, most likely due to the steric effects between alanine fragment and ring structure of tryptophan in the peptide ELDKWA and the G∧C base pair (Figure 2-3). As such a lysine residue was incorporated in the peptide sequence and twin G∧C base pairs, which could act as a spacer between the ring structure of the peptide and G∧C base pairs. This was achieved by coupling the alanine residue to the ε-amino group of lysine.

2.3.2. Synthesis of ELDKWAK-TB

ELDKWAK-TB was synthesized as in Figure 2-4 using Wang Resin as the solid support and the standard Fmoc protection SPPS strategy. The first amino acid arginine was attached to the resin with the addition of Fmoc-Glu(O*t*-Bu)-OH, (**2.2)** to Wang resin **(2.1)** that led to an esterification reaction between the hydroxyl groups on the resin and carboxyl group of Fmoc-Glu(O*t*-Bu)-OH. Then, a mixture of acetic anhydride and pyridine was added to allow capping of the free hydroxyl groups on the resin. The degree of substitution of the first amino acid on the resin was determined by the spectroscopic quantification of the fulvene-piperidine adduct at 301 nm. The Fmoc group of arginine resins was deprotected using a solution of piperidine in DMF. The resulting free amino group was then coupled to Fmoc-Leu-OH (**2.4**) The Fmoc groups were removed from the dipeptide (**2.5**) under basic conditions and the free amino group of the leucine residue was coupled to Fmoc-Asp(O*t*-Bu)-OH (**2.6**). Deprotection of the Fmoc group from the tripeptide **2.7**, followed by the coupling of Fmoc-Lys(Boc)-OH (**2.8**) resulted in the tetrapeptide **2.9**. After the Fmoc deprotection of the Fmoc-

Lys(Boc)-OH, reaction with the fifth amino acid Fmoc-Trp(Boc)-OH (**2.10**) resulted in the pentapeptide **2.11**.

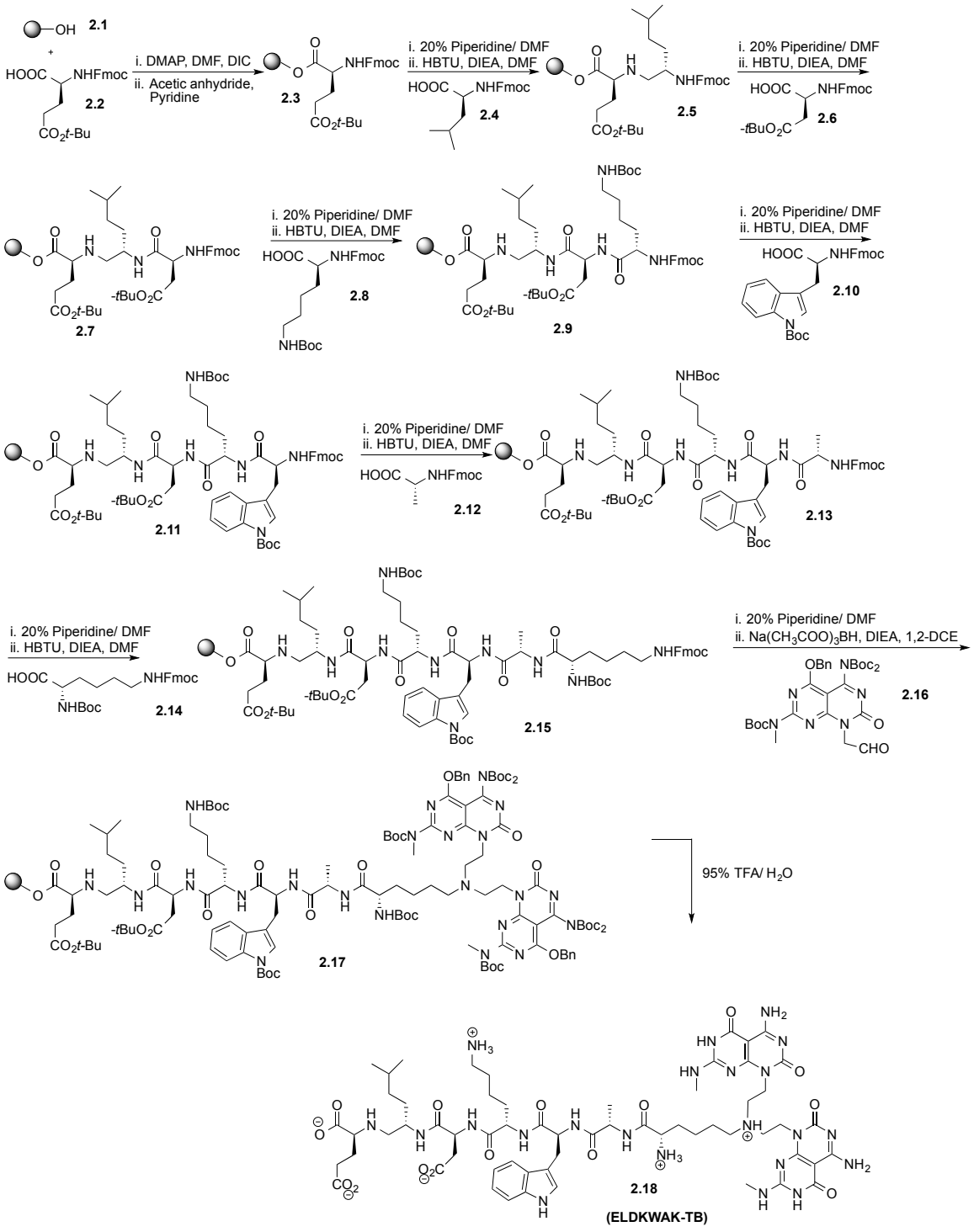

Figure 2-4: Synthetic scheme for the synthesis of ELDKWAK-TB

Fmoc-Ala-OH (**2.12**) was coupled after the removal of Fmoc group from the pentapeptide **2.11** to afford **2.13**. After subjecting the hexapeptide **2.13** to Fmoc deprotection, the last amino acid Boc-Lys(Fmoc)-OH (**2.14**) was added to give the desired compound **2.15** with a terminal Fmoc group. The protected G∧C base aldehyde (**2.16**) was then coupled to Wang resin bound peptide ELDKWAK to give twin G∧C base ELDKWAK (ELDKWAK-TB) via reductive amination reaction. Treatment of the resulting resin with TFA led to the removal of protecting groups and cleavage from the resin to produce the TFA salt of ELDKWAK-TB (**2.18**).

2.3.3. Characterization and self-assembly of ELDKWAK-TB

ELDKWAK-TB was characterized by mass spectrometry, NMR and elemental analysis to confirm the successful synthesis of the desired compound. In order to study the biological properties of ELDKWAK-TB, it was important that the latter self-assembled in aqueous conditions.

This was achieved by preparing the stock solution ELDKWAK-TB (1 mg/mL) in water and studying the self-assembly and morphology using scanning electron microscopy (SEM) imaging.[28] A wide range of different conditions (temperature, sonication times and aging) was used to stimulate and optimize the appropriate conditions for the self-assembly of ELDKWAK-TB. The images in Figure 2-5 suggest that ELDKWAK-TB formed very short RNTs immediately after repeated sonication and heating. However, these nanotubes aggregated after 1 hour to form large aggregates. We attempted to do transmission electron microscopy (TEM) of ELDKWAK-TB to get the average diameter. The TEM imaging did not show single RNTs because of aggregation, the average diameter was calculated to be approximately 4.9 $\pm$ 0.3 nm. This indicated that the outer diameter of the RNTs increased from 3.5 nm (RNTs without functionalization) to 4.9 nm with the hepta-peptide functionalization of the RNTs.

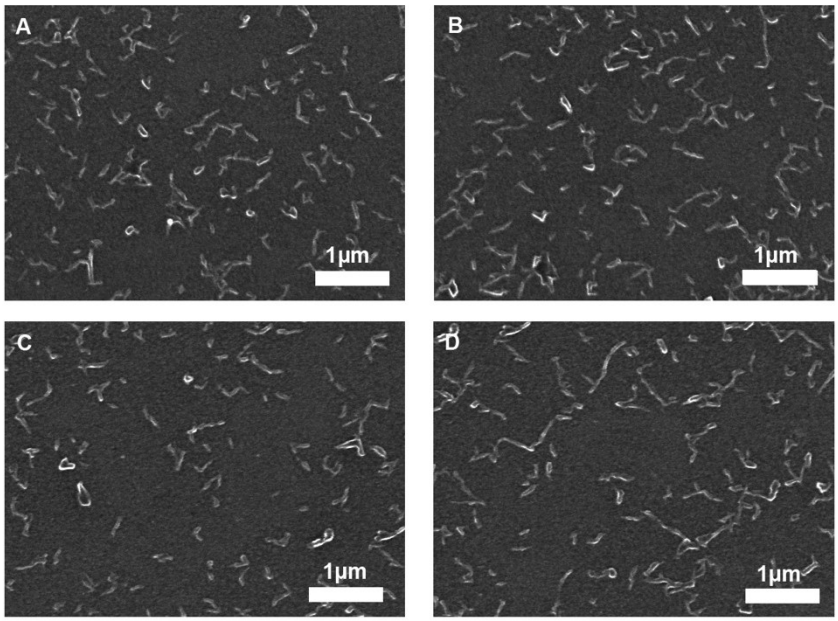

Figure 2-5: SEM images of ELDKWAK-TB RNTs in water (0.102 mM, at 10 min).

2.3.4. RGDSK-TB

The cell adhesion sequence RGD (arginine-glycine-aspartic acid), discovered in 1984, is the attachment site for many adhesive proteins and peptides.[24,25] RGD being the smallest active peptide can mimic a number of adhesive peptides to bind more than one integrin receptors on the cell surface.[26] The α-subunits of the RGD-binding integrins (α_5, α_8, α_V and α_{IIb}) belong to a subfamily of integrins as they resemble in their sequences as compared to non-RGD-binding receptors.[27]

A compound comprised of the peptide sequence RGDSK functionalized with one G∧C unit and twin G∧C moiety had previously been prepared by our group.[29] The RGDSK mono and twin G∧C RNTs have been used for studying osteoblast-integrin adhesion and ortheopedic applications.[29,30] The fragment SK (serine-lysine) acts as a spacer between the RGD sequence and the G∧C motifs.

2.3.5. Synthesis of RGDSK-TB

In the SPPS strategy of RGDSK-TB [25] (Figure 2-6), the first amino acid arginine Fmoc-Arg(Pbf)-OH (**2.19**) was conjugated to the Wang resin (**2.1**). The acetic

anhydride and pyridine mixture was then added in order to cap the free hydroxyl groups. The degree of substitution was determined on the resin by the spectroscopic quantification of fulvene-piperidine adduct at 301 nm.

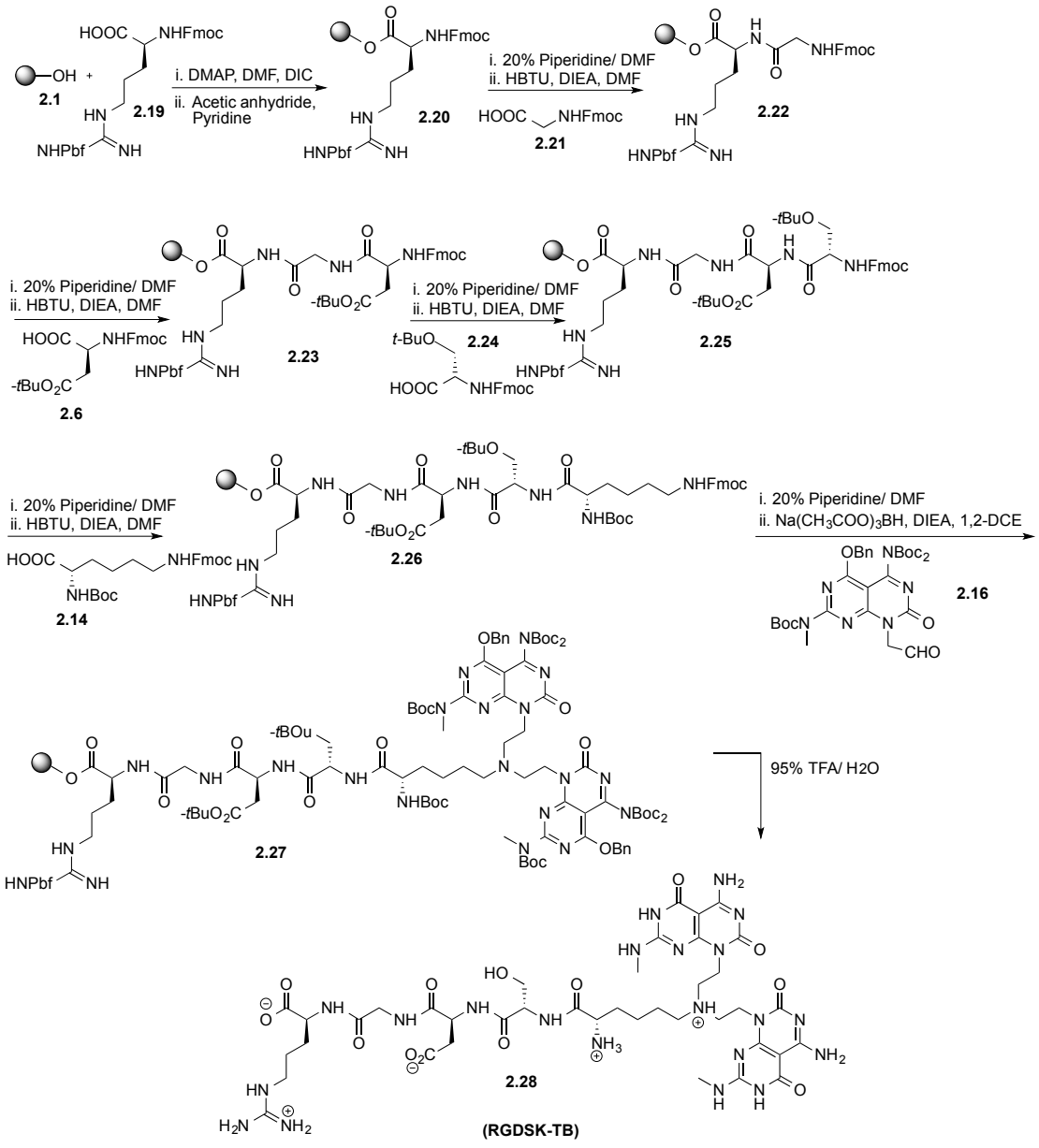

Figure 2-6: Synthetic scheme for the synthesis of RGDSK-TB.

A solution of piperidine in DMF was added to the Wang resin for deprotecting the Fmoc group on the arginine. The free amino group was then coupled to Fmoc-Gly-OH (**2.21**), which resulted in the dipeptide **2.22**. The Fmoc group on glycine

was deprotected under basic conditions and the free amino group of glycine was coupled to Fmoc-Asp(O*t*-Bu)-OH (**2.6**) in the same way as Fmoc-Gly-OH. The resulting tripeptide **2.23**, was deprotected and coupled with Fmoc-Ser(*t*-Bu)-OH (**2.24**) to form the tetrapeptide **2.25**. The final amino acid Boc-Lys(Fmoc)-OH (**2.14**) was coupled to the Fmoc-deprotected amine group of the tetrapeptide **2.25** to produce the pentapeptide **2.26**. The synthesis of the peptide RGDSK resulted in fragmentation at RG, so the incubation time for deprotection of Fmoc groups was optimized.

The G∧C base aldehyde (**2.16**) was coupled to peptide **2.26** after removal of the final Fmoc group via a reductive amination reaction that resulted in the formation of compound **2.27**. The desired compound RGDSK-TB **(2.28)** was obtained upon deprotection and cleavage from the resin under acidic conditions.

2.3.6. Characterization and self-assembly of RGDSK-TB

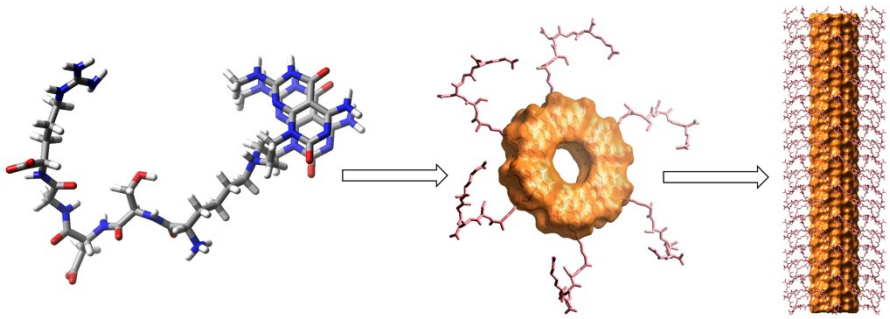

Figure 2-7: The predicted mode of self-assembly of RGDSK-TB.

The molecule RGDSK-TB was characterized using NMR spectroscopy, mass spectrometry and elemental analysis. Using molecular modeling study it was predicted that RGDSK-TB [31] would self-assemble independently by first forming the individual rosettes and then resulting in the formation of the RNTs (Figure 2-7) by stacking of the rosettes. SEM imaging was used to study the morphology of the nanostructures formed by RGDSK-TB. The images in Figure 2-8 illustrated that RGDSK-TB formed RNTs, which increased in length over time, as shown in Figure 2-9. It was found that the RGDSK-TB RNTs tend to aggregate when they were sonicated for longer time.

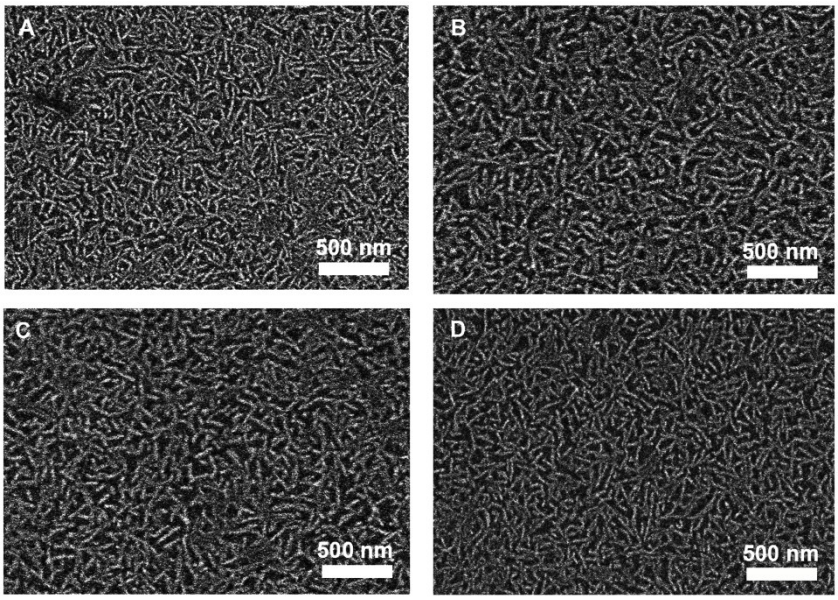

Figure 2-8: SEM images of RNTs formed by self-assembly of RGDSK-TB in water (0.113 mM, aged for 1 d).

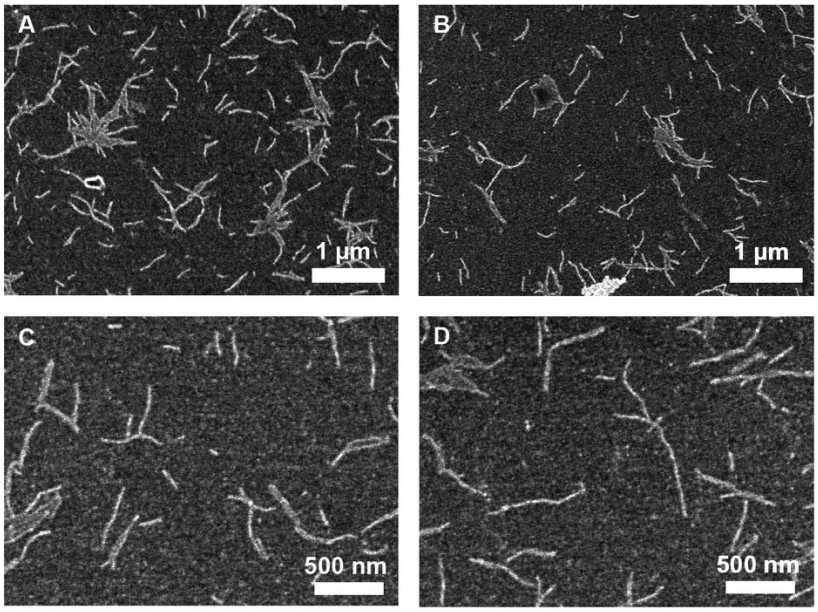

Figure 2-9: SEM images of RGDSK-TB in water (0.113 mM, aged for 4 d).

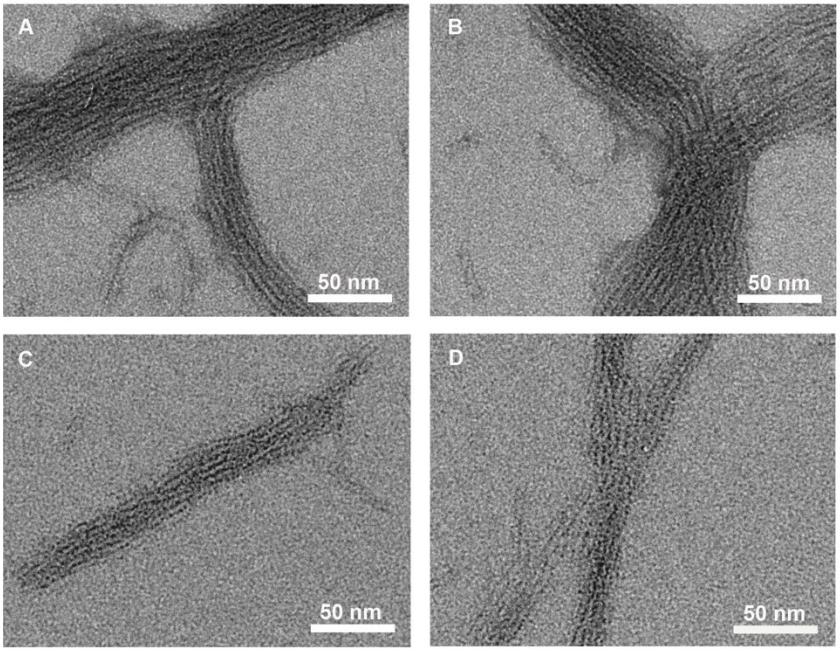

Figure 2-10: TEM images of RNTs formed by self-assembly of RGDSK-TB in water (0.113 mM, aged for 1 d).

TEM[28] was used to measure the diameter of the RNTs formed by RGDSK-TB. It was found that the RGDSK-TB RNTs have an average diameter of 4.3 $\pm$ 2.6 nm. The TEM images also confirmed the formation of nanostructures (Figure 2-10). The atomic force microscopy (AFM)[28] images (Figure 2-11) also revealed that RGDSK-TB formed nanotubular structures in a high aspect ratio.

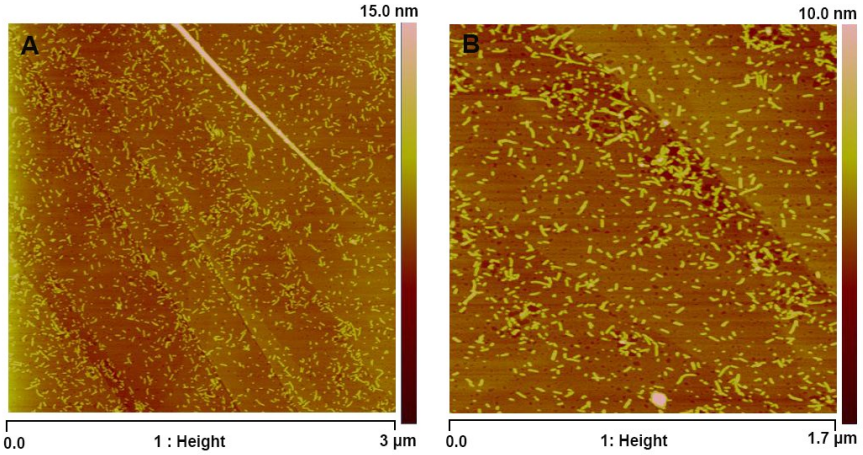

Figure 2-11: AFM images of RNTs formed by self-assembly of RGDSK-TB in water (0.113 mM, aged for 7 d) using HOPG substrate.

2.3.7. DRGSK-TB

A new twin G∧C motif (DRGSK-TB) containing peptide DRGSK was synthesized. The function of the scrambled version of RGD sequence, DRG (aspartic acid-arginine-glycine) was to act as the control for the RGD sequence for biological studies. The sequence SK was incorporated to DRG sequence as for RGD peptide prior to the G∧C coupling to act as a spacer between the peptide and the rings of twin G∧C bases.

2.3.8. Synthesis of DRGSK-TB

DRGSK-TB was synthesized by SPPS (Figure 2-12), whereby the first step involved the esterification of Fmoc-Asp(O*t*-Bu)-OH (**2.6**) to the Wang resin (**2.1**). Upon capping the remaining free hydroxyl groups on the resin, the degree of substitution of the first amino acid aspartic acid, was determined by the spectroscopic quantification of the fulvene-piperidine adduct at 301 nm.

Fmoc deprotection of the amino acids prior to each coupling reaction was carried out under basic conditions and the incubation time was optimized, as done for RGDSK-TB. The Wang resin supported with aspartic acid was coupled to the second amino acid Fmoc-Arg(Pbf)-OH (**2.19**), leading to the formation of the dipeptide **2.30**. This was followed by the third coupling reaction of the free amino group of the arginine residue with Fmoc-Gly-OH (**2.21**) resulting in the tripeptide **2.31**. The next two subsequent coupling reactions with Fmoc-Ser(*t*-Bu)-OH (**2.24**) and Boc-Lys(Fmoc)-OH (**2.14**), were carried out in the similar fashion as for RGDSK-TB that led to the formation of tetrapeptide **2.32** and pentapeptide **2.33**, respectively.

The G∧C base aldehyde (**2.16**) was coupled to the free amino group of the terminal lysine residues by a reductive amination reaction. The resulting product was finally deprotected to yield the DRGSK peptide functionalized twin G∧C motif **2.35** (DRGSK-TB).

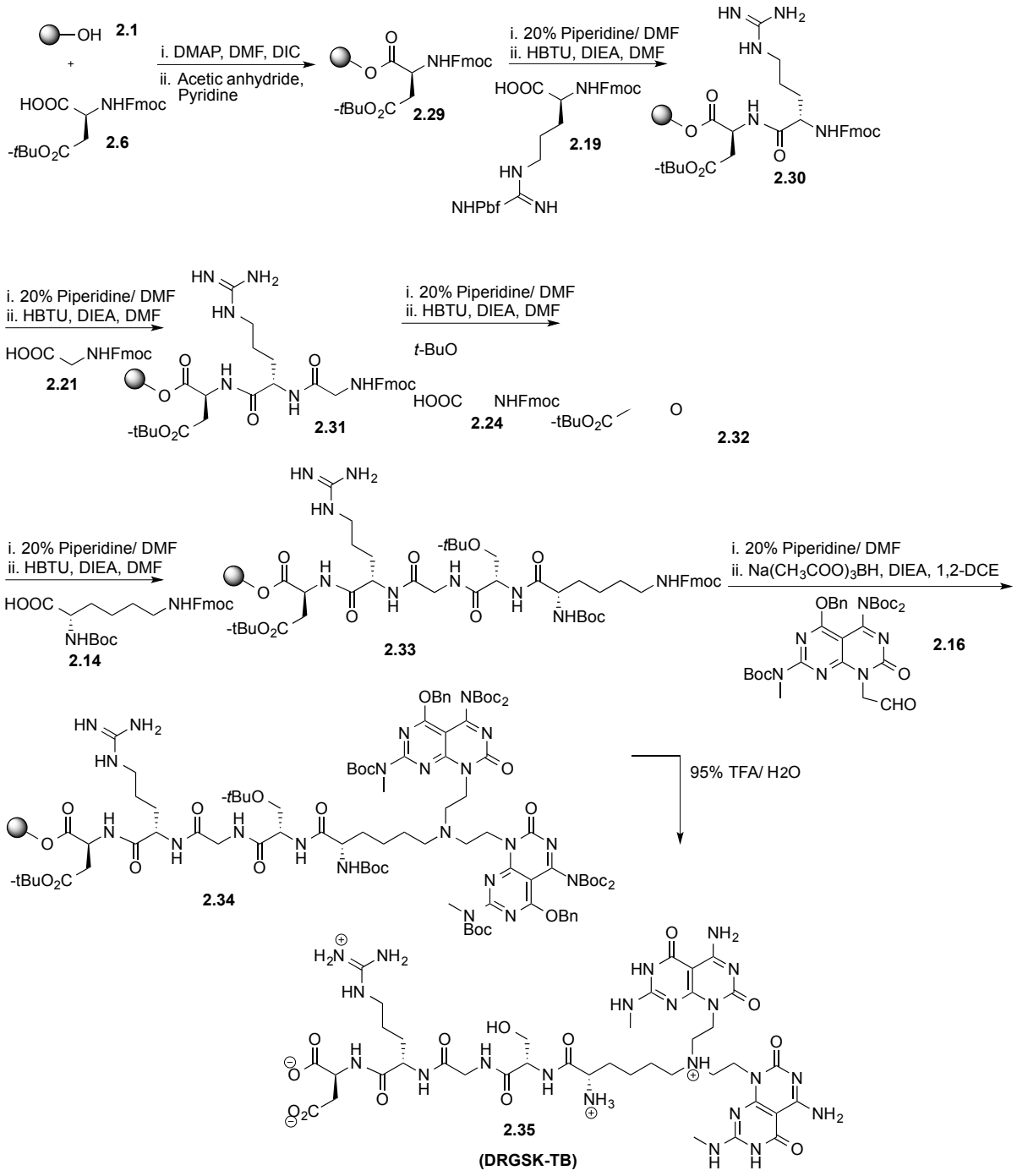

Figure 2-12: Synthetic scheme for the synthesis of DRGSK-TB.

2.3.9. Characterization and self-assembly of DRGSK-TB

NMR spectroscopy, mass spectrometry and elemental analysis were used to characterize and confirm the formation of DRGSK-TB.

The morphology of DRGSK-TB nanotubes was analyzed using SEM imaging (Figure 2-13). Various conditions for the self-assembly were tried and optimized as the compound DRGSK-TB had low solubility in water at high concentrations. The study indicated that DRGSK-TB required high heating conditions to form RNTs. Nanostructures were formed after aging the stock solution for 4 d.

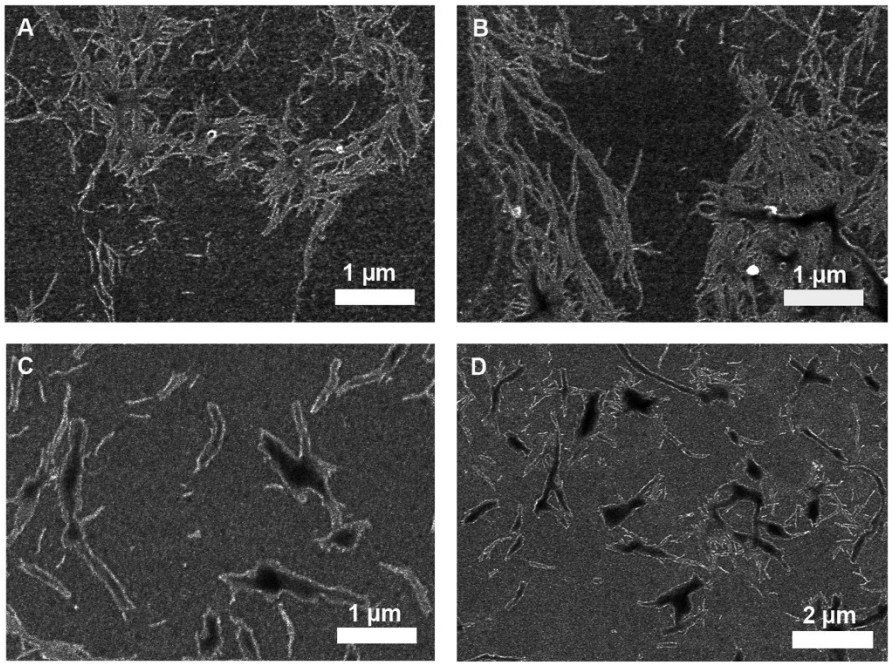

Figure 2-13: SEM images of RNTs formed by self-assembly of DRGSK-TB in water (0.144 mM, aged for 4 d).

The samples used for SEM were also used for TEM imaging (Figure 2-14) to also confirm the formation of nanotubular structures. The average diameter of the RNTs formed by DRGSK-TB was measured by TEM and was found to be 4.3 $\pm$ 0.2 nm. This value was comparable to value obtained for the diameter of the RGDSK-TB RNTs. The AFM imaging (Figure 2-15), however revealed a smaller diameter value than that obtained by TEM imaging. The AFM measurements can

lead to deformation and flattening of the RNTs upon the interaction of the soft nanomaterials (RNTs) with the AFM tip.[32]

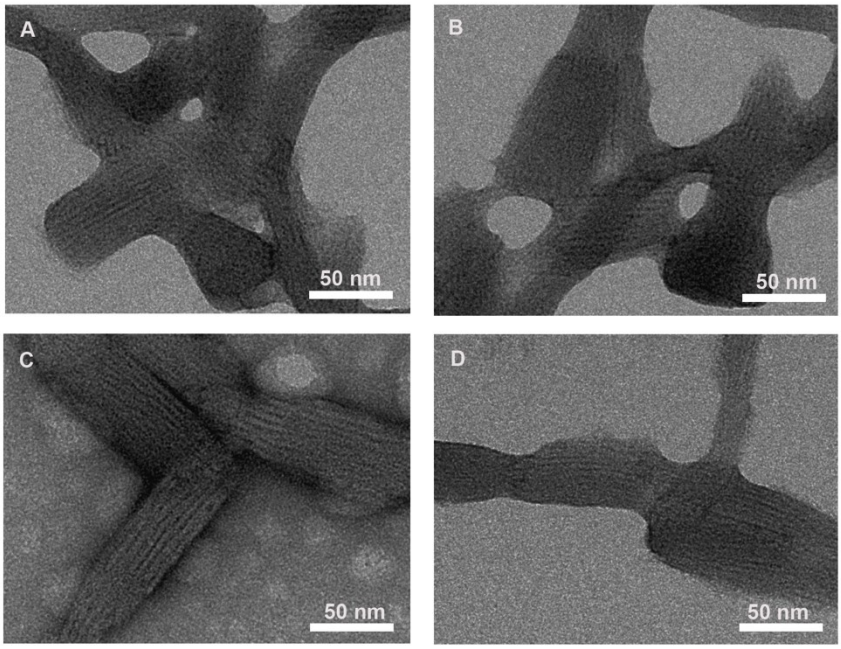

Figure 2-14: TEM images of RNTs formed by self-assembly of DRGSK-TB in water (0.144 mM, aged for 4 d).

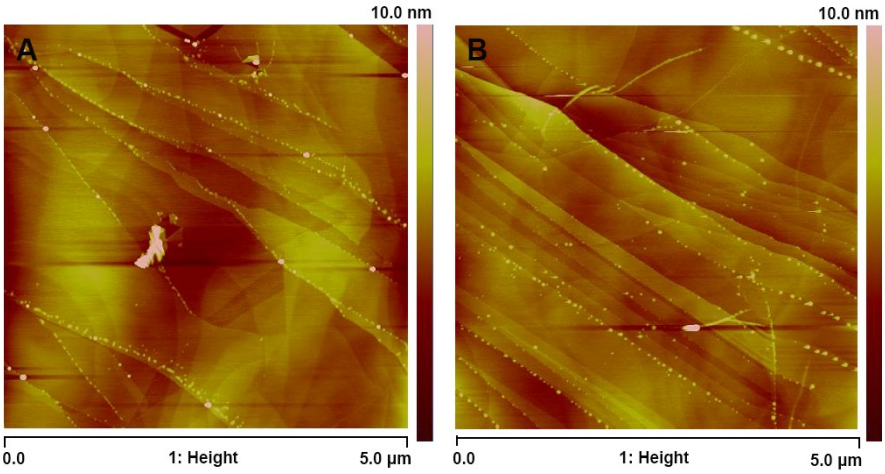

Figure 2-15: AFM images of RNTs formed by self-assembly of DRGSK-TB in water (0.144 mM, aged for 2 d) using HOPG substrate.

2.4. Conclusion

In this chapter, three twin G∧C motifs (ELDKWAK-TB, RGDSK-TB and DRGSK-TB), functionalized with bioactive peptides ELDKWAK, RGDSK and DRGSK were successfully synthesized using SPPS and characterized. These twin G∧C building blocks functionalized were self-assembled in water to form RNTs under different optimized conditions. The morphology of the RNTs was studied using SEM imaging and their average diameter was calculated using TEM measurements. The RNTs formed from the heptapeptide functionalized twin G∧C motif, ELDKWAK-TB, is a new nanocarrier that would act as a vehicle for carrying the HIV-1 antigen ELDKWA to the cells. This will be discussed in more detail in Chapter IV. The pentapeptide RGDSK functionalized twin G∧C (RGDSK-TB) RNTs would be used to study the effect of RGD sequence in promoting the binding and encapsulation of ELDKWAK-TB RNTs to the cells. DRGSK-TB (DRGSK functionalized with twin G∧C base) RNTs would be used as the control for RGDSK-TB in the biological studies.

2.5. Experimental Section

2.5.1. Materials

All materials for peptide synthesis namely, Wang resin, protected amino acids like Fmoc-Glu(O*t*-Bu)-OH, Fmoc-Leu-OH, Fmoc-Asp(O*t*-Bu)-OH, Fmoc-Lys(Boc)-OH, Fmoc-Trp(Boc)- OH, Fmoc-Ala-OH, Fmoc-Arg(Pbf)-OH, Fmoc-Gly-OH, Fmoc-Ser(*t*-Bu)-OH) and coupling agent 2-(1H-benzotriazol-1-yl)-1,1,3,3-tetramethyluronium hexafluorophosphate (HBTU) were purchased from NovaBiochem. Solvents for peptide synthesis and other reagents like diisopropylcarbodiimide (DIC), DMF, MeOH, DCM, piperidine, TFA, triisopropyl silane (TIS) and *N*-ethyl-*N*-isopropylpropan-2-amine (DIEA) were purchased from Sigma-Aldrich. DMF was distilled before use. All reactions were performed under an atmosphere of N_2, unless stated otherwise. Reagent grade DCM, MeOH and 1,2-dichloroethane (1,2-DCE) were purified on an MBraun solvent purification system. All other solvents and reagents were used without further purification. NMR spectra were in the specified deuterated solvents. The NMR data is presented as follows: chemical shift δ (ppm), multiplicity, coupling constant and integration. The following abbreviations were used to explain the multiplicities: s = singlet, d = doublet, t = triplet, m = multiplet, bs = broad singlet.

SEM and TEM carbon-coated 400-mesh grids were obtained from Electron Microscopy Sciences. Highly ordered pyrolytic graphite (HOPG) grids used for AFM imaging were obtained from MikroMasch USA, Inc. Uranyl acetate stain was also obtained from Electron Microscopy Sciences.

2.5.2. Synthesis of ELDKWAK-TB

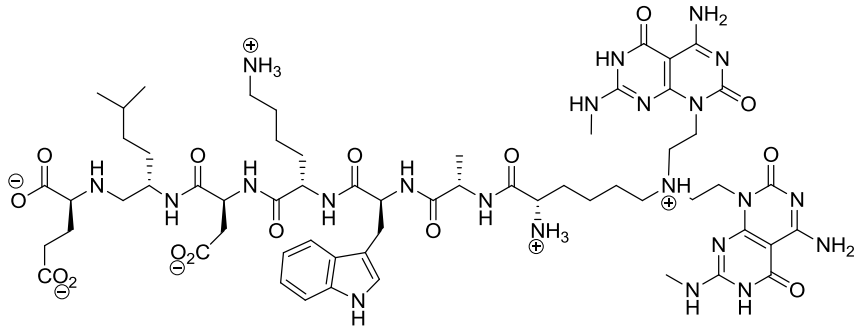

ELDKWAK-TB

DMF was added to Wang Resin (0.65 mmol/g, 500 mg, 0.325 mmol) in a 12 mL plastic syringe and was shaken for 20 min. After draining the solvent DMF, a mixture of Fmoc-Glu(O*t*-Bu)-OH (0.580 g, 1.365 mmol) and DMAP (0.033 g, 0.27 mmol) in DMF (3 mL) was added, and the reaction mixture was shaken for 1 h. DIC (211 μL, 1.365 mmol) was then added to the syringe and allowed to react overnight. The resin was filtered under vacuum and washed (4 x 10 mL) with DMF, MeOH and DCM. Then, the resin was treated with 50% acetic anhydride in pyridine in order to cap the free hydroxyl groups (2 x 5 min). DMF, MeOH and DCM (4 x 10 mL) were used to wash the resin. The latter was dried under vacuum, after which the degree of substitution of the hydroxyl groups on the resins was determined by the spectroscopic quantification of the fulvene-piperidine adduct at 301 nm. The UV-Vis spectra of two resin samples with mass 8.5 and 10.2 mg gave absorbance intensities of 0.333 and 0.367. A degree of substitution of 0.487 mmol/g was obtained, that corresponded to a yield of 75%.

$$\text{Degree of substitution} = \frac{101 \times \text{Absorbance at 301 nm}}{7.8 \times \text{mass of resin (mg)}}$$

The Wang resin substituted by glutamic acid derivative was treated with a solution of 20% piperidine in DMF (5 mL, 1 x 2 min, 1 x 10 min) to remove the Fmoc group. The resin with the glutamic acid residue was washed with DMF, MeOH and DCM (4x 10 mL). A mixture of Fmoc-Leu-OH (0.344 g, 0.973 mmol), HBTU (0.351 g, 0.925 mmol) and DIEA (338.4 μL, 1.946 mmol) in DMF

(2.5 mL) was added to the syringe. The reaction mixture was shaken for 3 h. After coupling, the resin was washed with DMF, MeOH and DCM (4 x 10 mL) and dried under vacuum. The yellow colour of the resin in the Kaiser test confirmed the completion of the amide coupling reaction.

The Fmoc group of leucine was deprotected from the resin bound dipeptide **(2.5)** using 20% piperidine in DMF (5 mL, 1 x 2 min, 1 x 10 min). The resin was washed with DMF, MeOH and DCM (4 x 10 mL) prior to coupling with the third amino acid. A mixture of Fmoc-Asp(O*t*-Bu)-OH (0.401 g, 0.973 mmol), HBTU (0.351 g, 0.925 mmol) and DIEA (338.4 μL, 1.946 mmol) in DMF (2.5 mL) was added to the syringe and the reaction mixture was shaken for 3 h. The resin was then washed with DMF, MeOH and DCM (4 x 10 mL) and dried under vacuum. The yellow color of the resin in the Kaiser test confirmed the completion of the coupling reaction.

The Fmoc group of aspartic acid was removed from the tripeptide **2.7** using 20% piperidine in DMF (5 mL, 1 x 2 min, 1 x 10 min). The resin beads were washed with DMF, MeOH and DCM (4 x 10 mL) before coupling with the fourth amino acid. A mixture of Fmoc-Lys(Boc)-OH (0.456 g, 0.973 mmol), HBTU (0.351 g, 0.925 mmol) and DIEA (338.4 μL, 1.946 mmol) in DMF (2.5 mL) was added to the syringe and the reaction mixture was shaken for 3 h. The resin was washed with DMF, MeOH and DCM (4 x 10 mL) and dried under vacuum. Kaiser test displaying yellow color of the resin confirmed the absence of free amino acids.

The tetrapeptide-functionalized resin **(2.9)** was treated with 20% piperidine in DMF (5 mL, 1 x 2 min, 1 x 10 min) to cleave the Fmoc group and was washed with DMF, MeOH and DCM (4 x 10 mL) before proceeding to coupling with the fifth amino acid. Fmoc-Trp(Boc)-OH (0.456 g, 0.973 mmol), HBTU (0.351 g, 0.925 mmol) and DIEA (338.4 μL, 1.946 mmol) in DMF (2.5 mL) was added to the syringe and the reaction mixture was shaken for 3 h. After the resin was washed with DMF, MeOH and DCM (4 x 10 mL) and dried under vacuum, Kaiser test was performed. The yellow color of the resin confirmed the absence of free amino acids.

The resin **(2.11)** was incubated with 20% piperidine in DMF (5 mL, 1 x 2 min, 1 x 10 min) to liberate the Fmoc group from the pentapeptide. The resin was washed with DMF, MeOH and DCM (4 x 10 mL). A solution of Fmoc-Ala-OH (0.303 g, 0.9732 mmol), HBTU (0.351 g, 0.925 mmol) and DIEA (338.4 µL, 1.9464 mmol) in DMF (2.5 mL) was added to the syringe and the reaction mixture was shaken for 3 h. After the resin was washed with DMF, MeOH and DCM (4 x 10 mL) and dried under vacuum. The completion of the coupling reaction was confirmed with the yellow color of the resin beads in the Kaiser test.

The resin was treated with 20% piperidine in DMF (5 mL, 1 x 2 min, 1 x 10 min) to remove the Fmoc group from the terminal alanine residue. The resin was washed with DMF, MeOH and DCM (4 x 10 mL), prior to coupling with the seventh amino acid, lysine. Boc-Lys(Fmoc)-OH (0.235 g, 0.500 mmol), HBTU (0.180 g, 0.500 mmol) and DIEA (174 µL, 1.000 mmol) in DMF (2.5 mL) was added to the peptide Glu-Leu-Asp-Lys-Trp-Ala bound resin (0.257 g, 0.125 mmol) in the syringe. The reaction mixture was shaken for 3.5 h, after which the resin was washed with DMF, MeOH and DCM (4 x 10 mL) and dried under vacuum.

The Wang resin with Glu-Leu-Asp-Lys-Trp-Ala-Lys (0.130 g, 0.058 mmol) were transferred to a new 12 mL plastic syringe and 20% piperidine in DMF (5 mL, 1 x 2 min, 1 x 10 min) was added to remove the Fmoc group. The solution was drained from the syringe and the resin was washed with DMF, MeOH and DCM (4 x 10 mL) and then dried under vacuum. G∧C base aldehyde, **2.16** (0.149 g, 0.232 mmol) in 1,2-DCE (2.5 mL) was added to the resin and was shaken overnight. Sodium triacetoxy borohydride (0.059 g, 0.278 mmol) and DIEA (73 µL, 0.418 mmol) were then added and shaken for 60 h. This procedure was repeated twice. The solution was drained and the resin was washed with DMF, MeOH and DCM (4 x 10 mL) and then dried under vacuum. The desired peptide functionalized with G∧C (ELDKWAK-TB) was deprotected and cleaved from the resin by adding a solution of TFA, TIS and water in the ratio of 95%: 2.5%: 2.5% and shaking the reaction mixture for 3 h. The resulting mixture was filtered and

removal of the solvent using rotatory evaporation afforded a viscous liquid. Cold ether (Et_2O) was added to the resulting viscous solution to precipitate the crude product. The precipitate was recovered by centrifugation at 1100 rpm for 10 min. The precipitate was washed with Et_2O (10 times) and the precipitate was dried in vacuum over a 40 °C oil bath for 3 d to yield the desired compound.

^{1}H NMR (600 MHz, d_6-DMSO) δ: 12.3 (bs, 3H), 10.21 (bs, 1H), 8.22 (bs, 8H), 7.26 (m, 4H), 7.12 (bs, 1H), 6.99-6.91 (m, 2H), 4.52-4.58 (m, 1H), 4.17-4.45 (m, 3H) 3.81 (t, 2H) 3.49 (m, 4H), 3.27 (m, 2H), 3.09-2.96 (m, 4H), 2.91- 2.86 (m, 6H), 2.806 (d, 2H), 2.73-2.69 (m, 2H), 2.61 (t, 2H), 2.51 (m, 12H), 2.38 (t, 1H), 2.28 (t, 6H), 1.99-1.94 (m, 2H), 1.83-1.79 (m, 3H) 1.67-1.22 (m, 6H), 1.01 (s, 6H), 0.85 (m, 6H). HRMS calcd for $C_{60}H_{90}N_{22}O_{15}$ $[M+H]^+$ 1357.69, found 1357.65; elemental analysis calcd for $(C_{60}H_{89}N_{22}O_{15})(TFA)_4(H_2O)_{4.5}(Et_2O)$: C, 43.32, H, 5.48, N, 15.65, found: C, 43.019, H, 5.282, N, 15.31.

2.5.3. Synthesis of RGDSK-TB

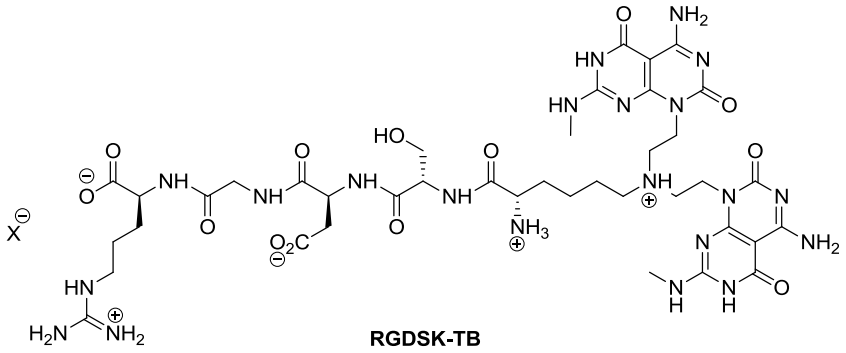

DMF was added to Wang resin (0.65 mmol/g, 300 mg, 0.195 mmol) in a 12 mL plastic syringe and was shaken for 20 min. After draining the solvent, a mixture of Fmoc-Arg(Pbf)-OH (0.531 g, 0.819 mmol) and DMAP (0.020 g, 0.162 mmol) in DMF (3 mL) was added. After shaking for 1 h, DIC (127 µL, 0.819 mmol) was added to the syringe and the reaction mixture was shaken overnight. The resin beads were filtered under vacuum and washed with DMF, MeOH and DCM (4 x 10 mL). They were then treated with 50% acetic anhydride in pyridine in order to

cap the free hydroxyl groups (2 x 5 min). Washing of the resin was done with (4 x 10 mL) DMF, MeOH and DCM and the resin beads were dried under vacuum. The degree of substitution was determined by the spectroscopic quantification of the fulvene-piperidine adduct at 301 nm. The UV-Vis spectra of the two resin samples of mass 7.3 and 7.6 mg gave absorbance intensities of 0.235 and 0.255. Using the expression for degree of substitution, an average value of 0.426 mmol/g was obtained that corresponded to a yield of 65%.

The Wang resin substituted by the arginine derivative was treated a solution of 20% piperidine in DMF (5 mL, 2 x 5 min). The resulting product was then washed with DMF, MeOH and DCM (4 x 10 mL). A mixture of Fmoc-Gly-OH (0.152 g, 0.511 mmol), HBTU (0.184 g, 0.485 mmol) and DIEA (178.6 μL, 1.022 mmol) in DMF (2.5 mL) was added to the syringe and the reaction mixture was shaken for 3.5 h. The resin beads were washed with DMF, MeOH and DCM (4 x 10 mL) and dried under vacuum. The yellow color of the resin in the Kaiser test confirmed the completion of the amide coupling reaction.

The Fmoc group of the glycine was deprotected using 20% piperidine in DMF (5 mL, 2 x 5 min). DMF, MeOH and DCM (4 x 10 mL) were used to wash the resin prior to coupling with the third amino acid. A solution mixture of Fmoc-Asp(O*t*-Bu)-OH (0.201 g, 0.511 mmol), HBTU (0.184 g, 0.485 mmol) and DIEA (178.6 μL, 1.022 mmol) in DMF (2.5 mL) was added to the syringe and the reaction mixture was shaken for 3.5 h. The resin was then washed with DMF, MeOH and DCM (4 x 10 mL) and dried under vacuum. The completion of the coupling reaction was confirmed by yellow color of the beads in the Kaiser test.

The Fmoc group of aspartic acid was removed from the tripeptide bound resin **(2.23)** using 20% piperidine in DMF (5 mL, 2 x 5 min) and the resin beads were washed with DMF, MeOH and DCM (4 x 10 mL) prior to coupling with the fourth amino acid. A solution of Fmoc-Ser(*t*-Bu)-OH (0.196 g, 0.511 mmol), HBTU (0.184 g, 0.485 mmol) and DIEA (178.6 μL, 1.022 mmol) in DMF (2.5 mL) was added to the syringe and the reaction mixture was shaken for 3.5 h. The beads were washed with DMF, MeOH and DCM (4 x 10 mL) and then dried

under vacuum. The Kaiser test displaying yellow color of the resin confirmed the absence of free amino acids.

The resin **(2.25)** was treated with 20% piperidine in DMF (5 mL, 2 x 5 min) to remove the Fmoc group from the serine residue. The resin beads were washed with DMF, MeOH and DCM (4 x 10 mL), before proceeding to coupling with the fifth amino acid, lysine. The final amino acid Boc-Lys(Fmoc)-OH (0.240 g, 0.511 mmol), HBTU (0.184 g, 0.485 mmol) and DIEA (178.6 μL, 1.022 mmol) in DMF (2.5 mL) was added to resin and the reaction mixture was shaken for 3.5 hours. After the coupling reaction, the resin was washed with DMF, MeOH and DCM (4 x 10 mL) and dried under vacuum.

The Wang resin with Arg-Gly-Asp-Ser-Lys (250 mg, 0.067 mmol) was transferred to a new 12 mL plastic syringe and 20% piperidine in DMF (5 mL, 2 x 5 min) was added to remove the Fmoc group from the lysine residue. The solution was drained from the syringe and the beads were washed with DMF, MeOH and DCM (4 x 10 mL) and then dried under vacuum. G∧C base aldehyde, **2.16** (0.173 g, 0.270 mmol) in 1,2-DCE (2.5 mL) was added to the resin and shaken overnight. Sodium triacetoxy borohydride (0.069 g, 0.324 mmol) and DIEA (86 μL, 0.485 mmol) were then added and shaken for 60 h. This reaction procedure was repeated twice. The solution was drained and the beads were washed with DMF, MeOH and DCM (4 x 10 mL) and dried under vacuum. The desired peptide functionalized with twin G∧C (RGDSK-TB) was deprotected and liberated from the resin by adding a solution of TFA, TIS and water mixture (95%: 2.5%: 2.5%) and shaking for 3 h. The resulting mixture was filtered and the solvent was removed by rotatory evaporation. Cold ether (Et_2O) was added to the resulting viscous solution to precipitate the crude product. The precipitate was recovered by centrifugation at 1100 rpm for 10 min. The precipitate was washed with Et_2O (10 times) and the precipitate was dried in vacuum over a 40 °C oil bath for 3 d to yield the desired compound.

^{1}H NMR (600 MHz, d_6-DMSO) δ: 12.6 (bs, 2H), 9.32 (bs, 2H), 8.61 (d, 1H), 8.41 (d, 1H), 8.22 (bs, 3H), 8.13 (d, 1H), 8.05 (t, 1H), 7.885 (t, 1H), 7.67 (t, 2H), 7.4

(bs, 4H), 7.3 (bs, 4H), 4.59 (m, 1H), 4.42 (m, 4H), 4.19 (m, 1H), 3.88 (m, 1H), 3.73-3.58 (m, 4H), 3.54 (m, 4H), 3.31 (m, 2H), 3.07 (m, 2H), 2.7 (d, 6H), 2.59 (m, 2H), 2.48 (m, 2H), 2.37 (m, 2H), 1.73- 1.7 (m, 4H) 1.58-1.47 (m, 1H), 1.36-1.35 (m, 2H), 1.038-1.25 (m, 1H). HRMS calcd for $C_{39}H_{60}N_{21}O_{13}$ $[M+H]^+$ 1030.46, found 1030.467; elemental analysis calcd for $(C_{39}H_{59}N_{21}O_{13})(TFA)_4(H_2O)_{6.4}(Et_2O)_{0.3}$: C, 35.57, H, 5.13, N, 18.07, found: C, 35.23, H, 4.734, N, 17.66.

2.5.4. Synthesis of DRGSK-TB

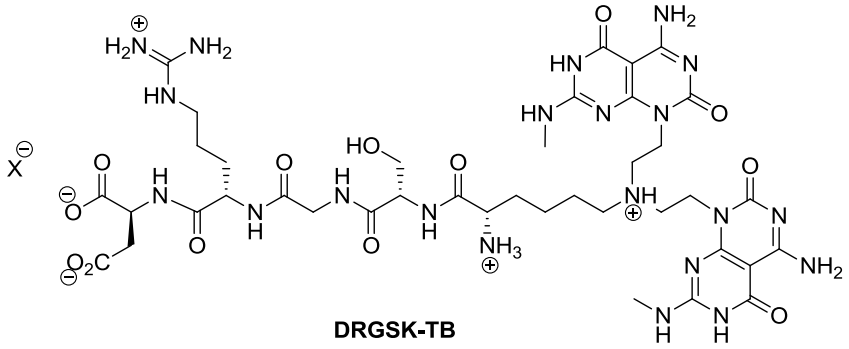

DRGSK-TB

DMF was added to Wang Resin (0.65 mmol/g, 500 mg, 0.325 mmol) in a 12 mL plastic syringe and was shaken for 20 min. After draining the solvent DMF, a solution mixture of Fmoc-Asp(O*t*-Bu)-OH (0.562 g, 1.365 mmol), DMAP (0.033 g, 0.270 mmol) in DMF (3 mL) was added. After 1 h of shaking, DIC (211 µL, 1.365 mmol) was added to the syringe and the reaction mixture was shaken overnight. The resin was filtered under vacuum and washed (4 x 10 mL) with DMF, MeOH and DCM. Then the resin was treated with 50% acetic anhydride in pyridine in order to cap the free hydroxyl groups (1 x 10 min, 2 x 20 min). The resin was washed with (4 x 10 mL) DMF, MeOH and DCM and dried under vacuum. The degree of substitution of hydroxyl groups was determined by the spectroscopic quantification of the fulvene-piperidine adduct at 301 nm. The UV-Vis spectra of the two resin samples with mass 5.9 and 6.6 mg gave absorbance

intensities of 0.235 and 0.255. A degree of substitution of 0.435 mmol/g was obtained that corresponded to a yield of 67%.

The Wang resin substituted by aspartic acid derivative was treated with a solution of 20% piperidine in DMF (5 mL, 1 x 2 min, 1 x 10 min) to remove the Fmoc group. The resin was washed with DMF, MeOH and DCM (4 x 10 mL) and a mixture of Fmoc-Arg(Pbf)-OH (0.565 g, 0.870 mmol), HBTU (0.314 g, 0.827 mmol) and DIEA (302.5 μL, 1.740 mmol) in DMF (2.5 mL) was added to the syringe. The reaction mixture was shaken for 3 h after which the resin was washed with DMF, MeOH and DCM (4 x 10 mL) and dried under vacuum. The yellow color of the resin in the Kaiser test confirmed the completion of the amide coupling reaction.

The Fmoc group of the arginine residue was deprotected from the dipeptide bound **(2.30)** resin using 20% piperidine in DMF (5 mL, 1 x 2 min, 1 x 10 min). Prior to coupling with the third amino acid, the resin beads were washed with DMF, MeOH and DCM (4 x 10 mL). A mixture of Fmoc-Gly-OH (0.258 g, 0.870 mmol), HBTU (0.314 g, 0.827 mmol) and DIEA (302.5 μL, 1.740 mmol) in DMF (2.5 ml) was added to the syringe and the reaction mixture was shaken for 3 h. The resin was washed with DMF, MeOH and DCM (4 x 10 mL) and then dried under vacuum. The yellow color of the resin in the Kaiser test confirmed the completion of the coupling reaction.

The Fmoc group was removed from the tripeptide functionalized resin **(2.31)** using 20% piperidine in DMF (5 mL, 1 x 2 min, 1 x 10 min) and the resin beads were washed with DMF, MeOH and DCM (4 x 10 mL) before coupling with the fourth amino acid. A solution of Fmoc-Ser(*t*-Bu)-OH (0.334 g, 0.870 mmol), HBTU (0.314 g, 0.827 mmol) and DIEA (302.5 μL, 1.740 mmol) in DMF (2.5 mL) was added to the syringe and the reaction mixture was shaken for 3 h. The resin was washed with DMF, MeOH and DCM (4 x 10 mL) and dried under vacuum. Kaiser test displaying yellow color of the resin confirmed the completion of coupling of the fourth amino acid derivative.

The resin beads were treated with 20% piperidine in DMF (5 mL, 1 x 2 min, 1 x 10 min) to remove the Fmoc group and washed with DMF, MeOH and DCM (4 x 10 mL), prior to coupling of the fifth amino acid, lysine. The last amino acid Boc-Lys(Fmoc)-OH (0.408 g, 0.870 mmol) was added to a mixture of HBTU (0.314 g, 0.827 mmol), DIEA (302.5 μL, 1.740 mmol) in DMF (2.5 mL). The reaction mixture was added to the resin and shaken for 3 h. The resin was then washed with DMF, MeOH and DCM (4 x 10 mL) and dried under vacuum. The yellow colour of the resin in the Kaiser test confirmed the completion of the amide coupling reaction.

The Asp-Arg-Gly-Ser-Lys functionalized Wang resin (0.200 g, 0.054 mmol) was transferred to a new 12 mL plastic syringe and 20% piperidine in DMF (5 mL, 1 x 2 min, 1 x 10 min) was added to remove the Fmoc group. The solution was drained from the resin and the beads were washed with DMF, MeOH and DCM (4 x 10 mL) and then dried under vacuum. G∧C base aldehyde **2.16** (0.139 g, 0.218 mmol) in 1,2-DCE (2.5 mL) was added to the resin and shaken overnight. Sodium triacetoxy borohydride (0.055 g, 0.261 mmol) and DIEA (68 μL, 0.392 mmol) were added and shaken for 60 h. This reaction was repeated twice after which the solution was drained and resin was washed with DMF, MeOH and DCM (4 x 10 mL) and dried under vacuum. The desired compound was deprotected and cleaved from the resin by adding a solution of TFA, TIS and water mixture (95%: 2.5%: 2.5%) and shaking for 3 h. The resulting mixture was filtered and the solvent was removed by rotatory evaporation. Cold ether (Et_2O) was added to the resulting viscous solution to precipitate the crude product that was recovered by centrifugation at 1100 rpm for 10 min. The precipitate was washed with Et_2O (10 times) and the precipitate was dried in vacuum over a 40 °C oil bath for 3 d to yield the desirable compound.

^{1}H NMR (600 MHz, d_6-DMSO) δ: 12.57 (bs, 2H), 9.53 (bs, 2H), 9.23 (bs, 2H), 9.13 (d, 1H), 8.52 (d, 1H), 8.44 (d, 2H), 8.23 (bs, 3H), 8.05 (d, 1H), 7.953 (t, 1H), 7.79 (t, 2H), 7.55 (bs, 4H), 7.32 (bs, 4H), 4.54 (m, 1H), 4.44 (m, 4H), 4.35 (m, 1H), 3.9-3.84 (m, 1H), 3.74- 3.56 (m, 4H), 3.36 (m, 4H), 3.07 (d, 6H), 2.93 (m,

2H), 2.69 (m, 2H), 2.48 (m, 2H), 2.50 (m, 2H), 1.75-1.69 (m, 4H) 1.51-1.49 (m, 1H), 1.41 (m, 2H), 1.040 (m, 1H). HRMS calcd for $C_{39}H_{60}N_{21}O_{13}$ $[M+H]^+$ 1030.46, found 1030.4661; elemental analysis calcd for $(C_{39}H_{59}N_{21}O_{13})(TFA)_{2.6}(H_2O)_3(Et_2O)_{0.1}$: C, 38.48, H, 5.26, N, 21.13, found: C, 38.1, H, 5.1, N, 21.46.

2.5.5. Characterization by Microscopy

A stock solution of 1 mg/mL of peptide-functionalized with twin G∧C motif (TB) was prepared in water using different conditions of heat and sonication to form RNTs. The stock solution was diluted to 0.2 mg/mL in water. A drop of the diluted solution of the RNT was deposited on the 400 square-mesh copper grids right after dilution and was dried by blotting with a filter paper after 30 s. The grids were air dried and then heated on a hotplate (70 °C) for 10 min prior to imaging in order to remove any residual solvents. SEM images were obtained at 30 kV accelerating voltage, 20 μA and a working distance of 5-8 mm on a high resolution Hitachi S–4800 cold field emission SEM.

TEM samples for RNTs were prepared by adding a droplet of the diluted RNT solution on the 400 square-mesh copper grid. After 30 s, the sample was blotted and air-dried. A droplet of 2% aqueous solution of uranyl acetate was deposited on the grid to stain the RNTs. The stain was blotted with a filter paper after 2 min and the grid was heated on a hot plate for 10 min. JEOL 2200 FS TEM–200kV Schottky field emission instrument equipped with an in-column omega filter was used for TEM imaging. Bright field TEM images were acquired using energy filtered zero loss beams (slit width 10ev).

For AFM measurement, clean HOPG and mica substrates (1 × 1 cm^2) were prepared and the RNT samples were deposited by spin-coating at 2500 rpm for 30 s to remove the excessive precipitation from the surface of the sample.

The morphology of the sample was visualized using a Digital Instruments/Veeco Instruments MultiMode Nanoscope IV AFM equipped with an E scanner. For optimal height profile, silicon cantilevers (MikroMasch USA, Inc.) with low spring constants of 4.5 N/m were used in tapping mode (TM-AFM). To obtain a clear image from the surface, low scan rate (0.5-1 Hz) and amplitude setpoint of 1 V were used in our measurement.

2.5.6. Sample preparation of ELDKWAK-TB

A stock solution of 1 mg/mL (0.510 mM) of ELDKWAK-TB was prepared in water by sonicating for 5 min and then heating for 30 s (sonication and heating was done repeatedly three times). The stock solution was diluted to 0.2 mg/mL (0.102 mM) for the SEM sample preparation.

2.5.7. Sample preparation of RGDSK-TB

The stock solution of RGDSK-TB, 1 mg/mL (0.614 mM) was dissolved in water and sonicated for 2 min. To prepare the SEM, TEM and AFM samples the stock solution was diluted to 0.2 mg/mL (0.113 mM) in water and was allowed to age. SEM and TEM images were obtained after 1 d and 4 d of aging. AFM imaging was done for sample aged for 7 d.

2.5.8. Sample preparation of DRGSK-TB

To study the self-assembly of DRGSK-TB, the stock solution of 1 mg/mL (0.718 mM) was prepared in water by heating at 90 °C for 30 min. The solution was then diluted to 0.2 mg/mL (0.144 mM) in water and allowed to age for 4 d. The SEM and TEM images were obtained for 4 d aged sample, and AFM images were obtained for the sample at 2 d.

2.9. References

1. Carpo L. Hormones, Freeman, New York, **1985**.
2. Boschmann M, König W. Peptide and Protein Hormones. Structure, Regulation, Activity. A Reference Manual. 284 Seiten, zahlreiche Abb. und Tab. VCH Verlagsgesellschaft Weinheim, New York, Basel, Cambridge **1993**. Preis: 198, DM. Nahrung, 38: 225.
3. *Pan W, Kastin AJ, Banks WA, Zadina JE.* Effects of peptides: a cross-listing of peptides and their central actions published in the journal Peptides from 1994 through 1998. *Peptides*. ***1999***. *20*(9): *1127*-38.
4. Sewald N, Jakubke H-D. Peptides: Chemistry and Biology, Second Edition. Wiley-VCH, Verlag GmbH & Co. KGaA. **2002**. Chapter1 (1-4).
5. Wiesm¨uller K-H, Fleckenstein B, Jung G. Peptide vaccines and peptide libraries. *Biol*. *Chem. Hoppe-Seyler*. ***2001***. *382*: *571*.
6. Zauner, W, Lingnau K, Mattner F, von Gabain A and Buschle M. Defined synthetic vaccines. *Biol*. *Chem. Hoppe-Seyler* ***2001***. *382*: *581*.
7. *Cochran AG*. Antagonists of protein-protein interactions. *Chem*. *Biol*. **2000**. *7*: *R85*-R94.
8. *Clackson T*, *Wells JA*. A hot spot of binding energy in a hormone-receptor interface. *Science*. ***1995***. *267: 383*-386.
9. du Vigneaud V, Ressler C and Trippett S. The Sequence of Amino Acids in Oxytocin, with a Proposal for the Structure of Oxytocin. *J. Biol. Chem.* **1953**. 205: 949-957.
10. Carpino LA, Ghassemi S, Ionescu D, Ismail M, Sadat-Aalaee D, Truran GA, Mansour E, Siwruk GA, Eynon JS, Morgan B. Rapid, continuous solution-phase peptide synthesis: Application to peptides of pharmaceutical interest. *Org. Process Res. Dev*. **2003**. 7, 28-37.
11. Merrifield RB. Solid phase peptide synthesis I: Synthesis of a tetrapeptide. *J. Am. Chem. Soc*. **1963**. 85: 2149-2154.
12. Journeay WS, Suri SS, Moralez JG, Fenniri H, Singh B. Low inflammatory activation by self-assembling Rosette nanotubes in human Calu-3 pulmonary epithelial cells. *Small*. **2008**. 4(6): 817-23.

13. Journeay WS, Suri SS, Moralez JG, Fenniri H and Singh B. Rosette nanotubes show low acute pulmonary toxicity in vivo. *Int. J. Nanomedicine*. **2008**. 3(3): 373-83.
14. Zhang L, Rakotondradany F, Myles AJ, Fenniri H, Webster TJ. Arginine-glycine-aspartic acid modified rosette nanotube-hydrogelcomposites for bone tissue engineering. *Biomaterials*. **2009**. 30(7): 1309-20.
15. Zhang L, Hemraz UD, Fenniri H, Webster TJ. Tuning cell adhesion on titanium with osteogenic rosette nanotubes. *J. Biomed. Mater. Res. A*. **2010**. 95(2): 550-63.
16. Alfsen A, Bomsel M. HIV-1 gp41 envelope residues 650-685 exposed on native virus act as a lectin to bind epithelial cell galactosyl ceramide. *J. Biol. Chem*. **2002**; 277(28): 25649-59.
17. Moralez JG, Raez J, Yamazaki T, Motkuri RK, Kovalenko A, Fenniri H. Helical rosette nanotubes with tunable stability and hierarchy. *J. Am. Chem. Soc*. **2005**, 127: 8307-8309.
18. Kaiser E, Colescott RL, Bossinger CD, Cook PI. Color test for detection of free terminal amino groups in the solid-phase synthesis of peptides. *Anal. Biochem*. **1970**. 34(2): 595-598.
19. Zagury, D, Bernard J, Cheynier R, Desportes I, Leonard R, Fouchard M, Reveil B, Ittele D, Lurhuma Z, Mbayo K, Wane J, Salaun J, Goussard B, Dechazal L, Burny A, Nara P and Gallo RC. A group-specific anamnestic immune reaction against HIV induced by a candidate vaccine against AIDS. *Nature* (London). **1988**. 332:728-731.
20. Chen YH, Xiao Y, Yu TW and Dierich MP. Epitope vaccine: a new strategy against HIV-1. *Immunol. Today*. **1999a**, 20: 588-589.
21. Xiao Y, Lu Y and Chen YH. Epitope-vaccine as a new strategy against HIV-1 mutation. *Immunol. Lett*. **2001**. 77: 3-6.
22. Xiao Y, Dong XN and Chen YH. Neutralizing antibodies: mechanism of neutralization and protective activity against HIV-1. *Immunol. Res*. **2002**, 25: 193-200.

23. Muster T, Steindl F, Purtscher M, Trkola A, Klima A, Himmler G, Rüker F, Katinger H. A conserved neutralizing epitope on gp41 of human immunodeficiency virus type 1. *J Virol*. **1993**. 67(11): 6642-7.
24. Pierschbacher MD, Ruoslahti E. The cell attachment activity of fibronectin can be duplicated by small fragments of the molecule. *Nature.* **1984a**. 309: 30-33.
25. Pierschbacher MD, Ruoslahti E. Variants of the cell recognition site of fibronectin that retain attachment-promoting activity. *Proc. Natl. Acad. Sci*. USA. **1984b**. 81: 5985-88.
26. Hautanen A, Gailit J, Mann DM, Ruoslahti E. Effects of modifications of the RGD sequence and its context on recognition by the fibronectin receptor. *J. Biol. Chem*. **1984b**. 264: 1437-42.
27. Pytela R, Suzuki S, Breuss J, Erle DJ, Sheppard D. Polymerase chain reaction cloning with degenerate primers: homology-based identification of adhesion molecules. *Methods Enzymol*. **1994**. 245: 420-51.
28. SEM, TEM and AFM imaging was done by Dr. Jae-Young Cho.
29. Dee KC, Andersen TT, Bizios RJ. Design and function of novel osteoblast-adhesive peptides for chemical modification of biomaterials. *Biomed. Mater. Res*. **1998**. 40: 371-377.
30. Childs A, Hemraz UD, Castro NJ, Fenniri H, Zhang LG. Novel biologically-inspired rosette nanotube PLLA scaffolds for improving human mesenchymal stem cell chondrogenic differentiation. *Biomed. Mater*. **2013**. 8(6): 065003.
31. Modeling of RGDSK-TB RNTs was done by Dr. Takeshi Yamazaki.
32. (a) Muir T, Morales E, Root J, Kumar I, Garcia B, Vellandi C, Jenigian D, Marsh T, Henderson E and Vesenka JJ. Scanning force microscopy studies of X-ray-induced double-strand breaks in plasmid DNA. *Vac. Sci. Technol. A*. **1998**. 16: 1172-1177.

    (b) DeRose JA and Revel JP. Studying the surface of soft materials (live cells) at high resolution by scanning probe microscopy: challenges faced. *Thin Solid Films*. **1998**. 331: 194-202.

    (c) Kasumov AY, Klinov DV, Roche PE, Gueron S and Bouchiat H.

Thickness and low-temperature conductivity of DNA molecules. *Appl. Phys. Lett*. **2004**. 84: 1007-1009.

Chapter 3

Co-assembly Study of Rosette Nanotubes (RNTs)

3.1. Introduction

Rosette nanotubes (RNTs) are nanocarriers comprised of DNA base analogue G∧C motifs that can be functionalized with short peptides or amino acids.[1,2,4] Lysine residues and short peptides functionalized mono G∧C base have previously been synthesized. These motifs can self-assemble in a hierarchical fashion in aqueous medium by 18 hydrogen bonds and hydrophobic effects to form a six-membered macrocycle known as rosette that stack to form RNTs by π-π stacking interactions.[3-5] The twin G∧C building block results in the formation of a more stable self-assembled RNTs, resulting from the stacking of hexameric twin-rosette maintained by 36 hydrogen bonds, and solvophobic effects. Reduced steric interactions and electrostatic repulsions due to a decrease in functional group density, contribute to the stability of these RNTs.[6]

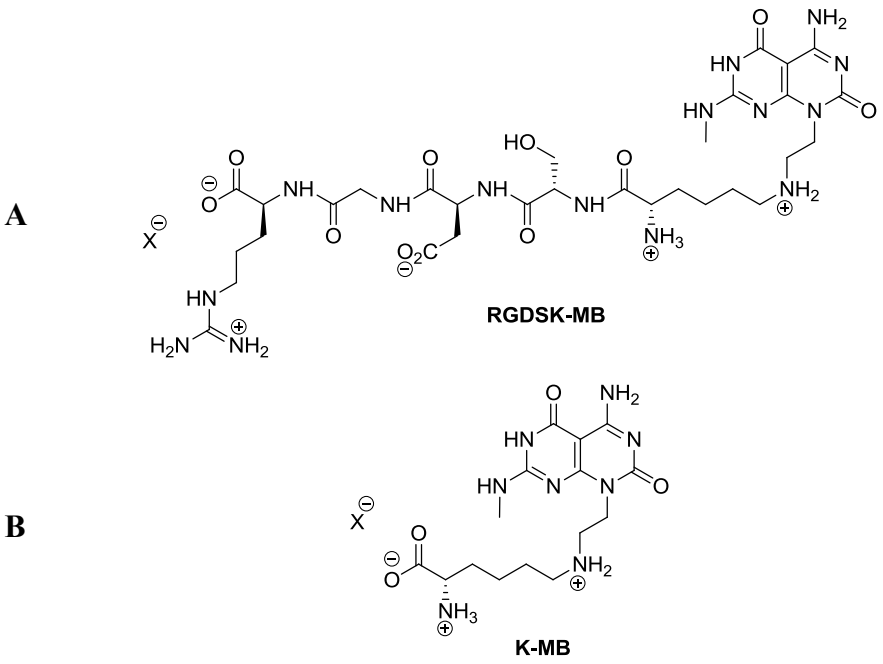

Figure 3-1: Structures of (A) peptide RGDSK functionalized mono G∧C motif (RGDSK-MB), and (B) lysine (K) functionalized mono G∧C motif (K-MB).

Another study revealed that administration of high dose of RNTs constituted of lysine-functionalized mono G∧C (K-MB) resulted in low lung inflammation *in vivo*. It was also shown that a formulation containing the peptide RGDSK

functionalized with single G∧C (RGDSK-MB) induced pro-inflammatory and apoptotic response *in vitro* in human carcinoma cell line Calu-3 acute lung inflammation. The RGDSK-MB monomer did not self-assemble on its own and a co-assembly was triggered by mixing it with K-MB (Figure 3-1) in a ratio of 5:95. It has previously been suggested that RNTs resulting from co-mixing a peptide-functionalized mono G∧C with lysine-functionalized mono G∧C, formed a stable system for osteogenic applications.[7-9] This stability can be further enhanced by designing the twin-G∧C variants.[10]

The aim of this project is to develop stable RNTs as a nanocarrier for the HIV-1 gp 41 epitope ELDKWA by the surface functionalization of RNTs with the peptide ELDKWA. In the previous chapter, we studied the synthesis of ELDKWA, incorporation of the lysine residue to the terminal end of the peptide ELDKWA and its functionalization with twin G∧C building blocks (ELDKWAK-TB). Several conditions of temperature, sonication and aging were used to aid in the self-assembly of ELDKWAK-TB. The self-assembly study and SEM imaging of ELDKWAK-TB (Figure 3-2) suggested that ELDKWAK-TB formed large aggregates instead of single RNTs, within one hour of the self-assembly process.

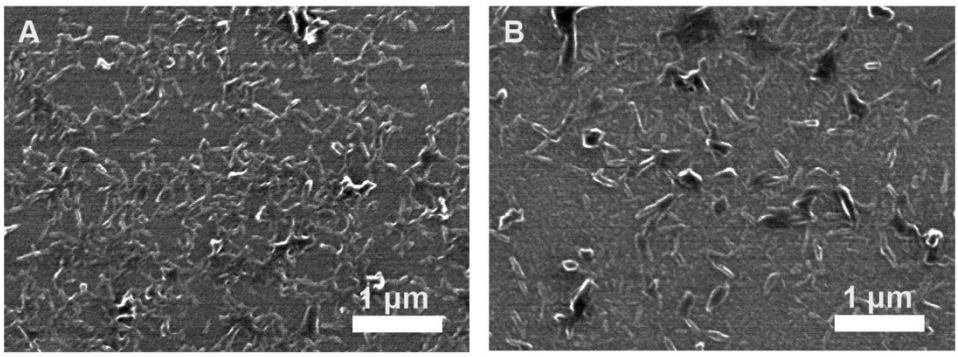

Figure 3-2: SEM images of formation of aggregates by ELDKWAK-TB RNTs.

In this chapter, we aim to achieve a stable nanotubular system by the co-assembly of lysine-functionalized twin G∧C base (K-TB) with ELDKWAK functionalized twin G∧C motif, ELDKWAK-TB (Figure 3-3). The morphology of the co-assembled K-TB/ELDKWAK-TB RNTs was studied by microscopic techniques

and the supramolecular chirality of the nanotubes was examined using circular dichroism (CD).

In the second part of this chapter, fluorescently-labeled RNTs were developed to study the encapsulation of the K-TB/ELDKWAK-TB RNTs *in vitro*. The self-assembly study of fluorescein isothiocyanate (FITC)-functionalized twin G∧C motif (FITC-TB) via SEM imaging revealed that the module does not lead to the formation of stable RNTs. However, when FITC-TB is co-assembled with the twin base linker, TBL (Figure 3-4), stable and well-dispersed RNTs are formed. Twin base linker, as we described in the previous chapter is the aminobutyl group functionalized twin G∧C motif that self-assembled in a hierarchical manner to form RNTs.[6] The formation of RNTs by co-assembly of FITC-TB with TBL was confirmed using SEM, TEM and AFM. The fluorescently-labeled FITC-TB/TBL RNTs, was then co-mixed with K-TB/ELDKWAK-TB RNTs and SEM and CD studies confirmed the formation of RNTs upon their co-mixing. This fluorescently-labeled RNT construct was used for *in vitro* studies to investigate their biological properties (see Chapter 4).

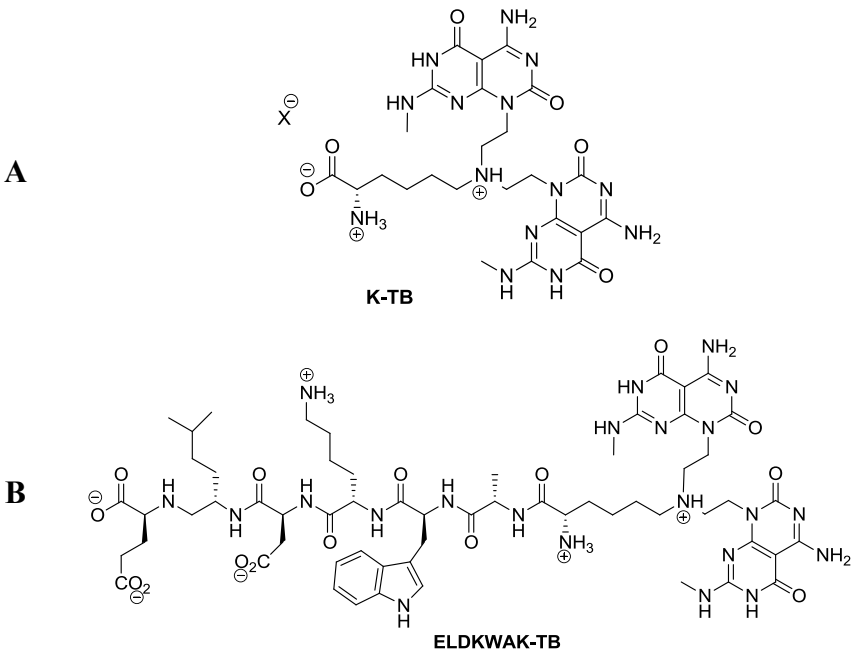

Figure 3-3: Structures of (A) lysine (K) functionalized twin G∧C motif (K-TB) and (B) ELDKWAK functionalized with twin G∧C bases (ELDKWAK-TB).

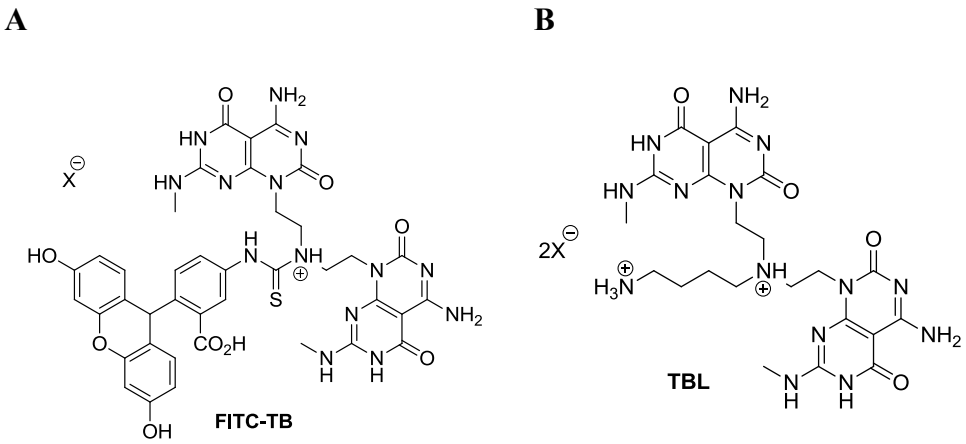

Figure 3-4: Structures of (A) FITC functionalized twin G∧C (FITC-TB) and (B) twin G∧C monomer with an aminobutyl group (TBL).

3.2. Results and Discussion

3.2.1. Self-assembly of K-TB

K-TB was synthesized by the standard Fmoc protection solid phase synthesis strategy and the final compound was characterized by mass spectroscopy, NMR and elemental analysis in our lab.[4,5]

In order to achieve the self-assembly of K-TB, a stock solution of 1 mg/mL (0.786 mM) was prepared in water. The solution was then sonicated for 5 min and heated for 30 s (repeated twice). The stock solution was then diluted in water to 0.05 mg/mL (0.039 mM) for SEM imaging, and to 0.0125 mg/mL (9 μM) for TEM and AFM imaging.

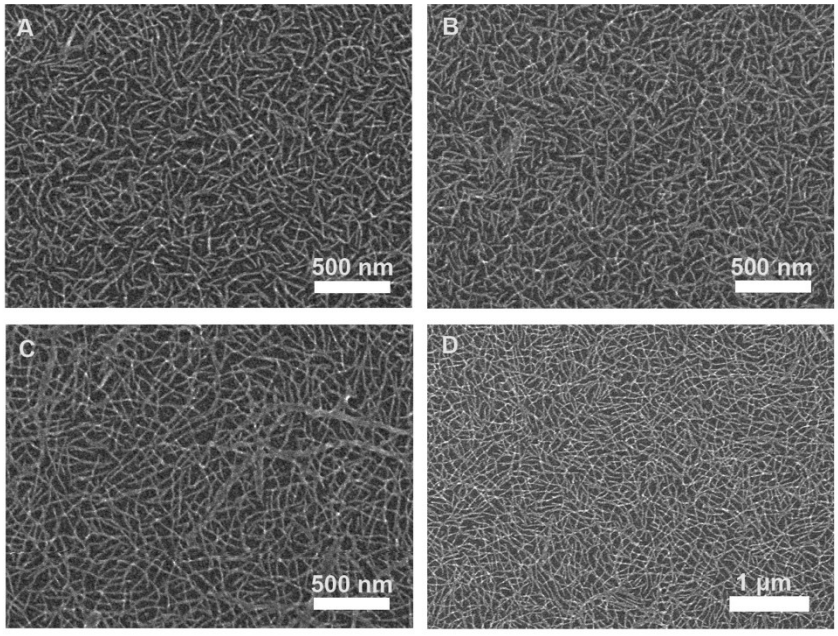

Figure 3-5: SEM images of RNTs formed by self-assembly of K-TB in water at 0.039 mM concentration (A and B aged at 1 h; C and D aged at 24 h).

The SEM imaging[11] suggested that K-TB forms short RNTs after 1 h (Figure 3-5, A and B) that increased in length after being aged for 24 h (Figure 3-5, C and D). The TEM imaging[11] (Figure 3-6) was done to confirm the formation of the nanotubes and obtain an average diameter of the nanotubes.

The average diameter of RNTs formed by self-assembly of K-TB was found to be 3.3 $\pm$ 0.2 nm by TEM measurements. The AFM images[11] in Figure 3-7, however, revealed nanotubes shorter in length as compared to the TEM images. This could likely be due to the spin coating method used to prepare samples for AFM measurements that might have severed the tubes. Drop casting was used for TEM and SEM sample preparation.

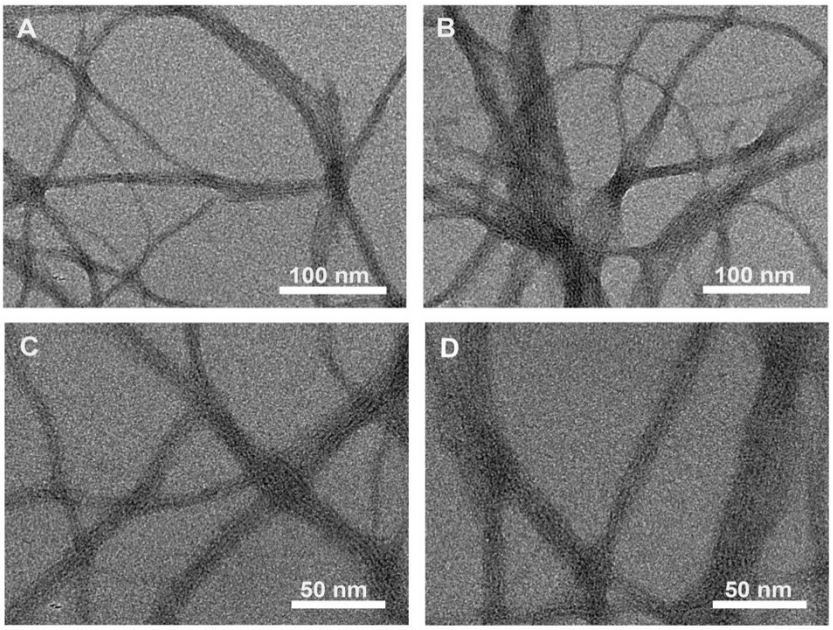

Figure 3-6: TEM images of RNTs formed by self-assembly of K-TB in water (9 μM, aged at 24 h).

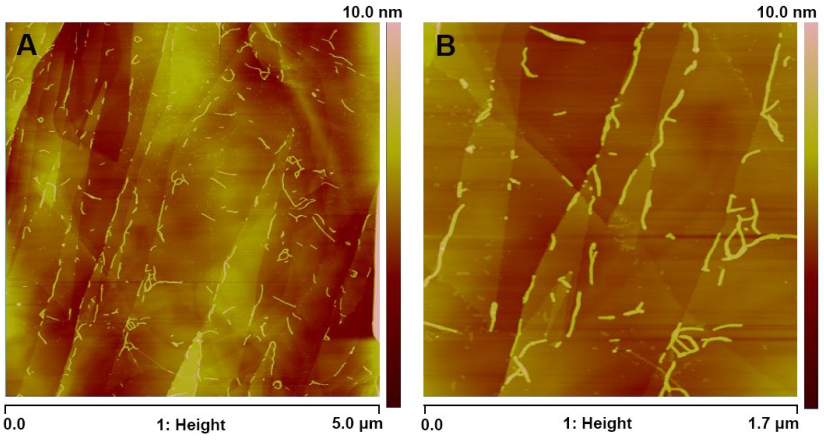

Figure 3-7: AFM images of RNTs formed by self-assembly of K-TB in water (9 μM, aged at 24 h) using HOPG substrate.

3.2.2. Co-assembly of K-TB with ELDKWAK-TB (Solution A)

In the previous chapter, we discussed that self-assembly of ELDKWAK-TB (Figure 3-2) does not lead to formation of single, well-dispersed RNTs; instead they form aggregates. So herein, we aim to develop stable RNTs by co-assembling K-TB with ELDKWAK-TB. K-TB forms stable and well-dispersed RNTs in aqueous solution as shown in Figure 3-8.

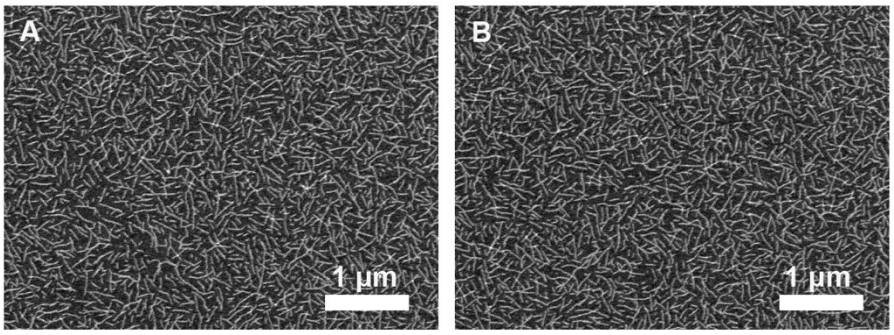

Figure 3-8: SEM images of well-dispersed RNTs formed by self-assembly of K-TB in water (0.039 mM, aged at 10 min).

We presume that co-assembly of ELDKWAK-TB with K-TB could lead to formation of more stable RNTs and improve the morphology of ELDKWAK-TB. In order to co-assemble K-TB with ELDKWAK-TB, a stock solution of 1 mg/mL (0.743 mM) was prepared in water in a molar ratio of 9:1. The solution was then sonicated for 5 min and heated for 30 s, and this procedure was repeated twice. The stock solution was then diluted to 0.05 mg/mL (0.037 mM) in water and allowed to age for 3 d prior to sample preparation for SEM, TEM and AFM.

The SEM imaging (Figure 3-9) revealed that the co-assembly of K-TB with ELDKWAK-TB in the molar ratio 9:1 leads to formation of stable nanotubular structures in a high aspect ratio. The co-assembled RNTs increased in length with time as evidenced in Figure 3-13.

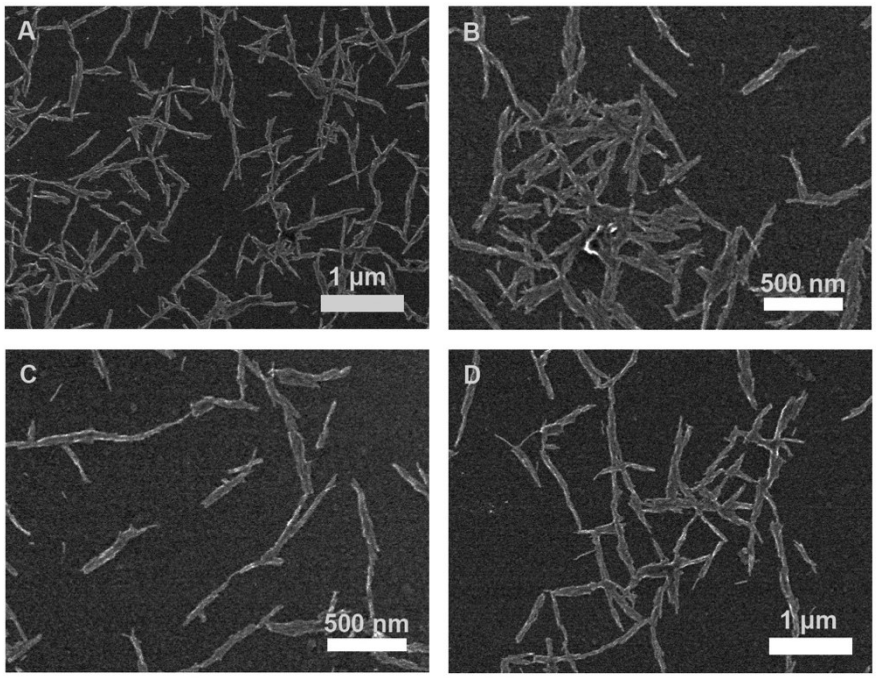

Figure 3-9: SEM images of RNTs formed by co-assembly of K-TB with ELDKWAK-TB in a molar ratio 9:1 in water (0.037 mM, aged for 3 d).

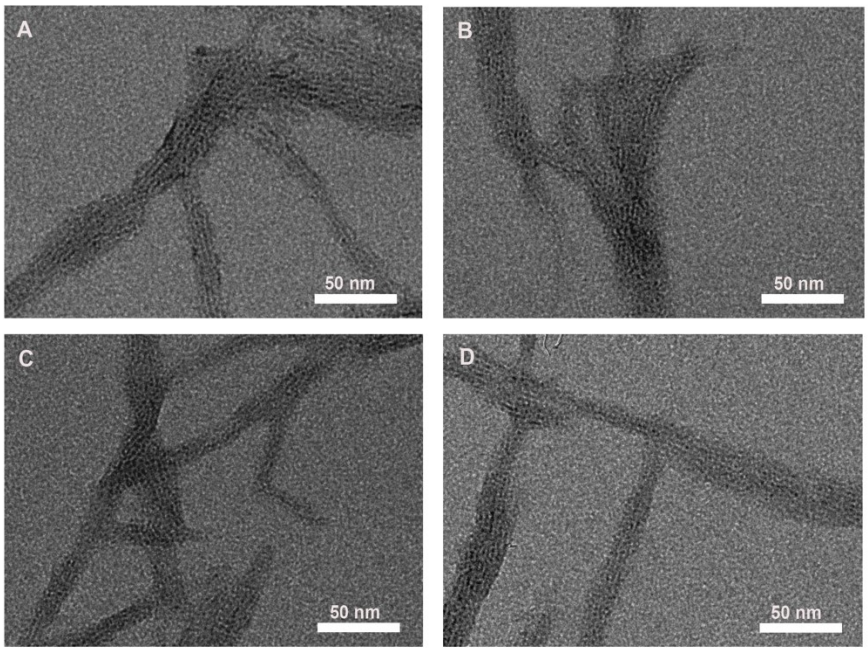

Figure 3-10: TEM images of RNTs formed by co-assembly of K-TB with ELDKWAK-TB in a molar ratio 9:1 in water (0.037 mM, aged for 3 d).

The TEM images (Figure 3-10) confirmed the formation of the nanostructures formed by K-TB/ELDKWAK-TB (9:1), designated as solution A. The TEM imaging does not show any visual difference between the RNTs formed by the co-assembly of K-TB with ELDKWAK-TB and the ones formed by the self-assembly of K-TB (Figure 3-6). As such, other experimental techniques to prove the co-assembly of K-TB with ELDKWAK-TB are discussed later in this chapter.

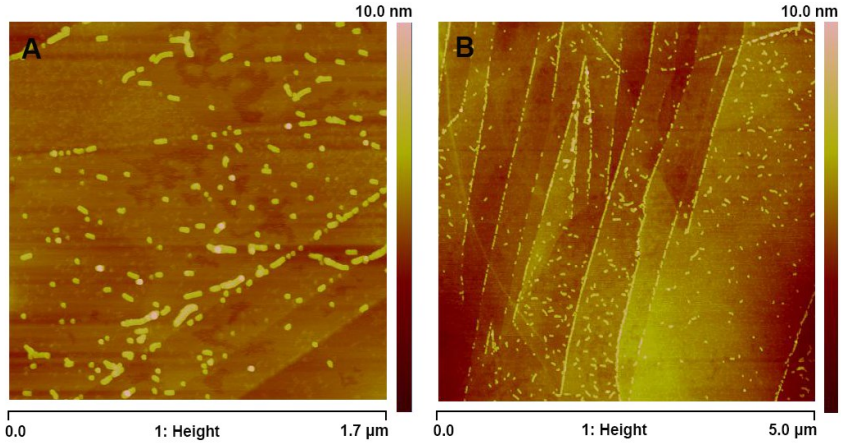

Figure 3-11: AFM images of RNTs formed by co-assembly of K-TB with ELDKWAK-TB in a molar ratio 9:1 in water (0.037 mM, aged for 3 d) using HOPG substrate.

The diluted samples of solution A used for TEM imaging were also used for AFM imaging. The AFM imaging (Figure 3-11) also showed the formation of nanostructures by the co-assembly of K-TB with ELDKWAK-TB. The morphology of the RNTs in AFM measurements are visually different from the one displayed by SEM and TEM imaging owing to the spin coating method of preparing sample for AFM.[14]

3.2.3. Study of time-dependence of co-assembly of K-TB with ELDKWAK-TB

As we discussed earlier in this chapter, the self-assembly of K-TB resulted in the formation of well-dispersed RNTs (Figure 3-12A) while the self-assembly of ELDKWAK-TB formed large aggregates in 1 h (Figure 3-12B).

The co-assembly of K-TB with ELDKWAK-TB (Solution A) led to formation of stable nanostructures at 1 h (Figure 3-12C).

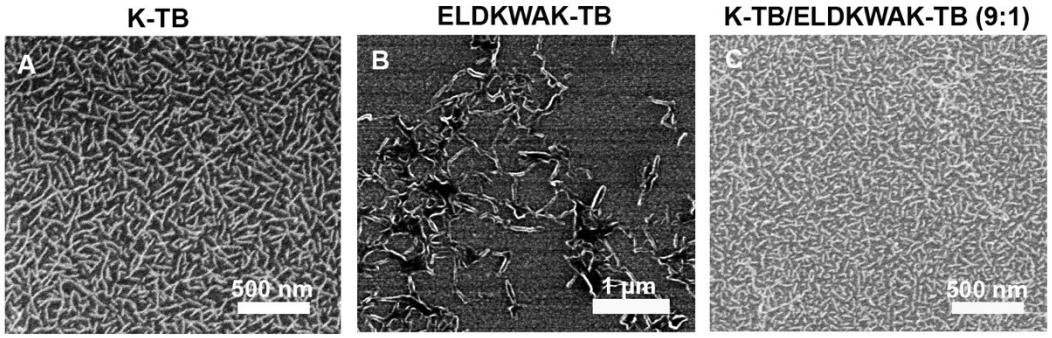

Figure 3-12: SEM images of RNTs formed by self-assembly of (A) K-TB at 0.05 mg/mL, (B) ELDKWAK-TB at 0.02 mg/mL and (C) co-assembly of K-TB with ELDKWAK-TB in a molar ratio 9:1 aged at 0 min.

A detailed study of time-dependence was done to investigate the formation of the K-TB RNTs and change in their morphology after undergoing a co-assembly process with ELDKWAK-TB in the molar ratio of 9:1 by SEM imaging (Figure 3-13). The stock solutions for K-TB and solution A was prepared as mentioned in section 3.2.2 and 3.2.3, respectively and were diluted to 0.05 mg/mL in water. These solutions were then allowed to age for different time periods of 0 min, 1 h, 1 d, 3 d and 7 d, prior to sample preparation for SEM imaging.

The SEM images in Figure 3-13, revealed that both the self-assembly of K-TB and the co-assembly of K-TB with ELDKWAK-TB (Table 3-1), both led to the formation of the short RNTs in a high aspect ratio at 0 min. While the self-assembly of K-TB resulted in formation of well-dispersed nanostructures that increased in length with time from 1 h to 7 d, the solution A RNTs were initially of shorter size (0 min and 1 h), which then increased in complexity and formed aggregates at 7 d.

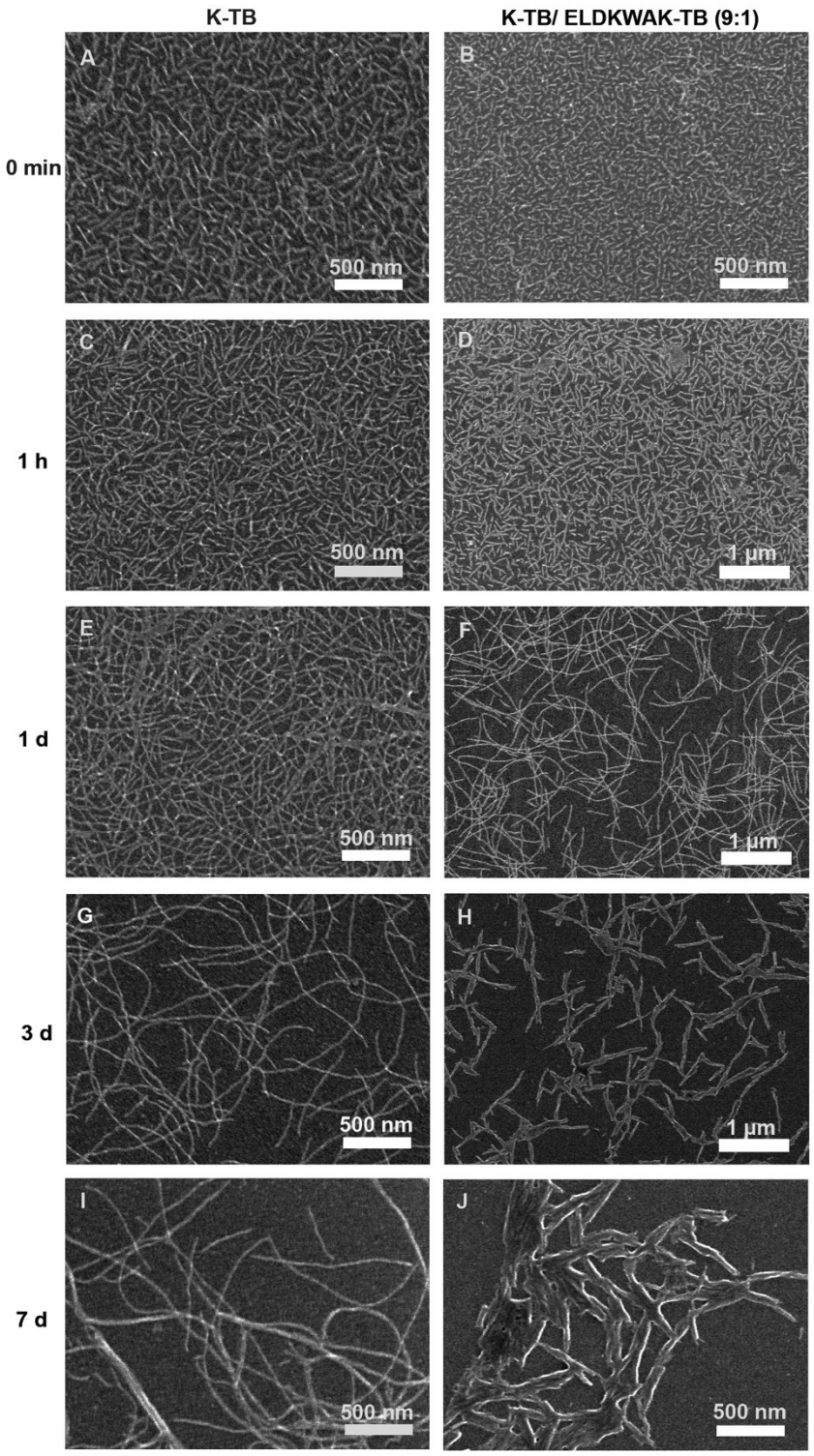

Figure 3-13: SEM images of K-TB (0.039 mM) and K-TB co-assembled with ELDKWAK-TB in a molar ratio 9:1 (0.037 mM) at different time intervals.

3.2.4. Circular Dichroism (CD) study of co-assembly of K-TB with ELDKWAK-TB

CD is a spectroscopic technique used to study supramolecular chirality based on the difference in the absorption of the left- and right-handed circular polarized light, due to presence of an optically active molecule.[12] Molecules such as proteins or DNA have characteristic CD spectra, particularly in the UV range. The superposition of the CD signals from the random orientation of the molecules in solution results in CD spectra that would indicate their chiral properties.[12-14]

The TEM imaging did not confirm a change in diameter upon co-assembly of K-TB with ELDKWAK-TB, although a change in morphology was observed by SEM and TEM. Therefore, CD was used to prove the co-assembly of K-TB with ELDKWAK-TB.

As such, CD was used to study the supramolecular organization of the self-assembly of K-TB and ELDKWAK-TB. The CD spectra (Figure 3-14) of both K-TB and ELDKWAK-TB solutions in water (50 μM) gave a bisignate signal (centered at 253 and 300 nm and, 230 nm) at 0 min.

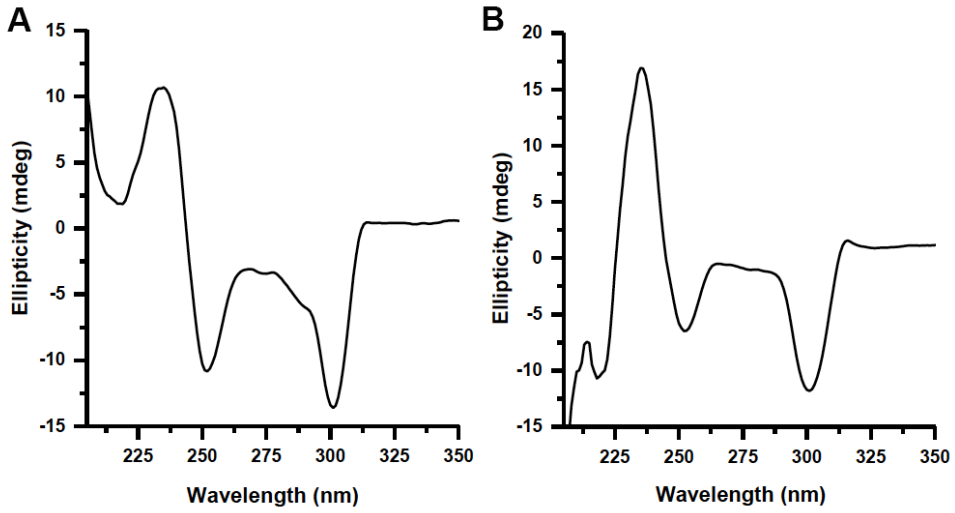

Figure 3-14: CD spectra of (A) self-assembly of K-TB, and (B) ELDKWAK-TB (50 μM, aged at 0 min).

The time-dependent CD studies were done to investigate any change in the supramolecular arrangement and the stability of the nanotubes upon co-assembly. The stock solution (1 mg/mL) that was prepared for SEM imaging was diluted to 50 µM in water to record the CD spectra. The CD signals of unstirred aqueous solutions of K-TB, ELDKWAK-TB and solution A were recorded from 350 to 205 nm, at time ranging from 0 h to 168 h (Figure 3-15).

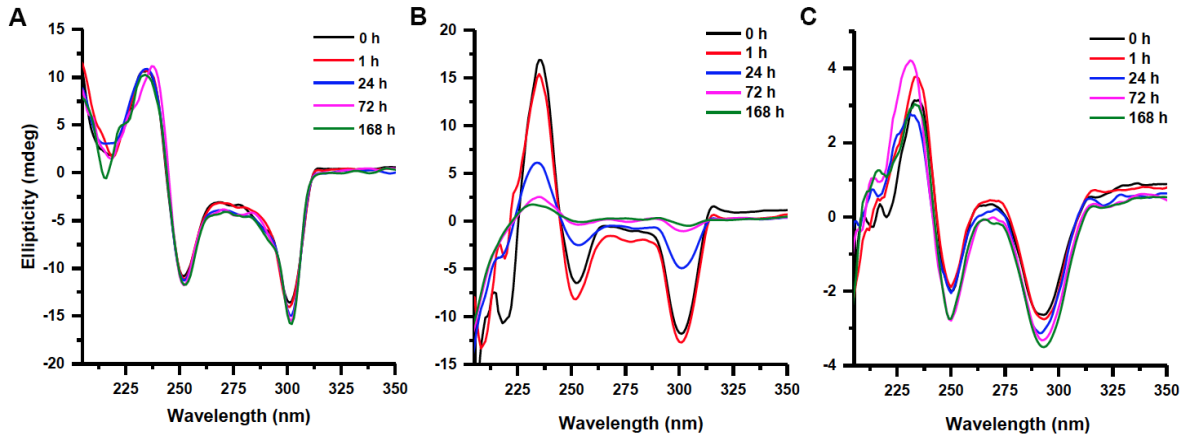

Figure 3-15: Time-dependent CD study of (A) K-TB, (B) ELDKWAK-TB, and (C) solution A, at a concentration of 50 µM.

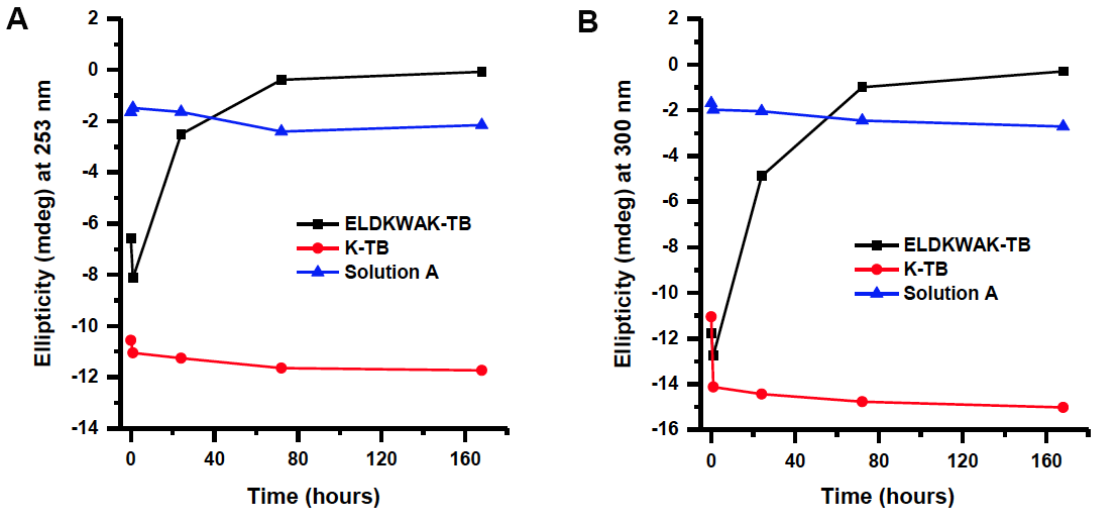

Figure 3-16: Time-dependent CD study of K-TB and ELDKWAK-TB, and solution A, at a concentration of 50 µM, at 253 nm (A) and 300 nm (B)

The CD profile of self-assembled K-TB (Figure 3-15A and 3-16) displayed strong negative CD signal of -10.6 and -11.1 mdeg at 253 and 300 nm respectively at 0 min. The negative CD signal at 253 nm did not show any significant change while it increased from -11.1 to -15.0 mdeg at 300 nm with increase in time from 0 h to 168 h. The bisignate Cotton effect did not reveal considerable growth of RNTs, which suggested that the self-assembly of K-TB was fast.

The CD spectra of self-assembled ELDKWAK-TB at 0 min (Figure 3-15B and 3-16) showed CD signal of -6.6 and -11.8 mdeg at 253 and 300 nm, respectively. The negative CD intensity increased to -8.1 and -12.8 mdeg at 253 and 300 nm, respectively, after 1 h of the self-assembly process. The intensity of the CD signal, however showed a considerable decrease after 1 h of the self-assembly (from 1 h to 168 h). This decrease in the CD intensity can be related to the possible aggregation of the nanotubes as suggested in the SEM imaging in Figure 3-12, hence losing the preferential supramolecular twist.

Solution A gave a CD signal of -2.0 and -2.6 mdeg at 250 and 294 nm, respectively that is much lower than that of K-TB RNTs at 0 h (Figure 3-15C and 3-16). RNTs in Solution A have a majority portion of K-TB, yet their CD signal is lower than the CD signal of K-TB. This implies that K-TB is not undergoing a homogenous self-assembly in solution A, or else it would have produced a CD intensity of about -9 mdeg (based on 90% of -10.6 and -11.1 mdeg at 253 and 300 nm).

Solution A co-assembled RNTs showed slow but steady growth over time, unlike the self-assembled ELDKWAK-TB RNTs, which undergoes a sharp decrease in CD signal with time. This suggested that co-assembly leads to the formation of stable RNTs with steady growth over time.

3.2.5. Co-assembly of TB-FITC with TBL (Solution B)

FITC-functionalized twin G∧C (FITC-TB)[15] and the twin G∧C monomer with an aminobutyl group (TBL)[15] has previously been synthesized and characterized. The FITC-TB has very low solubility in water (less than 0.1 mg/mL) due to which self-assembly under aqueous condition is a challenging process. While RNTs can be obtained for FITC-TB, the RNTs are not stable and undergo aggregation. The solubility of FITC-TB in water can be improved by its co-assembly with TBL, leading to formation of the stable RNTs. This process resulted into well-dispersed and more stable RNTs, compared to homogenous FITC-TB RNTs.

A stock solution of 0.5 mg/mL of FITC-TB with TBL in a molar ratio of 1:15 was prepared in water. The solution was then sonicated and heated several times. The solution was then diluted to to 0.025 mg/mL and 0.0125 mg/mL in water. The SEM imaging (Figure 3-17) revealed the formation of short, well-dispersed nanostructures. The nanotubes were stable for a period of 6 months.

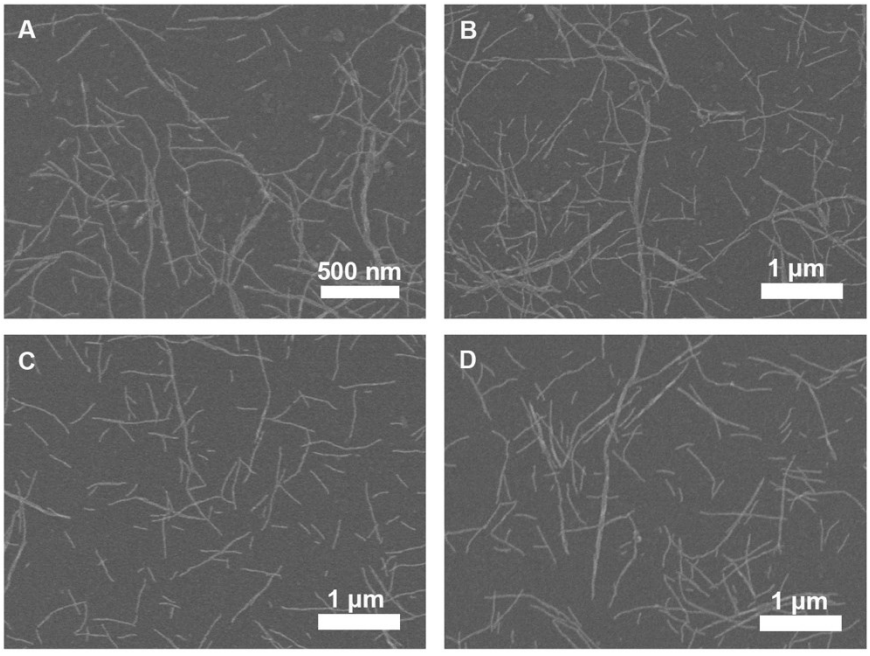

Figure 3-17: SEM images of FITC-TB co-assembled with TBL in the molar ratio 1:15 (A and B at concentration 0.025 mg/mL and 0.0125, and C and D at concentration 0.0125 mg/mL; aged for 30 d).

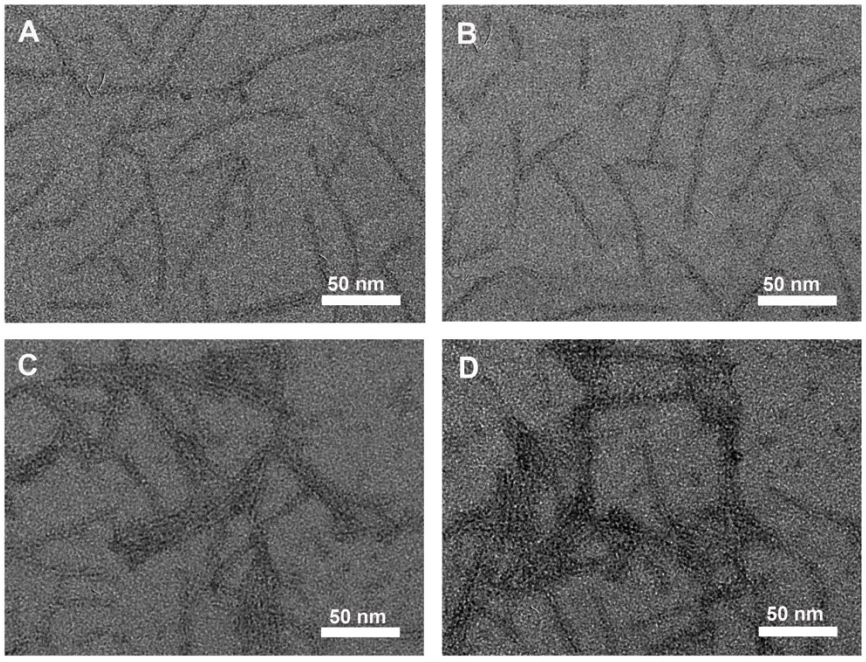

Figure 3-18: TEM images of FITC-TB co-assembled with TBL in the molar ratio 1:15 (0.025 mg/ml, aged for 30 d).

The diluted solution (0.025 mg/mL) of FITC-TB/TBL (1:15) (designated as solution B) was also used for TEM and AFM imaging. The TEM (Figure 3-18) and AFM images (Figure 3-19) revealed and confirmed the well-dispersed, short nanostructures as visualized by the SEM imaging.

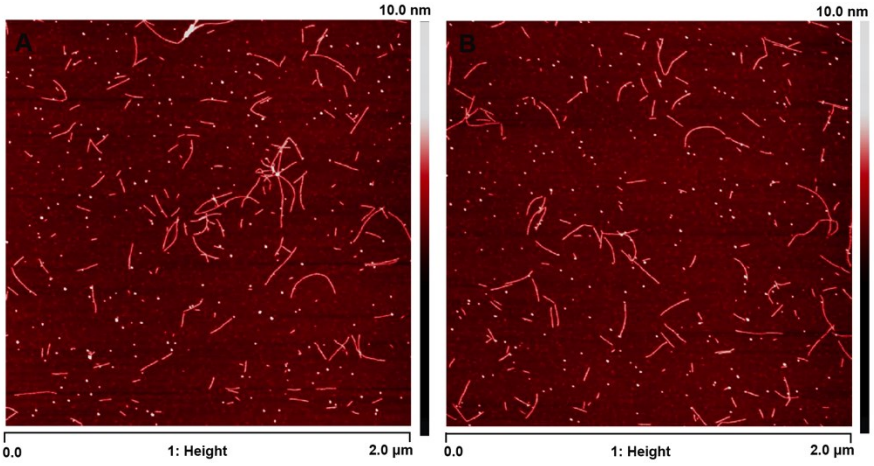

Figure 3-19: AFM images of FITC-TB co-assembled with TBL in the molar ratio 1:15 (0.025 mg/mL, aged for 30 d) using mica substrate.

3.2.5. Co-mixing of FITC-TB/TBL (1:15) with K-TB/ELDKWAK-TB (9:1) in the ratio 10:1

The fluorescent RNT construct with an HIV-1 epitope was developed by co-mixing Solution A with Solution B. A stock solution of 1 mg/mL RNTs was prepared by adding 80 µL of Solution B to 4 µL Solution A RNT solution as shown in Table 3-1. The solution was then diluted in water to 0.05 mg/mL and sonicated for 2 min. The SEM imaging in Figure 3-20 illustrated the morphology of RNTs in solution B at 1 h and 1 d. While there is a change in the morphology upon the addition of Solution A RNTs, the resulting mixture still produced stable RNTs, as required for our study (Chapter 4).

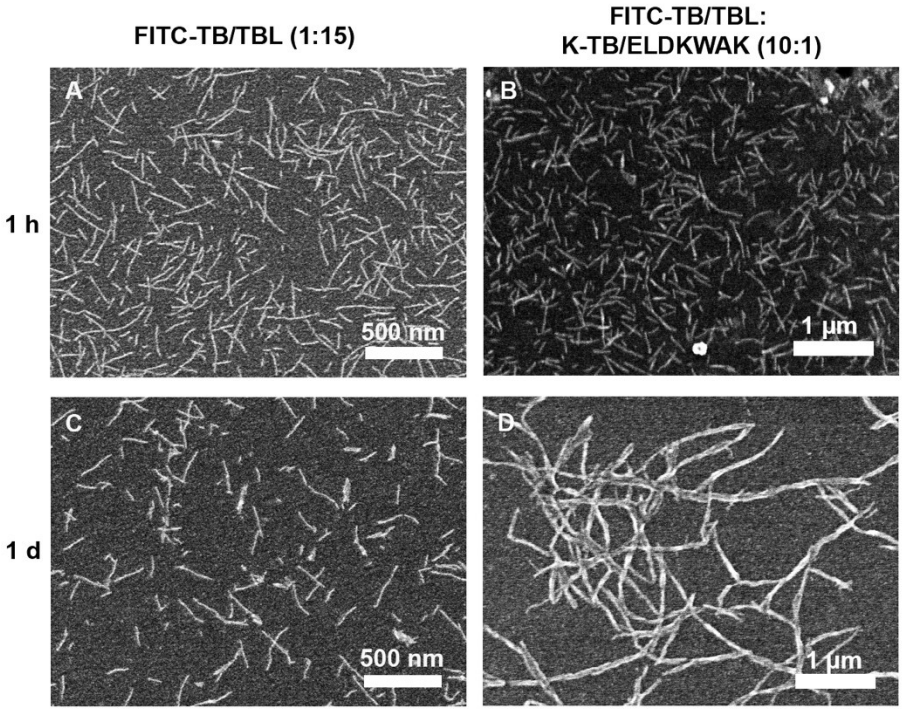

Figure 3-20: SEM images of (A and C) FITC-TB/TBL (1:15) (B and D) co-mixing of FITC-TB/TBL (1:15) with K-TB/ELDKWAK-TB (9:1) in a ratio of 10:1 (0.05 mg/mL).

3.3. Conclusion

In this chapter, we described the process of self-assembly of TB-K that resulted in the formation of stable nanotubular structures. The RNTs formed by K-TB were characterized by SEM, TEM and AFM imaging. We also established that co-assembly of ELDKWAK-TB with K-TB would promote ELDKWAK-TB to assemble into stable hybrid nanotubes, which otherwise formed large aggregates. The morphology of the RNTs formed by the co-assembly of K-TB with ELDKWAK-TB in a molar ratio 9:1 was studied using microscopic techniques (SEM, TEM and AFM). A detailed study of time-dependence gave the evidence of a change in the morphology of K-TB and K-TB/ELDKWAK-TB RNTs with time using SEM imaging, but did not confirm the co-assembly process. The CD studies were used to confirm the co-assembly between K-TB and K-TB/ELDKWAK-TB, which gave evidence of slow, yet a steady growth of the heterogenous RNTs. This was in agreement with an expected lower degree of self-assembly compared to the homogenous K-TB RNTs.

We further studied the co-assembly of FITC-TB co-assembled with TBL in a molar ratio 1:15 to form fluorescent-labeled RNTs, as the self-assembly of FITC-TB alone did not result in stable RNTs. The FITC-TB/TBL RNTs were characterized by SEM, TEM and AFM imaging. These RNTs were then co-mixed with K-TB/ELDKWAK-TB (9:1) in the weight ratio of 10:1 and were visualized using SEM imaging. The fluorescently-labeled K-TB/ELDKWAK-TB RNTs construct were used for the *in vitro* cell studies (Chapter 4).

3.4. Experimental design

3.4.1. Characterization by microscopy

A stock solution of 1 mg/mL of peptide-functionalized twin G∧C motif was prepared in water using different conditions of heat and sonication to form RNTs. The stock solution was diluted in water. A drop of the diluted solution of the RNT was deposited on the 400 square-mesh copper grids right after dilution and was dried by blotting with a filter paper after 30 s. The grids were air dried and then heated on a hotplate (70 °C) for 10 min prior to imaging in order to remove any residual solvent. SEM images were obtained at 30 kV accelerating voltage, 20 μA and a working distance of 5-8 mm on a high resolution Hitachi S-4800 cold field emission SEM.

TEM samples for RNTs were prepared by adding a droplet of the diluted RNT solution on the 400 square-mesh copper grid. After 30 s, the sample was blotted and air-dried. A droplet of 2% aqueous solution of uranyl acetate was deposited on the grid to stain the RNTs. The stain was dried with a filter paper after 2 min and the grid was heated on a hot plate for 10 min. JEOL 2200 FS TEM–200kV Schottky field emission instrument equipped with an in-column omega filter was used for TEM imaging. Bright field TEM images were acquired using energy filtered zero loss beams (slit width 10ev).

For AFM measurement, clean HOPG and mica substrates (1 x 1 cm^2) were prepared and the RNT samples were deposited by spin coating at 2500 rpm for 30 s to remove the excess solution from the surface of the sample.

The morphology of the sample was visualized using a Digital Instruments/Veeco Instruments MultiMode Nanoscope IV AFM equipped with an E scanner. For optimal height profile, silicon cantilevers (MikroMasch USA, Inc.) with low spring constants of 4.5 N/m were used in tapping mode (TM-AFM). To obtain a clear image from the surface, low scan rate (0.5-1 Hz) and amplitude setpoint of 1 V were chosen in our measurement.

3.4.2. Circular Dichroism (CD) spectroscopy

The CD spectra for all the samples were recorded on a JASCO J-810 spectropolarimeter. The stock solutions of all the samples were prepared at a concentration of 1 mg/mL in water. After subjecting the stock solution to the required conditions of heat and sonication, they were diluted to 50 μM in water. The CD spectra were recorded at different aging periods and were scanned from 350-205 nm at a rate of 100 nm/min. A quartz cuvette of sample volume 3-5 mL and a pathlength of 1 cm was chosen for CD measurement.

3.4.3. Sample preparation of K-TB

K-TB has previously been made in Fenniri's group using the standard Fmoc-based SPPS. A stock solution of 1 mg/mL (0.786 mM) of TB-K was prepared in water by sonicating for 5 min and heating for 30 s. This procedure was repeated twice. The solution was then diluted to 0.05 mg/mL (0.039 mM) in water and allowed to age for 1 h and 1 d, for SEM imaging. The stock solution was diluted to 0.0125 mg/mL (9 μM) for TEM imaging. The K-TB solution was diluted to 50 μM in water for the CD studies.

3.4.4. Sample preparation of K-TB co-assembled with ELDKWAK-TB (9:1)

A stock solution of 1 mg/mL (0.743 mM) of K-TB co-assembled with ELDKWAK-TB in the molar ratio 9:1 was prepared in water by repeatedly sonicating for 5 min and heating for 30 s (three times). The stock solution was allowed to age for 3 d and diluted to 0.05 mg/mL (0.037 mM) in water for sample preparation of SEM, TEM and AFM imaging. The solution was diluted to 50 μM in water to obtain the CD spectra.

3.4.5. Time-dependent CD study of K-TB and K-TB/ELDKWAK-TB (9:1)

The samples for K-TB and K-TB/ELDKWAK-TB (9:1) were prepared in water as mentioned above. The SEM images and the CD spectra were obtained for these samples at different aging periods of 0 min, 1 h, 1 d, 3 d and 7 d.

3.4.6. Sample preparation of FITC-TB co-assembled with TBL (1:15)

A stock solution of 0.5 mg/mL of FITC-TB co-assembled with TBL in the molar ratio 1:15 was prepared in water by dissolving 0.9 mg TBL and 0.1 mg of FITC-TB in 2 mL of water. The solution was then heated and sonicated repeatedly for several times. The stock solution was the diluted to 0.025 mg/mL and 0.0125 mg/mL in water for SEM imaging.

3.4.7. Sample preparation of co-mixing FITC-TB/TBL (1:15) with K-TB/ ELDKWAK-TB (9:1) in the volume ratio (10:1)

The stock solution of FITC-TB co-assembled with TBL (1:15) was co-mixed with the stock solution of K-TB/ELDKWAK-TB (9:1) in the weight ratio of 10:1 with the final concentration of 1 mg/mL and was sonicated for 2 min. The solution was then diluted to 0.05 mg/mL for SEM imaging and to 50 μM for CD studies.

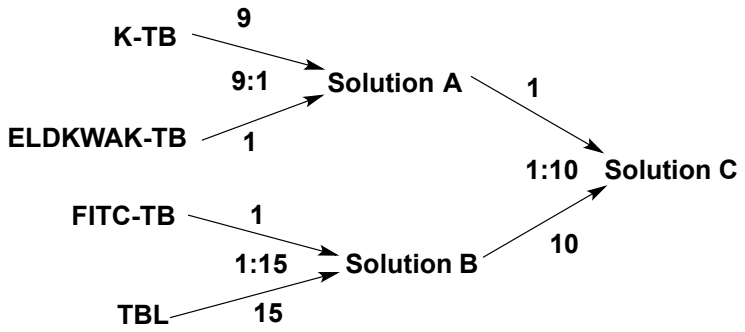

Table 3-1: Summary of the ratio of the individual components of the co-mixed RNTs.

3.4.8. Sample preparation of co-mixing FITC-TB/TBL (1:15) with K-TB/ELDKWAK-TB (9:1) in the ratio (10:1)

The stock solution of FITC-TB co-assembled with TBL (1:15) was co-mixed with the stock solution of K-TB/ELDKWAK-TB (9:1) in the ratio of 10:1 with the final concentration of 1 mg/mL and was sonicated for 2 min.

3.4.9. Time-dependent SEM and CD study of co-mixing FITC-TB/TBL (1:15) with K-TB/ELDKWAK-TB (9:1) in the volume ratio of 10:1

The samples that were prepared for the SEM and the CD studies were allowed to age for 1 h and 1 d for studying the behavior of the RNTs with respect to time. SEM imaging was done on these RNT samples at different aging periods.

3.5. References

1. Chun AL, Moralez JG, Webster TJ and Fenniri H. Helical rosette nanotubes: a biomimetic coating for orthopedics? *Biomaterials*. **2005**. 26(35): 7304-9.
2. Zhang L, Hemraz UD, Fenniri H and Webster TJ. Tuning cell adhesion on titanium with osteogenic rosette nanotubes. *J. Biomed. Mater. Res. A*. **2010**. 95(2): 550-63.
3. (a) Fenniri H, Mathivanan P, Vidale KL, Sherman DM, Hallenga K, Wood KV and Stowell JG. Helical rosette nanotubes: Design, self-assembly and characterization. *J. Am. Chem. Soc*. **2001**. 123: 3854-3855. (b) Fenniri H, Deng B-L and Ribbe AE. Helical rosette nanotubes with tunable chiroptical properties. *J. Am. Chem. Soc*. **2002**. 124: 11064-11072. (c) Fenniri H, Deng B-L, Ribbe AE, Hallenga, K, Jacob J and Thiyagarajan P. Entropically driven self-assembly of multichannel rosette nanotubes. *Proc. Natl. Acad. Sci. U.S.A*. **2002**. 99: 6487-6492.
4. El-Bakkari M, Beingessner RL, Alshamsan A, Cho JY and Fenniri H. Electrostatic and steric effect of peptides functionalized on self-assembled rosette nanotubes. *Mater. Res. Soc. Symp. Proc*. **2011**. 1316
5. Hemraz UD, El-Bakkari M, Yamazaki T, Cho JY, Beingessner RL and Fenniri H. "Chiromers: Conformation-driven mirror-image supramolecular chirality isomerism identified in a new class of helical rosette nanotubes," *Nanoscale*. **2014**.
6. Moralez JG, Raez J, Yamazaki T, Motkuri RK, Kovalenko A, Fenniri H. Helical rosette nanotubes with tunable stability and hierarchy. *J. Am. Chem. Soc*. **2005**. 127(23): 8307-9.
7. Suri SS, Rakotondradany F, Myles AJ, Fenniri H, Singh B. The role of RGD-tagged helical rosette nanotubes in the induction of inflammation and apoptosis in human lung adenocarcinoma cells through the P38 MAPK pathway. *Biomaterials*. **2009**. 30(17): 3084-90.

8. Suri SS, Mills S, Aulakh GK, Rakotondradany F, Fenniri H and Singh B. RGD-tagged helical rosette nanotubes aggravate acute lipopolysaccharide-induced lung inflammation. *Int. J. Nanomedicine*. **2011**. 6: 3113-23.
9. Le MH, Suri SS, Rakotondradany F, Fenniri H, Singh B. Rosette nanotubes inhibit bovine neutrophil chemotaxis. *Vet. Res*. **2010**. 41(5): 7.
10. Zhang L, Hemraz UD, Fenniri H, Webster TJ. Tuning cell adhesion on titanium with osteogenic rosette nanotubes. *J. Biomed. Mater. Res. A*. **2010**. 95(2): 550-63.
11. SEM, TEM and AFM imaging were done by Dr. Jae-Young Cho.
12. Berova N, Nakanishi K, Woody RW. Circular Dichroism, Principles and Applications. Wiley-VCH, New York, **2000**.
13. Fan Z, Govorov AO. Plasmonic circular dichroism of chiral metal nanoparticle assemblies. *Nano Lett*. **2010**. 10: 2580-2587.
14. Kuzyk A, *et al*. DNA-based self-assembly of chiral plasmonic nanostructures with tailored optical response. *Nature.* **2012**. 483: 311-314.
15. FITC-TB and TBL was synthesized and characterized by Dr. Usha D. Hemraz.

Chapter 4

Biological Studies of Rosette Nanotubes for HIV-1 Therapy

4.1. Introduction

For the past three decades, the development of an effective vaccine to prevent the human immunodeficiency virus (HIV) infection have been a major challenge for scientists. The genetic diversity of the HIV-1 strains around the globe and their continuous evolution in the populations that give them a mutational escape from the immune responses is the key obstacle in the HIV-1 vaccine development.[1-6] To date, there are 13 different subtypes and sub-sub-types of HIV-1 strain known, distributed according to the geographical or epidemiological basis. There is 15-20% of variation in the envelope proteins within the subtype and up to 35% variation between the subtype.[1,2,7] This genetic variation in the HIV-1 sequences poses a hurdle in the design of a viable global vaccine.

A recent breakthrough in the HIV research was the RV144 Thai trial that proved to the world that a vaccination against HIV-1 strain might be effective in lowering the risk of acquiring an HIV-1 infection, although the results were very marginal.[8] Subsequently, a number of broadly potent neutralizing antibodies specific to various epitopes of the HIV-1 envelope (Env) were characterized.[9] Yet, none of the vaccines developed were effective in stimulating the desired immune response against the HIV-1 strains. Inducing the required immune response still remains a major challenge for researchers. A study by Barouch *et al*. reported that the development of the HIV-1 mosaic vaccine SHIV-SF162P3, provided partial protection to the rhesus macaques against the simian-human immunodeficiency virus by overcoming the limitations due to the genetic diversity of the strain.[10]

A study based on HIV-1 neutralization assays reveals that the sera of 25% of the individuals carrying HIV can generate broadly neutralizing antibodies in their body during the course of HIV infection.[11] Out of the three monoclonal neutralizing antibodies that specifically bind to the CD4 binding site, one of them designated as VRC01, can neutralize more than 90% of the naturally occurring strains on expression.[12] The crystal structure of VRC01 in complex with HIV-1 glycoprotein 120 (gp120) protein was determined indicating that the antibody directly binds to the initial CD4 attachment site of the virus. The specific binding

of VRC01 to the envelope protein accounts for its broad neutralizing ability.[13] In order to develop a vaccine that has the ability to illicit the production of VRC01 antibodies, it is important to understand their mechanism of generation. It has been observed that individuals infected with HIV-1 have large amounts of gp120 and it takes several years for their immune system to make VRC01-like antibodies. The reason for the delay in producing antibodies is still unknown.[14,15]

The alternative forms of protein and methods of their exposure to the immune system have been developed to induce maximal binding of these modified proteins to the CD4 binding site.[16] This approach was also used to target other sites on the HIV-1 Env, specifically the HIV-1 gp41. Neutralizing monoclonal antibodies like 2F5 have been identified to be specific to a HIV-1 gp41 epitope that has one of the few conserved sequences, which can allow broad neutralization of the various strains of HIV-1.[17]

A number of strategies have been designed to reduce the risk of infection of HIV-1 strains.[18] Virus-like particles (VLPs) is one of strategies used to develop vaccines against hepatitis B and HIV. VLPs are nanoparticles that do not use DNA or RNA from the virus but have the ability to reproduce the structure and size of the actual virus by the engineered method to generate modified antigens. These antigens displayed on the VLPs can be taken up by the antigen-presenting cells (APCs) and illicit the immune responses after the required immunization.[18-20] Various attempts have been made to develop vaccines for HIV by immunizing the individuals carrying HIV, with inactivated viruses, peptides, viral vectors and *ex vivo* generated dendritic cells (DCs).[21-23] A study involving DCs loaded with different HIV strains suggested that DC-based vaccines are considered to be an important part of modern strategy for vaccine development against HIV infection.[24] Nanotechnology have been used in the past few years to overcome the challenges faced by scientists to develop diagnostics and therapeutics for HIV/AIDS.

In the present study we aim to develop a therapy against HIV-1 by using rosette nanotubes (RNTs) as the nano-carrier for the HIV-1 gp41 epitope specific for the

neutralizing antibody 2F5. To achieve this objective, the twin G∧C motifs were functionalized with the peptide sequence ELDKWA-the epitope on the HIV-1 gp41 specific for 2F5. The synthesis and characterization of the twin G∧C base with ELDKWAK (ELDKWAK-TB, lysine incorporated between the peptide ELDKWA and the twin G∧C base), and its self-assembly to form RNTs in aqueous environment was studied in Chapter 2. The SEM images in Figure 4-1A showed the aggregate formation by the self-assembly process of ELDKWAK-TB that can be avoided by co-assembling with lysine-functionalized twin G∧C motif, K-TB (Figure 4-1C).

In the previous chapter, we focused on the co-assembly studies of the G∧C motifs functionalized with different sequences in order to develop a fluorophore-labeled RNT construct for the cell uptake study using the DCs. In this study we first co-assembled the ELDKWAK-TB RNTs with the TB-K in the molar ratio of 1:9 (Solution A) (Figure 4-1C) to form a stable twin base RNT system. This ELDKWAK-TB/K-TB RNT system was then co-mixed with a fluorescent RNT system, FITC-TB/TBL (Figure 4-1D). FITC-TB/TBL RNTs were formed by co-assembling FITC functionalized twin G∧C motif (FITC-TB) with twin-base linker (TBL) in the molar ratio of 1:15 (Solution B), as FITC-TB does not form stable RNTs in aqueous conditions.

In this chapter we study the biological properties of the ELDKWAK-TB/K-TB RNTs co-mixed with FITC-TB/TBL system by treating the dendritic cell line JAWS II with the RNT construct. We also studied the binding of the ELDKWAK-TB /K-TB RNTs to the neutralizing antibody 2F5 specific for the HIV-1 gp41 epitope.

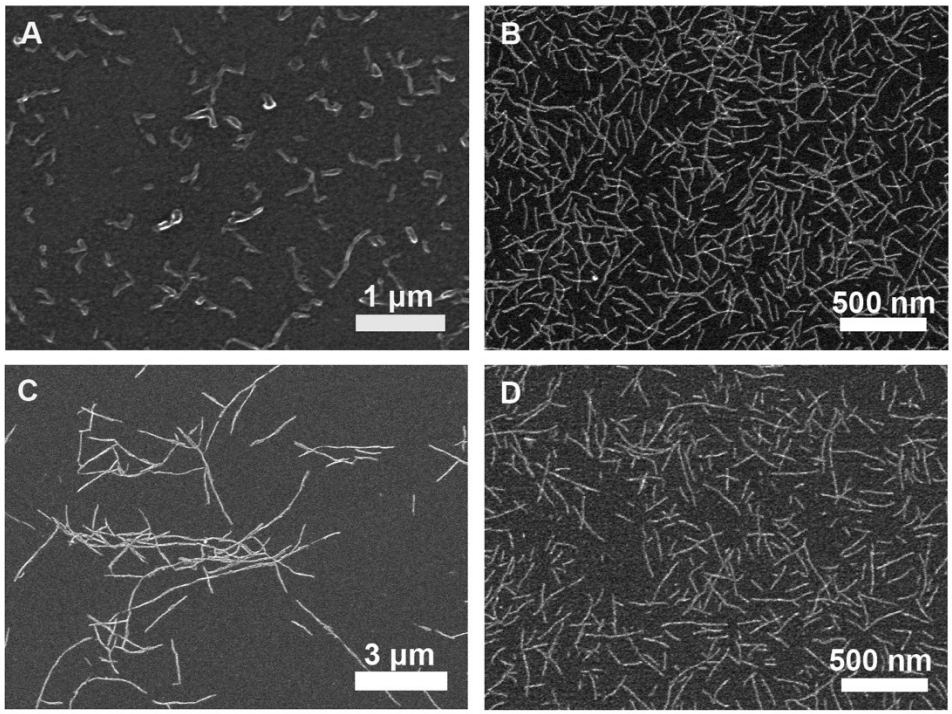

Figure 4-1: SEM images of RNTs formed in water by (A) self-assembly of ELDKWAK-TB (B) self-assembly of K-TB (C) co-assembly of K-TB with ELDKWAK-TB in the molar ratio 9:1 (D) co-mixing of FITC-TB/TBL (1:15) with K-TB/ELDKWAK-TB (9:1) in the weight ratio of 1:10.

4.2. Results and Discussion

To study biological applications of RNTs, monocytic immature dendritic cell line JAWS II was cultured using alpha minimum essential medium (AMEM).

4.2.1. Study of concentration-dependence of cellular uptake of RNTs

The development of the RNTs constituting of FITC-TB/TBL (1:15) and K-TB/ ELDKWAK-TB (9:1) (Figure 4-1) were studied and confirmed in chapter 3. We studied the uptake of the fluorescent RNT construct in a concentration dependent manner by JAWS II cells via confocal fluorescence microscopy.

Confocal microscopy has been used in biomedical research to study the distribution and the localization of various molecules inside the cells and tissues. A confocal microscope has the advantage over the conventional microscope as it produces images with much better resolution and contrast along with enhanced sentivity.[25]

In order to study the uptake of Solution A (K-TB/ELDKWAK-TB (9:1)) RNTs by the JAWS II dendritic cells, they were co-mixed with Solution B (FITC-TB/TBL (1:15)) RNTs in the ratio of 10:1 and 1:10 (Table 4-1) and sonicated for 2 min prior to their treatment into the DCs. The cells were then incubated for 24 hours after the transfection of 0.25, 0.5 and 1 μg/mL (μM) of the Solution B RNTs and Solution B co-mixed with Solution A in the ratio 1:10 and 10:1.

The confocal images in Figure 4-2 suggested an obvious increase in the fluorescence signal with the increase in the concentration of the RNTs encapsulated in the cells. The images also showed an increased fluorescence signal with the greater amount of FITC-TB/TBL in the RNTs construct.

RNT Sample	Volume of Solution B, 0.5 mg/ml	Volume of Solution A, 1 mg/ml	Ratio
Solution B: Solution A	80 µl	4 µl	10:1
Solution B: Solution A	8 µl	40 µl	1:10

Table 4-1: Summary of the ratio of the individual components of the co-mixed RNTs.

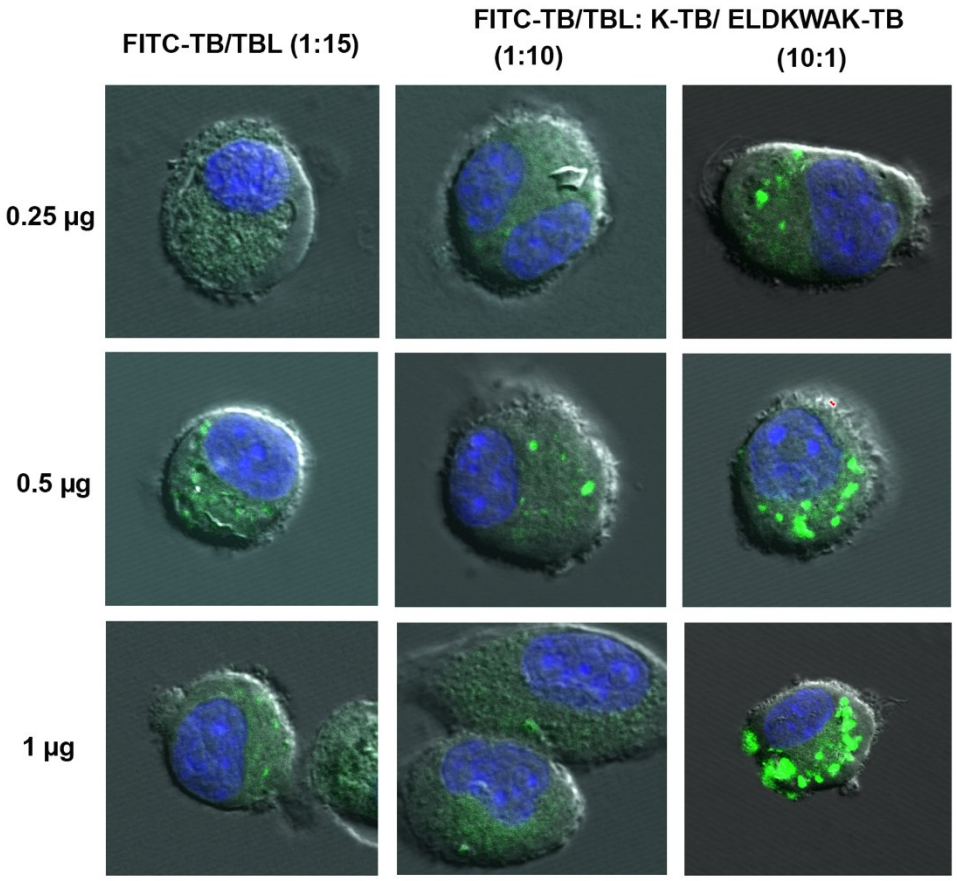

Figure 4-2: Confocal imaging and superposition of three images of cellular uptake of RNTs at different concentrations (0.25, 0.5 and 1 µg/mL) in the JAWS II cells. Blue: nuclei (DAPI), green: FITC-labeled RNTs.

A 3D image of the DCs with encapsulated RNTs was obtained to further confirm the uptake of the RNTs by the Z-stack analysis. The Z-stack analysis is done by

capturing the image of slices of the cells and then stacking them on top of each other to get a 3D image. The green fluorescent signal in the 3D confocal image in Figure 4-3 indicated the green colored RNTs surrounding the blue nucleus in the cells (the nucleus is stained with DAPI). This justified that the RNTs are present inside the cells.

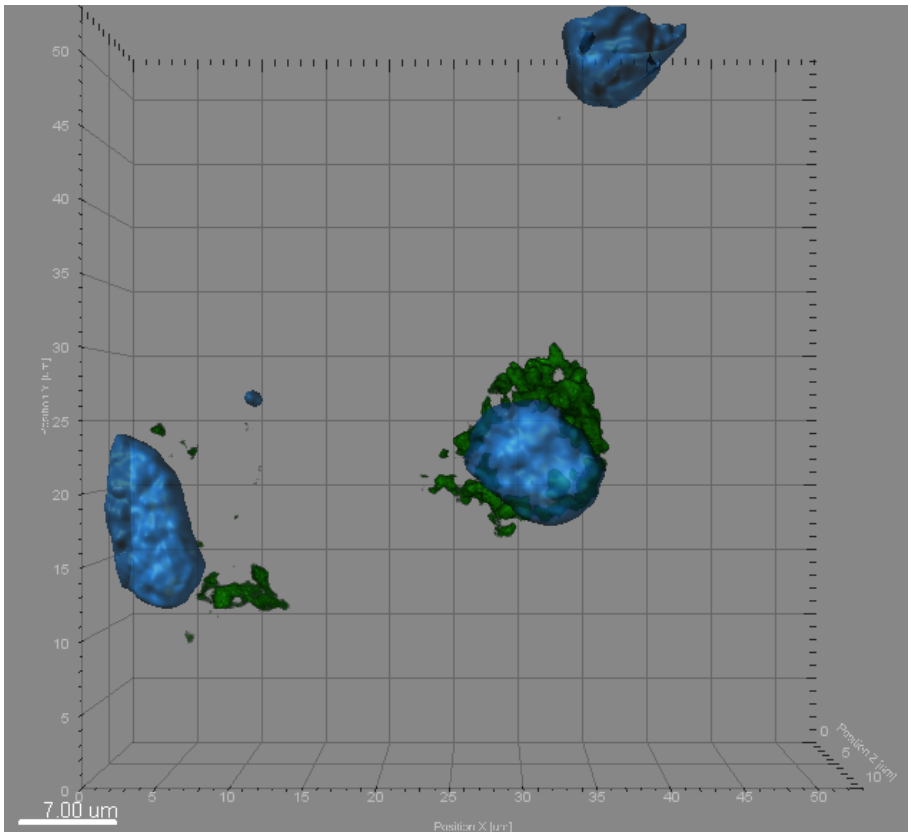

Figure 4-3: 3D confocal images of JAWS II cells transfected with FITC-labeled RNTs for 24 h. Blue: nuclei (DAPI), green: FITC-labeled RNTs. Scale bar = 7 µm.

4.2.2. Study of time-dependence of cellular uptake of RNTs

A time study for the cellular encapsulation of RNTs was conducted to examine the effect of time on the uptake of RNTs by the cells. DCs were transfected with 1 μg/ml RNTs comprised of Solution B and Solution B co-mixed with Solution A in the ratio 1:10 and 10:1. The cells were incubated for different periods of time, 3, 6, 12, 24, 36 and 48 h after treatment with RNTs. The confocal images of dendritic cells (Figure 4-3) revealed an elevated green fluorescent signal, indicating an increase in the uptake of RNTs by the cells. Incubation of the cells for 3-6 h after the transfection of RNTs showed minimal uptake of RNTs. The cellular uptake of nanotubes increased progressively from 12-48 h of incubation by the cells. The confocal imaging studies revealed that 24 h of incubation of cells with RNTs was sufficient for cellular uptake of the RNTs.

The results that were obtained from the time study of cellular encapsulation of RNTs by confocal imaging were confirmed by the quantification measurement of fluorescence in the cells by flow cytometry. Flow cytometry is a laser-based technique that is used in biotechnology for cell counting, cell sorting and biomarker detection. Flow cytometer can detect the fluorescence signal in the fixed cells and yield a histogram plot, as shown in Figure 4-4. The dendritic cells were treated with 1 μg/ml each of Solution B RNTs and Solution B RNTs co-mixed with Solution A RNTs in the ratio 1:10 and 10:1, similar to the confocal imaging experiments. The cells were treated with RNTs, incubated for different time periods and were then fixed. Since a small number of cells in flow cytometry experiment required longer times for fluorescence measurement. A large population of treated cells was used as compared to confocal imaging for smooth fluorescence measurement. The fluorescence measurement of the RNTs inside the cells was carried out within 24 hours for optimum flow cytometry results.

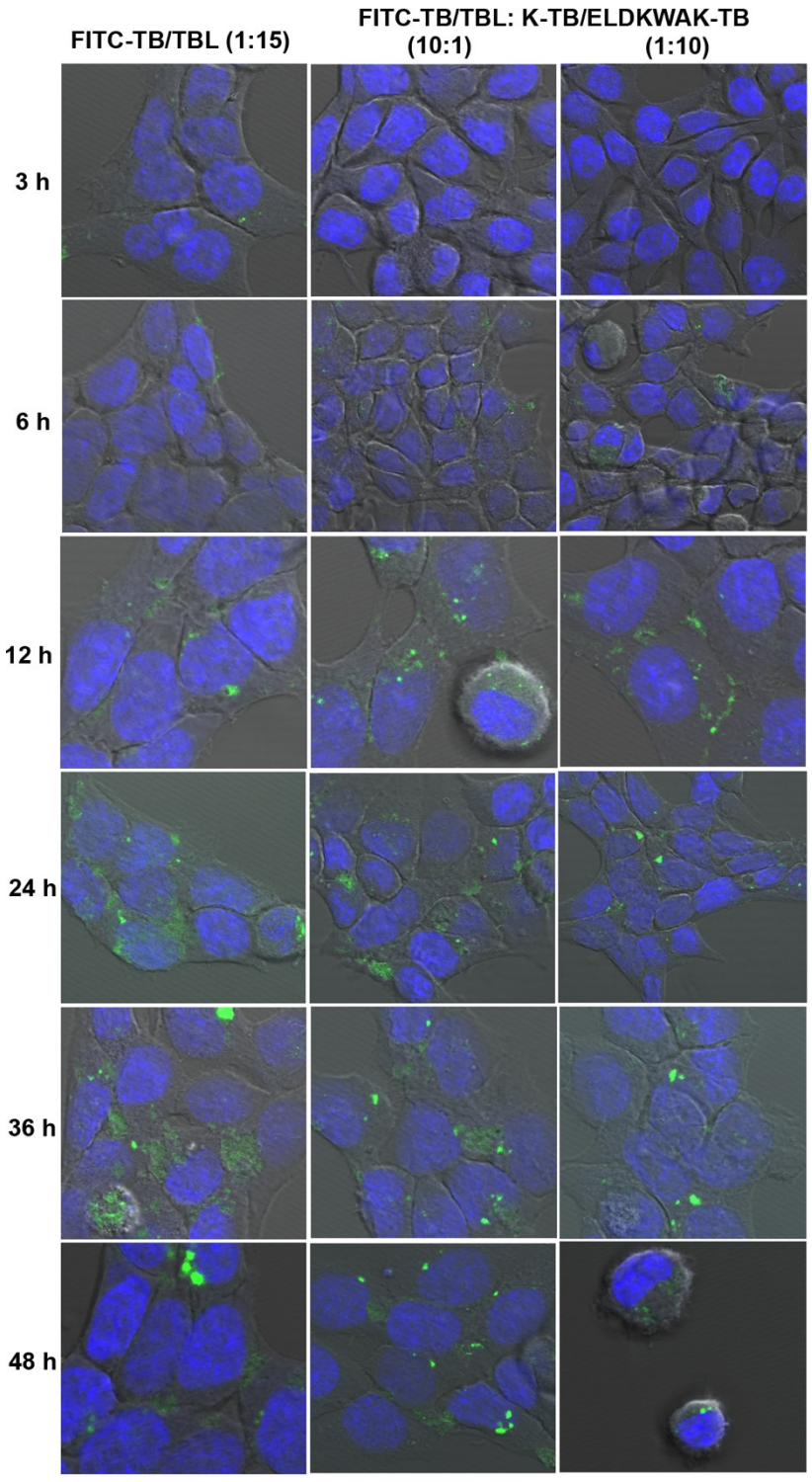

Figure 4-4: Confocal imaging of cellular uptake of RNTs at different times (3, 6, 12, 24, 36, 48 h at 1 μg/mL concentration of RNTs) in the JAWS II cells. Blue: nuclei (DAPI), green: FITC-labeled RNTs.

The histogram plots obtained from the flow cytometry measurement were compared to the confocal imaging data. The histogram plots in Figure 4-5 suggested that the quantified fluorescence measurement showed minimal uptake of fluorescent RNTs at 3 h and the encapsulation of RNTs in the cells increased with treatment groups that were incubated for 12 h. The histogram plot deviated towards the right side (region of high fluorescence intensity), indicating higher fluorescence at 24-48 h. These results were comparable to the confocal images that indicated more fluorescence with Solution B RNTs and Solution B co-mixed with Solution A RNTs in the ratio 10:1 as compared to 1:10 ratio.

The flow cytometry results were in agreement with the time-dependent increase in the uptake of the RNTs from 3-48 h by the confocal imaging.

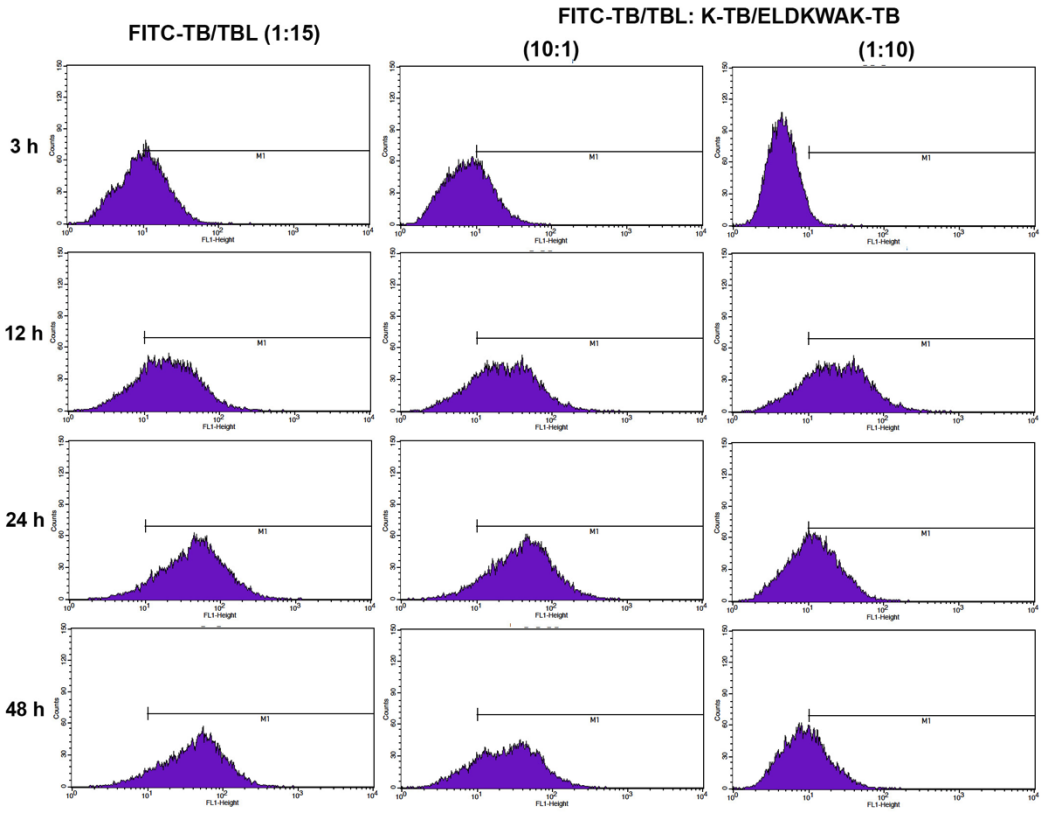

Figure 4-5: Histogram plots of measuring the cellular uptake of RNTs at different times (3, 12, 24, 36, 48 h at 1 μg/ml concentration of RNTs) in the JAWS II cells.

4.2.3. Effect of co-mixing of RGDSK-TB and DRGSK-TB on the cellular uptake of the FITC-labeled K-TB/ELDKWAK-TB RNTs

We discussed in Chapter 2 that peptide sequence RGD aids in promoting cell-adhesion and its scrambled version, DRG, would be used as a control. Although Solution A RNTs showed significant encapsulation, we were interested in exploring whether this encapsulation can be enhanced by the cell-promoting adhesive nanocarriers. As such, RGDSK-TB and its scrambled version DRGSK-TB were synthesized and self-assembled into RNTs. These RNTs were added to the Solution A co-mixed with Solution B RNTs to study their effect on the encapsulation. The RGDSK-TB and DRGSK-TB RNTs were added to the RNTs formed by Solution B co-mixed with Solution A RNTs in different ratios as shown in Table 4-2.

RNT Sample	Volume of Solution B, 0.5 mg/ml	Volume of Solution A, 1 mg/ml	Volume of RGDSK-TB or DRGSK-TB, 1 mg/ml	Ratio
Solution B: Solution A: RGDSK-TB or DRGSK-TB	8 µl	40 µl	4 µl	1:10:1
Solution B: Solution A: RGDSK-TB or DRGSK-TB	80 µl	4 µl	4 µl	10:1:1

Table 4-2: Summary of the ratio of the individual components of the co-mixed RNTs.

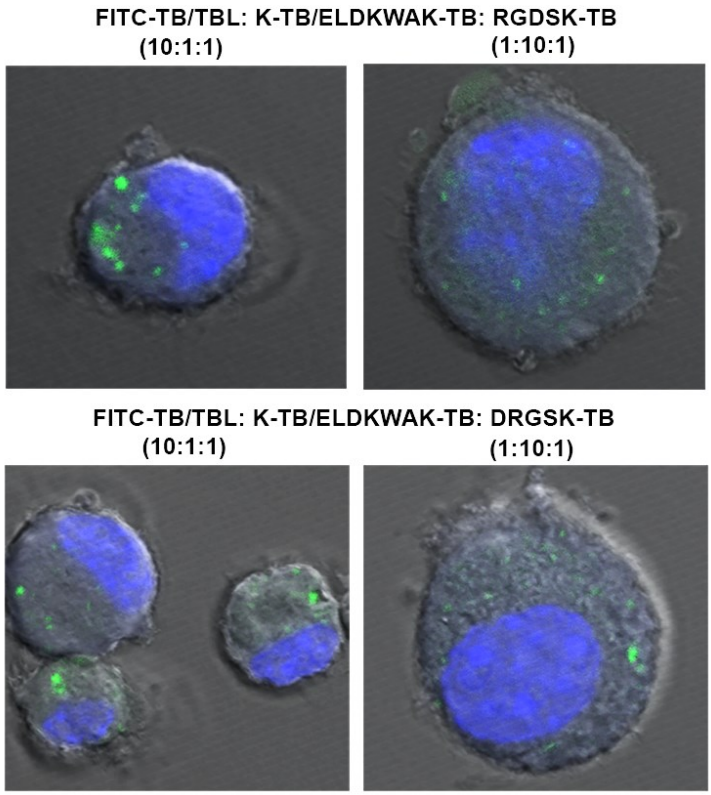

Figure 4-6: Confocal images of the effect of RGDSK-TB and DRGSK-TB on the cellular uptake of FITC-labeled K-TB/ELDKWAK-TB (Solution A) RNTs in the JAWS II cells. Blue: nuclei (DAPI), green: FITC-labeled RNTs.

The confocal images in Figure 4-6 displayed the green fluorescent signal after the treatment of cells with RNTs comprising of RGDSK-TB and/or DRGSK-TB and the Solution A co-mixed with Solution B. These results were similar and comparable to the fluorescence seen in the cells treated with Solution B RNTs (Figure 4-3) under the same conditions. The confocal images did not show any considerable difference in the uptake of RNTs upon addition of RGDSK-TB or DRGSK-TB RNTs. These results were confirmed by the quantification of fluorescence through flow cytometry.

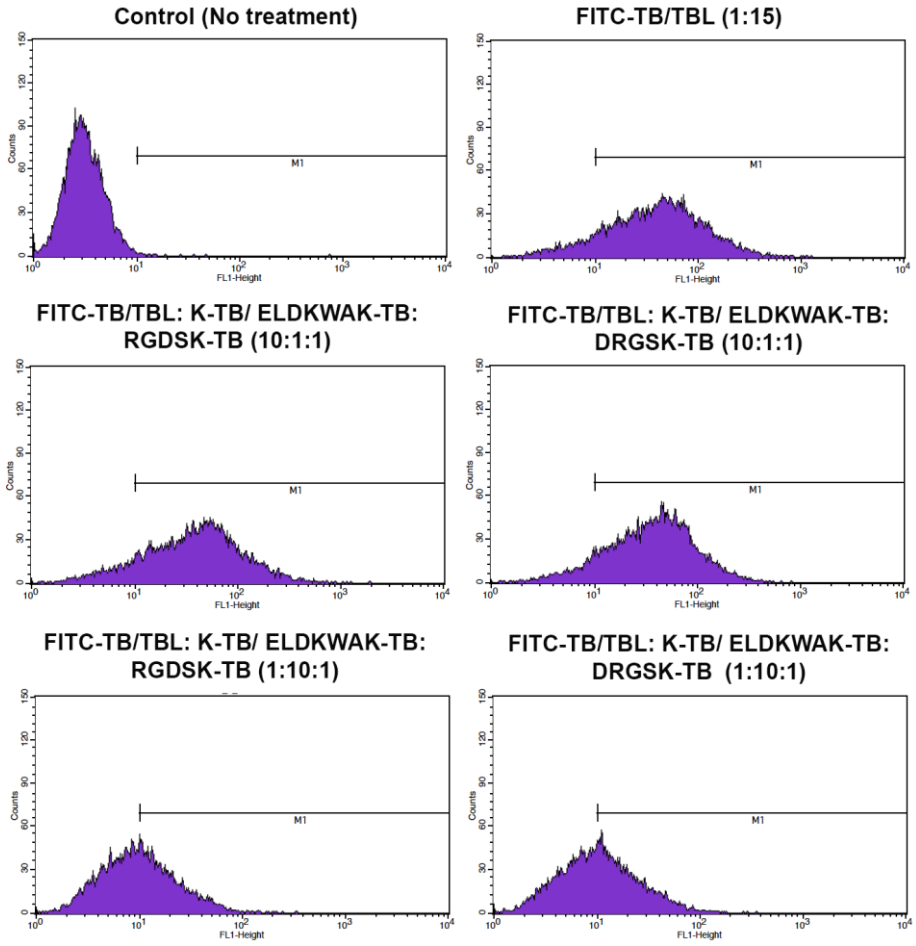

Figure 4-7: Histogram plots of effect of addition of RGDSK-TB and DRGSK-TB RNTs on the cellular uptake of FITC-labeled K-TB/ELDKWAK-TB RNTs (in the ratio 1:10 and 10:1) in the JAWS II cells.

The histogram plots (Figure 4-7), were obtained by the flow cytometry measurement after the treatment of RNTs constituting of RGDSK-TB and DRGSK-TB, each co-mixed with Solution B and Solution A RNTs (in the weight ratio as shown in Table 4-2) in the DCs. This was done to confirm the flow cytometry results with the confocal imaging data and quantify the fluorescence signal in the fixed cells. The green fluorescence signal peak shifted towards the area of more fluorescence signal with transfection of Solution B: Solution A: RGDSK-TB RNTs and Solution B: Solution A: DRGSK-TB RNTs in the ratio 10:1:1, as in case of Solution B RNTs treatment in the cells. The fluorescence measurements suggested that the peak deviated from the no treatment group

(control) towards the right (region of higher fluorescence) when the DCs were treated with Solution B, Solution A and RGDSK-TB and/or DRGSK-TB RNTs in the volume ratio 10:1:1. This shift was less than that of the fixed cells treated with respective RNTs in the ratio 1:10:1. These results were found to be similar to the confocal imaging study.

4.2.4. Co-localization study of the cellular uptake FITC-labeled RNTs

Co-localization is used to describe the presence of two or more fluorescent probes in the same physical location in the cells. The co-localization study of the RNTs in the DCs was used to examine the compartmentalization of the RNTs in the sub-cellular parts of the cells.

The LysoTracker probe is a fluorescent acidotropic dye available in different colors that are used to label and track the acidic components or organelles in the cells.[26] LysoTracker dyes have been used in biomedical research to investigate the biosynthesis and pathogenesis pathways in endosomal compartments of the cell.[27]

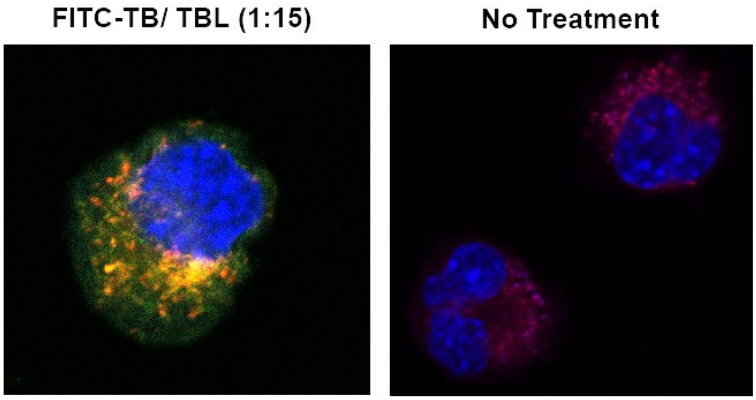

Figure 4-8: Confocal images of co-localization of FITC-labeled RNTs in the JAWS II cells. Blue: nuclei (DAPI), green: FITC-labeled RNTs, red: acidic components (LysoTracker Red), orange: FITC-labeled RNTs co-localized in acidic components of the cell.

After the transfection with 1 μM of FITC-TB/TBL RNTs, DCs were stained with LysoTracker Red DND-99 at 2 μM concentration for 20 min. Lysotracker Red stains the acidic components like endosomes in the cell. In the confocal images

(Figure 4-8), the orange color in the cells surrounding the blue nucleus showed the co-localization of RNTs in the acidic components of the cells as compared to the no treatment (control) group, where there is absence of the orange color and the endosomal organelles are stained red.

4.2.5. Enzyme-linked immunosorbent assay (ELISA) for K-TB/ELDKWAK-TB (9:1) RNTs.

The immunoassay technique with a radioactive label, known as radioactive immunoassay (RIA), was first developed by Solomon Berson and Rosalyn Yallow in 1960 to measure the endogenous insulin in plasma.[28] Due to the limitations of radioactively labeling of antigens and antibodies, there was an attempt by the scientists in 1970s and 1980s to successfully develop immunoassays with an enzyme as a reporter label.[29] Consequently, several variants of enzyme-labeled immunoassays were developed.[30]

ELISA is a simple technique that is based on a principle of binding of an antigen (peptide, protein, hormone or antibody) to its specific antibody (Ab) that enabled the detection of antigens in very small quantities in samples (blood, serum, plasma, urine or any fluid). The antigens are generally immobilized on a 96-well plate. The antigens then bind to its specific capture Ab (primary Ab) and the resulting complex is then subsequently detected by the enzyme-labeled secondary Ab. The chromogenic or fluorophore substrate for the enzyme gives the color or fluorescence that can be quantitatively measured through the colorimetric reading that indicates the presence of antigens.

We developed an ELISA to study the binding of ELDKWA peptide on the RNTs (constituting of K-TB/ELDKWAK-TB in the molar ratio 9:1) to its specific antibody HIV-1 gp41 monoclonal Ab (mAb) 2F5. Herein, we coated a polystyrene 96-well plate with Solution A RNTs with concentrations varying from 0-125 μg/mL. The RNTs were then allowed to bind to the unlabeled primary Ab (HIV-1 gp41 mAb 2F5) and were detected by the labeled secondary Ab (goat anti-human IgG (H+L) conjugated to HRP). TMB substrate was added to develop

a blue color, after which the stop solution was added. The absorbance was measured in the ELISA plate reader at 450 nm.

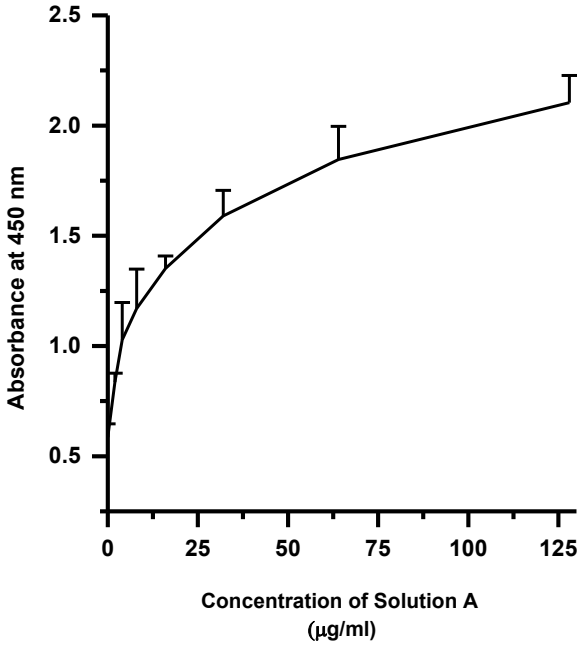

Figure 4-8: ELISA with absorbance at 450 nm versus concentration of K-TB/ELDKWAK-TB (Solution A) RNTs.

The absorbance obtained at 450 nm was plotted against the concentration of Solution A RNTs and the resulting curve showed a subsequent rise in the absorbance with increase in the concentration of the RNTs.

In another experiment, a 96-well plate was coated with Solution A RNTs, TBL (a RNT without any bioactive peptide side chain) RNTs and the peptide, ELDKWA at concentration of 0, 10, 20 and 40 μg/mL. The two RNT samples and the peptide, ELDKWA were then allowed to bind the unlabeled primary Ab, followed by detection by the enzyme-labeled secondary Ab. The substrate for the enzyme gave a blue color that was stopped by the stop solution and its absorbance was measured at 450 nm.

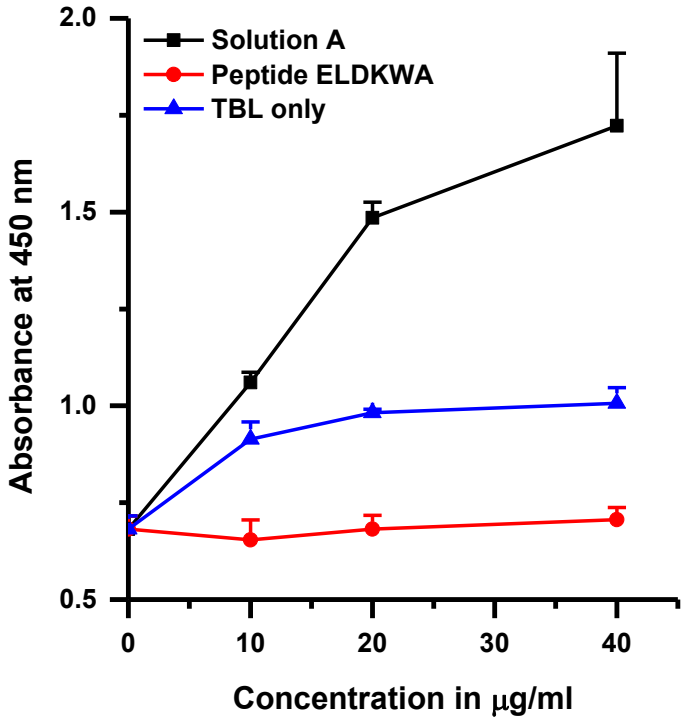

Figure 4-9: ELISA measuring the absorbance at 450 nm with respect to the concentration of Solution A (K-TB/ELDKWAK-TB) RNTs and the controls (TBL and peptide ELDKWA).

The absorbance measured at 450 nm (Figure 4-9) suggested a binding of Solution A RNTs with the HIV-1 mAb 2F5. However the absorbance with the peptide ELDKWA did not show any rise in the absorbance from 0-40 μg/mL. The absorbance measured for the TBL RNTs (without any bioactive peptide) was a little more than that of the peptide, ELDKWA. The RNT construct (K-TB/ELDKWAK-TB) carrying the HIV gp41 antigen ELDKWA, showed an elevation in the absorbance at 450 nm, much greater than the absorbance of TBL. These results suggested that nano-assembly played an important role in presenting the antigen (ELDKWA) and facilitated its binding to the 2F5 antibody.

An experiment was conducted to study the competition of binding of Solution A RNTs and the peptide ELDKWA with the specific Ab, 2F5. The 96-well plate

was coated with the Solution A RNTs, the peptide ELDKWA and the Solution A RNTs mixed with the peptide ELDKWA, each at a concentration of 0, 10, 20 and 40 μg/mL. The RNT samples coated onto the plate were allowed to bind the capture Ab, 2F5. The binding of the primary Ab was detected by the secondary HRP-conjugated Ab upon the development of the blue color with the substrate. The absorbance was measured at 450 nm after the addition of the stop solution.

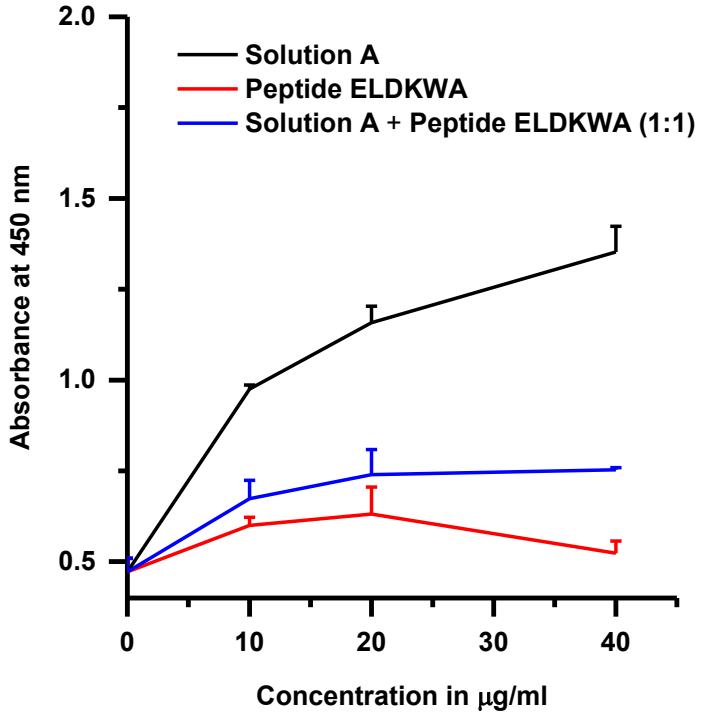

Figure 4-10: ELISA measuring the absorbance at 450 nm with respect to the concentration of Solution A RNTs and the controls (peptide ELDKWA and peptide ELDKWA co-mixed with Solution A RNTs in the volume ratio of 1:1).

The graph in Figure 4-10 showed an enhanced absorbance measurement at 450 nm in case of Solution A RNTs, indicating the strong binding of the ELDKWA sequence to the primary Ab, 2F5. The peptide ELDKWA alone, however did not result in a considerable rise in the absorbance from the 0 μg/ml concentration. This implied that the Solution A RNTs played an important role in the specific antigen-antibody binding. In addition, it was observed that when the peptide

ELDKWA solution was mixed with the Solution A RNTs (with K-TB/ELDKWAK-TB, 9:1), the absorbance was higher than the peptide alone. This reiterates the importance of the nanostructures in promoting the binding of the HIV-1 gp 41 epitope, ELDKWA to its specific mAb, 2F5.

These results confirmed the fact that RNTs played an important role in presenting antigen to its specific antibody and promoted the antigen-antibody binding specificity.

4.3. Conclusion

In this chapter we showed that the DCs successfully uptake the K-TB/ELDKWAK-TB RNTs (Solution A), implying that the receptors on the DCs recognize the ELDKWA peptide and encapsulate the RNTs. The cell uptake study of Solution A RNTs labeled with the fluorescent RNTs (FITC-TB/TBL) using confocal imaging and flow cytometry showed an increase in a concentration-dependent and time-dependent manner. Although these RNTs were sufficient to be up taken by the cells by itself, addition of RGDSK-TB RNTs (RGD sequence aids in cell adhesion) and DRGSK-TB (DRG, for control) RNTs to the Solution A RNTs did not show any considerable effect on their cell uptake.

The co-localization study provided evidence that the K-TB/ELDKWAK-TB RNTs get co-localized into the acidic lysosomal compartments of the cell when the cells were stained with LysoTracker Red dye (stains the acidic components of the cell). An ELISA was developed to prove that supramolecular assembly of the ELDKWAK functionalized twin G∧C motif can aid in the binding of the peptide to its specific antibody, 2F5, whereas the peptide ELDKWA alone did not show any binding even with increase in concentration.

4.4. Materials and Methods

4.4.1. Materials

JAWS II cell line and alpha minimum essential medium (AMEM) with ribonucleosides and deoxyribonucleosides were purchased from ATCC. Reagents for cell culture like fetal bovine serum (FBS), 0.5% trypsin-EDTA (1X), phenol red, 200 mM L-glutamine and 10 U/mL of penicillin-streptomycin were purchased from GIBCO. Mouse granulocyte-macrophage colony-stimulating factor (GM-CSF) was obtained from R&D systems. Cell labeling reagents LysoTracker Red DND-99 was purchased from Invitrogen. Cell mounting media and DAPI were obtained from Department of Experimental Oncology, University of Alberta. 3,3',5,5'-tetramethylbenzidine (TMB) liquid substrate for ELISA, stop solution for TMB, gelatin from bovine skin (type B), paraformaldehyde were obtained from Sigma-Aldrich. Coverslips and slides for confocal imaging were purchased from VWR. Primary antibody (Ab), HIV-1 gp41 monoclonal Ab (2F5) at 1 mg/mL concentration was obtained from NIH AIDS Reagent program. Secondary antibody, goat anti-human IgG (H+L) conjugated to HRP was obtained from Life Technologies Inc.

4.4.2. Cell culture

Immature monocytic dendritic cell line JAWS II from mouse model, strain C57BL/6 were cultured with AMEM with ribonucleosides and deoxyribonucleosides, 5 ng/mL of GM-CSF, 20% FBS, 4mM L-glutamine and 10 U/mL of penicillin-streptomycin in an incubator at 37 °C and 5% CO_2 atmosphere. The cells were sub-cultured at a sub-cultivation ratio of 1:2 using 0.5% trypsin-EDTA (1X), phenol red. Cells were de-attached after addition of 0.5% trypsin-EDTA (1X), phenol red and incubating the cells at 37 °C for about a minute.

4.4.3. Sample preparation for confocal imaging and flow cytometry

Peptide KAWKDLE functionalized with a twin G∧C motif (ELDKWAK-TB) and K-TB (lysine functionalized twin G∧C motif) were synthesized, as shown in

chapters 2 and 3. A stock solution of 1 mg/mL of RNTs constituting of K-TB co-assembled with ELDKWAK-TB in a molar ratio 9:1 was prepared (Solution A) as in chapter 3 (Section 3.4.4). A stock solution of 0.5 mg/mL of fluorescein isothiocyanate dye functionalized with twin G∧C base (FITC-TB) was co-assembled with twin base linker (TBL) in a molar ratio 1:15 (Solution B) as in section 3.4.6 (Chapter 3). The Solution A sample was co-mixed with Solution B in the ratio of 1:10 and 10:1 for the treatment of cells as mentioned in Table 4-1.

The buffers used were phosphate buffer saline (PBS, NaCl 137 mmol/L, 0.02% KCl, 0.144% Na_2HPO_4, 0.024% KH_2PO_4, pH 7.4), cell sorting buffer (1X PBS, 1mM EDTA, 25 mM HEPES, pH 7.0, 1% FBS, 0.2 μm filter sterilize).

4.4.4. Confocal imaging

For confocal imaging, the JAWS II dendritic cells (in AMEM) were seeded onto the circular cover slips in a 12-well plate. Cells in the plate were incubated at 37 °C for 24 h so that there is 50-60% confluency. After 24 h the medium was discarded from the wells. RNTs, constituting Solution A co-mixed with Solution B in the volume ratio of 1:10 and 10:1, were added to 1 ml of AMEM without FBS and antibiotic. The RNT solution in AMEM (1 mL) was added into each well and incubated at 37 °C for 24 h. After incubation, the AMEM with RNTs was discarded and the wells were washed with 700 μL of 1X PBS (twice for 30 s). The cells were fixed by adding 4% paraformaldehyde solution in 1X PBS for 15 min at room temperature. The cover slip was mounted on the slide by adding 1 drop of mounting media with DAPI on the slide. The slides were stored at 4 °C until imaging.

The cells were imaged using the confocal laser-scanning microscope (Zeiss LSM 710) at Department of Experimental Oncology, University of Alberta. Confocal images were analyzed and processed using the Zeiss LSM software, ZEN 2010. The channels used to observe FITC-labeled RNTs, DAPI-labeled nucleus and acidic compartments labeled by LysoTracker Red were FITC (green), DAPI (blue) and Cy3 (Red) respectively. In order to get a 3D construct images of the

cells, the images were sliced in the z-direction using z-stack on ZEN software and the images were processed to 3D image by Imaris software.

4.4.5. Concentration-dependence study of cell uptake of RNTs

Dendritic cells in 12-well plate were treated with 0.25, 0.5 and 1 μg/mL of Solution B RNTs, and RNTs formed by co-mixing Solution B with Solution A in the volume ratio of 1:10 and 10:1 for 24 h at 37 °C incubator. The cells were washed with PBS, fixed with paraformaldehyde and stained with DAPI as described above for confocal imaging.

4.4.6. Time-dependence study of cell uptake of RNTs

Dendritic cells in 12-well plate were treated with 1 μg/mL RNTs (Solution B, Solution B co-mixed with Solution A in the volume ratio of 1:10 and 10:1) for 3, 6, 12, 24 and 48 h at 37 °C incubator. The cells were imaged after fixing them and staining them with DAPI.

4.4.7. Co-localization study

After the treatment with 1 μg/mL Solution B RNTs in a 12-well plate in a 37 °C incubator for 24 h, the cells were washed with PBS. They were then incubated with 1 ml of LysoTracker Red DND-99 (2 μM) in AMEM without FBS and antibiotic at 37 °C for 20 min. The cells were again washed with PBS, fixed and stained with DAPI for imaging.

4.4.8. Effect of RGDSK-TB and DRGSK-TB on the cell uptake of RNTs

To study the effect of RGDSK-TB and DRGSK-TB on the cell uptake of K-TB/ELDKWAK-TB RNTs, 1 part each of RGDSK-TB and DRGSK-TB was added to Solution B RNTs co-mixed with Solution A in the weight ratio of 1:10 and 10:1 as shown in Table 4-2. The cells with 60% confluency were treated with these co-assembled RNTs for 24 hours. The cells were washed, fixed and stained.

4.4.9. Flow cytometry

Approximately 100,000 dendritic cells in 1mL of AMEM were seeded onto a 12-well plate and incubated at 37 °C for 24 h**.** The medium was discarded after 24 hours and the cells were treated with 1 mL of 1 μM RNT solution in AMEM without FBS and antibiotic. The cells were again incubated at 37 °C for 24 hours**.** The medium with RNTs was discarded and the wells were washed with 1X PBS (700 μL), twice. The cells were detached from the wells by adding 300 μL of 0.5% trypsin-EDTA and incubating the cells at 37 °C for 2-3 min. 1X PBS (700 μL) was added to all the wells. The cells in PBS from wells were pooled so that there were approximately 700,000-800,000 cells and transferred to the falcon tube. The cells in the falcon tube were centrifuged at 1100 rpm for 5 min. A transparent pellet of cells was formed at the bottom. The supernatant was discarded and 2 mL of 1% paraformaldehyde solution in 1X PBS was added. The cells were allowed to fix for 20 min at room temperature. The cells were again centrifuged at 1100 rpm for 5 min. The supernatant was discarded and 1 mL of cell sorting buffer was added. The buffer was mixed well such that the cell pellet breaks into single cells. The solution was then transferred to the flow cytometer tube so that there were approximately 700,000 to 800,000 cells per mL of the buffer. The samples were covered with aluminum foil and stored at 4 °C until analysis. The signal of FITC-labeled RNTs was measured in the fixed dendritic cells by the FACS Calibur Flow cytometer by BD Biosciences.

4.4.10. Time-dependence study of the cell uptake of RNTs

The cells seeded in 12 well plates were treated with 1 μg/ml RNTs (Solution B, Solution B co-mixed with Solution A in the volume ratio of 1:10 and 10:1) for 3, 6, 12, 24 and 48 h at 37 °C incubator. A control with no treatment was also prepared in the same manner to compare with treatment groups and signal was measured by FACS Calibur flow cytometer.

4.4.11. Effect of RGDSK-TB and DRGSK-TB on the cell uptake of RNTs

The effect of RGDSK-TB and DRGSK-TB on the cell uptake of K-TB/ELDKWAK-TB RNTs was also studied using flow cytometer. The cells were treated as for confocal imaging as described in this chapter (section 4.4.4).

4.4.12. Enzyme-linked immunosorbent assay (ELISA)

The polystyrene 96-well plate was coated with Solution A RNTs, TBL RNTs only without any peptide and only the peptide ELDKWA with concentration varying from 0-40 μg/mL. The RNTs were then allowed to bind the unlabeled primary antibody (HIV-1 gp41 monoclonal Ab 2F5) and detected by the labeled secondary antibody (goat anti-human IgG (H+L) conjugated to HRP). TMB substrate was added to develop color that was stopped by the stop solution.

Buffers for ELISA:

a. Antigen (RNTs) coating buffer: 1X PBS
b. Blocking buffer (2% gelatin from bovine skin in 1X PBS)
c. Antibody dilution buffer (0.1% gelatin from bovine skin in 1X PBS)
d. Washing buffer: PBST (1X PBS with 0.05% tween 20)

Procedure for ELISA:

a. **Coating with antigen:** The 96-well plate was coated with 100 μl of 0, 10, 20 and 40 μg/mL of the RNT solution in 1X PBS. The plate was incubated overnight at 4 °C.
b. **Blocking:** After an overnight incubation, the plate was washed 4 times with PBST. Then 100 μL of blocking buffer was added and incubated at 37 °C for 1 h.
c. **Coating with primary antibody (Ab):** The plate was washed 4 times with PBST. After washing, 100 μL of 1 μg/mL of primary Ab (HIV-1 gp41 mAb 2F5) in 0.1% dilution buffer was added to the wells. The plate was incubated at room temperature for 2 h with slow shaking.
d. **Coating with secondary Ab:** The plate was washed 4 times with PBST and 100 μL of secondary Ab (goat anti-human IgG (H+L) conjugated to HRP)

diluted to 1:6000 ratio in dilution buffer was added to the wells. The plate was the incubated with slow shaking at room temperature for 30 min.

e. **Detection:** After washing the plate with PBST (5 times), 100 µL of TMB substrate was added to the wells. The plate was incubated on the shaker at room temperature for 10 min. Then 100 µL of stop solution for TMB was added and the absorbance was measured at 450 nm with slow shaking.

4.4.13. Preparation of the standard curve

The multi-well plates were coated with Solution A RNTs with concentrations of 0, 2, 4, 8, 16, 32, 64, 128 µg/mL in 1X PBS with incubation at 4 °C overnight. After an overnight incubation, ELISA was carried out as described above (section 4.4.12) and the absorbance was measured at 450 nm.

4.4.14. ELISA for TB-K/ ELDKWAK-TB (9:1) RNTs with controls

The 96-well plate was coated with RNTs with concentrations of 0, 10, 20 and 40 µg/mL Solution A, K-TB, TBL (twin base linker), ELDKWA peptide and Solution A RNTs mixed with peptide ELDKWA in 1:1 ratio, in 1X PBS with incubation at 4 °C overnight. Then ELISA was carried out as described in section section 4.4.12 and the absorbance was measured at 450 nm.

4.5. References

1. Ndung'u T, Weiss RA. On HIV diversity. *AIDS.* **2012**. 26: 1255-1260.
2. Taylor BS, Sobieszcyk ME, McCutchan FE, Hammer SM. The challenge of HIV-1 subtype diversity. *N. Engl. J. Med*. **2008**. 358: 1590-1602.
3. Gaschen B, et al. Diversity considerations in HIV-1 vaccine selection. *Science*. **2002**. 296: 2354-2360.
4. Korber BT, Foley B, Gaschen B, Kuiken C. Epidemiological and immunological implications of the global variability of HIV-1. In: Pantaleo G, Walker BD eds. *Retroviral Immunology: Immune Response and Restoration. New Jersey: Humana Press*. **2001**. 1-32.
5. Korber BT, Letvin NL, Haynes BF. T-cell vaccine strategies for human immunodeficiency virus, the virus with a thousand faces. *J. Virol*. **2009**. 83: 8300-8314.
6. Barouch DH, Korber B. HIV-1 vaccine development after Step. *Ann. Rev. Med*. **2009**. 61: 2.
7. Hemelaar J, et al. Global and regional distributions of HIV-1 genetic subtypes and recombinants in 2004. *AIDS*. **2006**. 20: W13-W23.
8. Rerks-Ngarm S, Pitisuttithum P, Nitayaphan S, Kaewkungwal J, Chiu J, Paris R, Premsri N, Namwat C, de Souza M, Adams E, et al. MOPH-TAVEG Investigators. *N. Engl. J. Med*. **2009**. 361: 2209-2220.
9. Klein F, Mouquet H, Dosenovic P, Scheid JF, Scharf L, and Nussenzweig MC. *Science*. **2013**. 341: 1199-1204.
10. Barouch DH, Stephenson KE, Borducchi EN, Smith K, Stanley K, McNally AG, Liu J, Abbink P, Maxfield LF, Seaman M.S, *et al*. *Cell*. **2013**. 155: 531-539.
11. Stamatatos L, Morris L, Burton DR, Mascola JR. Neutralizing antibodies generated during natural HIV infection: good news for an HIV vaccine? *Nat Med*. **2009**. 15(8): 866-70.
12. Wu X, Yang ZY, Li Y, Hogerkorp CM, Schief WR, Seaman MS, et al. Rational design of envelope identifies broadly neutralizing human monoclonal antibodies to HIV. *Science*. **2010**. 329: 856-61.

13. Zhou T, Georgiev I, Wu X, Yang ZY, Dai K, Finzi A, et al. Structural basis for broad and potent neutralization of HIV by antibody VRC01. *Science*. **2010**. 329: 811-7.
14. Li Y, Migueles SA, Welcher B, Svehla K, Phogat A, Louder MK, et al. Broad HIV neutralization mediated by CD4-binding site antibodies. *Nat. Med*. **2007**. 13: 1032-4.
15. Walker LM, Simek MD, Priddy F, Gach JS, Wagner D, Zwick MB, et al. A limited number of antibody specificities mediate broad and potent serum neutralization in selected HIV infected individuals. *PLoS. Pathog*. **2010**. 6(8): 1-14.
16. Kwong PD, Mascola JR, Nabel GJ. Rational design of vaccines to elicit broadly neutralizing antibodies to HIV-1. *Cold Spring Harb Perspect Med*. **2011**. 1(1): 007278
17. Guenaga J, Dosenovic P, Ofek G, Baker D, Schief WR, Kwong PD, et al. Heterologous epitope-scaffold prime: boosting immuno-focuses B cell responses to the HIV gp41 2F5 neutralization determinant. *PLoS One*. **2011**. 6(1): 1-12.
18. Antonis AF, Bruschke CJ, Rueda P, Maranga L, Casal JI, *et al*. A novel recombinant virus-like particle vaccine for prevention of porcine parvovirus-induced reproductive failure. *Vaccine*. **2006**. 24: 5481–5490.
19. Young SL, Wilson M, Wilson S, Beagley KW, Ward V and Baird MA. Transcutaneous vaccination with virus-like particles. *Vaccine*. **2006**. 24(26): 5406-12.
20. Dell K, Koesters R, Linnebacher M, Klein C and Gissmann L. ntranasal immunization with human papillomavirus type 16 capsomeres in the presence of non-toxic cholera toxin-based adjuvants elicits increased vaginal immunoglobulin levels. *Vaccine*. **2006**. 24(13): 2238-47.
21. Levy Y. Preparation for antiretroviral interruption by boosting the immune system. *Curr. Opin. HIV. AIDS*. **2008**. 3: 118-123.
22. Johnston MI and Fauci AS. HIV vaccine development-improving on natural immunity. *N. Engl. J. Med*. **2011**. 365: 873-875.

23. Saunders KO, Rudicell RS and Nabel GJ. The design and evaluation of HIV-1 vaccines. *AIDS*. **2012**. 26: 1293-1302.
24. Garcia F and Routy JP. Challenges in dendritic cells-based therapeutic vaccination in HIV-1 infection Workshop in dendritic cell-based vaccine clinical trials in HIV-1. *Vaccine*. **2011**. 29: 6454-6463.
25. Rigby PJ and Goldie RG. Confocal microscopy in biomedical research. *Croat. Med. J*. **1999**. 40(3): 346-52.
26. (a) Cytometry suppl 7, 77 abstract #426B (1994); (b) Mol Biol Cell 5, 113a abstract #653 (1994); (b) Griffiths G, Hoflack B, Simons K, Mellman I, Kornfeld S. The mannose 6-phosphate receptor and the biogenesis of lysosomes. *Cell*. **1988**. 52(3): 329-341.
27. de Duve C. The lysosome in retrospect. In Dingle JT and Fell HB. eds, Lysosomes in Biology and Pathology. *Amsterdam: North-Holland Publishing Company*. **1969**. pp. 3-40.
28. Yalow RS, Berson SA. Immunoassay of endogenous plasma insulin in man. *Clin. Invest*. **1960**. 39: 1157-75.
29. Miles LEM, Hales CN. Labeled antibodies and immunological assay systems. *Nature*. **1968**. 219: 186-9.
30. Schuurs AHWM, van Weemen BK. Enzyme-immunoassay: a powerful analytical tool [Review]. *J. Immunoassay*. **1980**. 1: 229-49.

Chapter 5

Bibliography

References

1. Alfsen A, Bomsel M. HIV-1 gp41 envelope residues 650-685 exposed on native virus act as a lectin to bind epithelial cell galactosyl ceramide. *J. Biol. Chem*. **2002**. 277: 25649-25659.
2. Aline F, Brand D, Pierre J, Roingeard P, Severine M, Verrier B, et al. Dendritic cells loaded with HIV-1 p24 proteins adsorbed on surfactant free anionic PLA nanoparticles induce enhanced cellular immune responses against HIV-1 after vaccination. *Vaccine*. **2009**. 27:5284-91.
3. Allen TM, Cullis PR. Drug delivery systems: entering the mainstream. *Science*. **2004**. 303:1818-22.
4. Antonis AF, Bruschke CJ, Rueda P, Maranga L, Casal JI, *et al*. A novel recombinant virus-like particle vaccine for prevention of porcine parvovirus-induced reproductive failure. *Vaccine*. **2006**. 24: 5481–5490.
5. Azad N, Rojanasakul Y. Nanobiotechnology in drug delivery. *Am. J. Drug Deliv*. **2006**. 4: 79–88. Bethune DS, Kiang CH, de Vries MS, Gorman G, Savoy R, Vazquez J, Beyers R. Cobalt-catalysed growth of carbon nanotubes with single-atomic-layer walls. *Nature*. **1993**. 363: 605.
6. Bancherau J, Steinman RM. Dendritic cells and control of immunity. *Nature*. **1998**. 392: 245-52.
7. Banchereau J, Palucka AK. Dendritic cells as therapeutic vaccines against cancer. *Nat. Rev. Immunol*. **2005**. 5:296-306.
8. Barouch DH, Korber B. HIV-1 vaccine development after Step. *Ann. Rev. Med*. **2009**. 61: 2.
9. Barouch DH, Stephenson KE, Borducchi EN, Smith K, Stanley K, McNally AG, Liu J, Abbink P, Maxfield LF, Seaman M.S, *et al*. *Cell*. **2013**. 155: 531-539.
10. Berova N, Nakanishi K, Woody RW. Circular Dichroism, Principles and Applications. Wiley-VCH, New York, **2000**.
11. Bethune DS, Kiang CH, de Vries MS, Gorman G, Savoy R, Vazquez J, Beyers R. Cobalt-catalysed growth of carbon nanotubes with single-atomic-

layer walls. *Nature*. **1993**. 363: 605.

12. Bharali DJ, Pradhan V, Elkin G, Qi W, Hutson A, Mousa SA, et al. Novel nanoparticles for the delivery of recombinant hepatitis B vaccine. *Nanomedicine*. **2008**. 4:311-7.
13. Blanco P, Palucka AK, Pascual V, Banchereau J. Dendritic cells and cytokines in human inflammatory and autoimmune diseases. *Cytokine and Growth Factor Reviews*. **2008**. 19 (1): 41–52.
14. Bonifaz L, Bonnyay D, Mahnke K, Rivera M, Nussenzweig MC, Steinman RM. Efficient targeting of protein antigens to the dendritic cell receptor DEC-205 in the steady state leads to antigen presentation on MHC class I products and peripheral $CD8^+$ T cell tolerance. *J. Exp. Med.* 2002. 196:1627–38.
15. Borzsonyi G, Johnson RS, Myles AJ, Cho JY, Yamazaki T, Beingessner RL, Kovalenko A, Fenniri H. Rosette nanotubes with 1.4 nm inner diameter from a tricyclic variant of the Lehn-Mascal G∧C base. *Chem. Commun. (Camb)*. **2010**. 46(35): 6527-9.
16. Borzsonyi G, Alsbaiee A, Beingessner RL, Fenniri H. Synthesis of a tetracyclic G∧C scaffold for the assembly of rosette nanotubes with 1.7 nm inner diameter. *J. Org. Chem*. **2010**. 75(21): 7233-9.
17. Boschmann M and König W. Peptide and Protein Hormones. Structure, Regulation, Activity. A Reference Manual. 284 Seiten, zahlreiche Abb. und Tab. VCH Verlagsgesellschaft Weinheim, New York, Basel, Cambridge **1993**. Preis: 198, DM. Nahrung, 38: 225.
18. Brandenberger C, Rowley NL, Jackson-Humbles DN, Zhang Q, Lewandowski RP, Wagner JG, Chen W, Kaminski NE, Baker GL, Worden RM, Harkema JR. Engineered silica nanoparticles act as adjuvants to enhance allergic airway disease in mice. *Part. Fibre Toxicol*. **2013**. 10: 26.
19. Bramwell VW, Eyles JE, and Alpar HO. Particulate delivery systems for biodefense subunit vaccines. *Advanced Drug Delivery Reviews*. **2005**. 57 (9): 1247–1265.
20. Burton DR, Pyati J, Koduri R, Sharp SJ, Thornton GB, Parren PWHI, Sawyer LS, Hendry RM, Dunlop N, Nara PL. Efficient neutralization of primary

isolates of HIV-1 by a recombinant human monoclonal antibody. *Science.* **1994**. 266: 1024–1027.

21. Burton DR. A vaccine for HIV type 1: the antibody perspective. *Proc. Natl. Acad. Sci U. S. A.* **1997**. 94: 10018–10023.
22. Cambi A, Lidke DS, Arndt-Jovin DJ, Figdor CG, Jovin TM. Ligandconjugated quantum dots monitor antigen uptake and processing by dendritic cells. *Nano Lett*. **2007**. 7: 970–977.
23. Carpino LA, Ghassemi S, Ionescu D, Ismail M, Sadat-Aalaee D, Truran GA, Mansour E, Siwruk GA, Eynon JS and Morgan B. Rapid, continuous solution-phase peptide synthesis: Application to peptides of pharmaceutical interest. *Org. Process Res. Dev*. **2003**. 7, 28-37.
24. Carpo L. Hormones, Freeman, New York, **1985**.
25. Chadwick S, Kriegel C, and Amiji M. Nanotechnology solutions for mucosal immunization. *Advanced Drug Delivery Reviews*. **2010**. 62 (4-5): 394–407.
26. Chan DC, Kim PS. HIV entry and its inhibition. *Cell.* **1998**. 93: 681–684.
27. Chen YH, Xiao Y, Yu TW and Dierich MP. Epitope vaccine: a new strategy against HIV-1. *Immunol. Today*. **1999a**, 20: 588-589.
28. Chen Y, Webster TJ. Increased osteoblast functions in the presence of BMP-7 short peptides for nanostructured biomaterial applications. *J. Biomed. Mater. Res. A*. **2009**. 91(1): 296-304.
29. Childs A, Hemraz UD, Castro NJ, Fenniri H, Zhang LG. Novel biologically-inspired rosette nanotube PLLA scaffolds for improving human mesenchymal stem cell chondrogenic differentiation. *Biomed. Mater*. **2013**. 8(6): 065003.
30. Chun AL, Moralez JG, Webster TJ, Fenniri H. Helical rosette nanotubes: a more effective orthopaedic implant material. *Nanotechnology*. **2004**. 15: S234–S239.
31. Chun AL, Moralez JG, Webster TJ and Fenniri H. Helical rosette nanotubes: a biomimetic coating for orthopedics? *Biomaterials*. **2005**. 26(35): 7304-9.
32. *Clackson T, Wells JA.* A hot spot of binding energy in a hormone-receptor interface. *Science. 1995. 267: 383*-386.

33. *Cochran AG*. Antagonists of protein-protein interactions. *Chem*. *Biol*. **2000**. *7*: *R85*-R94.
34. Cohen J. Jitters jeopardize AIDS vaccine trials. *Science.* **1993**. 262:980–981.
35. Cohen J. AIDS vaccine trial produces disappointment and confusion. *Science*. **2003**. 299: 1290–1291.
36. Conley AJ, Kessler JA, Boots LJ, Tung JS, Arnold BA, Keller PM, Shaw AR, Emini EA. Neutralization of divergent human immunodeficiency virus type 1 variants and primary isolates by IAM-41-2F5, an anti-gp41 human monoclonal antibody. *Proc. Natl. Acad. Sci U. S. A*. **1994**. 91: 3348–3352.
37. Copland MJ, Rades T, Davies NM, Baird MA. Lipid based particulate formulations for the delivery of antigen. *Immunol. Cel Biol*. **2005**. 83: 97–105.
38. Cubillos-Ruiz JR, Engle X, Scarlett UK, Martinez D, Barber A, Elgueta R, *et al*. Polyethylenimine-based siRNA nanocomplexes reprogram tumor-associated dendritic cells via TLR5 to elicit therapeutic antitumor immunity. *J. Clin. Invest*. **2009**. 119:2231-44.
39. Cui D, Tian F, Ozkan CS, Wang M, Gao H. Effect of single wall carbon nanotubes on human HEK293 cells. *Toxicol. Lett.* **2005**. 155(1): 73–85.
40. (a) Cytometry suppl 7, 77 abstract #426B (1994); (b) Mol Biol Cell 5, 113a abstract #653 (1994); (b) Griffiths G, Hoflack B, Simons K, Mellman I, Kornfeld S. The mannose 6-phosphate receptor and the biogenesis of lysosomes. *Cell*. **1988**. 52(3): 329-341.
41. de Duve C. The lysosome in retrospect. In Dingle JT and Fell HB. eds, Lysosomes in Biology and Pathology. *Amsterdam: North-Holland Publishing Company*. **1969**. pp. 3-40.
42. Dee KC, Andersen TT and Bizios RJ. Design and function of novel osteoblast-adhesive peptides for chemical modification of biomaterials. *Biomed. Mater. Res*. **1998**. 40: 371-377.
43. De Gregorio E, D'Oro U, Wack A. Immunology of TLR-independent vaccine adjuvants. *Current Opinion in Immunology*. **2009**. 21 (3): 339–345.

44. Dell K, Koesters R, Linnebacher M, Klein C and Gissmann L. ntranasal immunization with human papillomavirus type 16 capsomeres in the presence of non-toxic cholera toxin-based adjuvants elicits increased vaginal immunoglobulin levels. *Vaccine*. **2006**. 24(13): 2238-47.
45. Delves PJ, Roitt IM. The immune system. Part 1. *N. Engl. J. Med*. **2000**. 343: 3–49.
46. Delves PJ, Roitt IM. The immune system. Part 2. *N. Engl. J. Med.* **2000**. 343: 108–17.
47. Donnelly JJ, Wahren B, Liu MA. DNA vaccines: progress and challenges. *J. Immunol*. **2005**. 175: 633–639.
48. Dresselhaus, M. S., Dresselhaus, G. & Eklund, P. C. Science of Fullerenes and Carbon Nanotubes (Academic, New York). 1996.
49. Dresselhaus, M. S.; Dresselhaus, G.; Sugihara, K.; Spain, I. L.; Goldberg, H. A. Graphite Fibers and Filaments; Springer-Verlag: New York. **1988**.
50. Driscoll KE. TNF-α and MIP-2: role in particle-induced inflammation and regulation by oxidative stress. *Toxicol. Lett*. **2000**. 112–113: 177–183.
51. Driscoll KE, Carter JM, Hassenbein DG, Howard B. Cytokines and particle-induced inflammatory cell recruitment. *Environ. Health Perspect.* **1997**. 105: 1159–1164.
52. D'Souza SE, Ginsberg MH, Plow EF. Arginyl-glycyl-aspartic acid (RGD): a cell adhesion motif. *Trends Biochem. Sci*. **1991**. 16(7): 246-50.
53. du Vigneaud V, Ressler C and Trippett S. The Sequence of Amino Acids in Oxytocin, with a Proposal for the Structure of Oxytocin. *J. Biol. Chem.* **1953**. 205: 949-957.
54. El-Bakkari M, Beingessner RL, Alshamsan A, Cho JY and Fenniri H. Electrostatic and steric effect of peptides functionalized on self-assembled rosette nanotubes. *Mater. Res. Soc. Symp. Proc*. **2011**. 1316
55. Eldridge JH, Staas JK, Meulbroek JA, Tice TR, Gilley RM. Biodegradable and biocompatible poly(DL-lactide-co-glycolide)microspheres as an adjuvant for staphylococcal enterotoxin B toxoid which enhances the level of toxin-neutralizing antibodies. *Infect. Immun*. **1991**. 59: 2978–2986.

56. Fan Z, Govorov AO. Plasmonic circular dichroism of chiral metal nanoparticle assemblies. *Nano Lett*. **2010**. 10: 2580-2587.
57. Fenniri H, Mathivanan P, Vidale KL, et al. Helical rosette nanotubes: design, self-assembly, and characterization. *J. Am. Chem. Soc*. **2001**. 123(16): 3854–3855.
58. Fenniri H, Deng BL, Ribbe AE. Helical rosette nanotubes with tunable chiroptical properties. *J. Am. Chem. Soc*. **2002**. 124(37): 11064–11072.
59. Fenniri H, Deng BL, Ribbe AE, Hallenga K, Jacob J, Thiyagarajan P. Entropically driven self-assembly of multichannel rosette nanotubes. *Proc. Natl. Acad. Sci. U S A*. **2002**. 99(2):6487–6492.
60. FITC-TB and TBL was synthesized and characterized by Dr. Usha D. Hemraz.
61. Garcia F and Routy JP. Challenges in dendritic cells-based therapeutic vaccination in HIV-1 infection Workshop in dendritic cell-based vaccine clinical trials in HIV-1. *Vaccine*. **2011**. 29: 6454-6463.
62. Gaschen B, et al. Diversity considerations in HIV-1 vaccine selection. *Science*. **2002**. 296: 2354-2360.
63. Gomez-Gualdrón DA, Burgos JC, Yu J, Balbuena PB. Carbon nanotubes: engineering biomedical applications. *Prog. Mol. Biol. Transl. Sci*. **2011**. 104: 175–245.
64. Goodman RB, Pugin J, Lee JS, Matthay MA. Cytokine-mediated inflammation in acute lung injury. *Cytokine & Growth Factor Rev*. **2003**. 14: 523–535.
65. Goya GF, Marcos-Campos I, Fernandez-Pacheco R, Saez B, Godino J, Asin L, et al. Dendritic cell uptake of iron-based magnetic nanoparticles. *Cell Biol. Int*. **2008**. 32:1001-5.
66. Guermonprez P, Valladeau J, Zitvogel L, Thery C, Amigorena S. Antigen presentation and T cell stimulation by dendritic cells. *Annu. Rev. Immunol*. **2002**. 20: 621-67.
67. Guenaga J, Dosenovic P, Ofek G, Baker D, Schief WR, Kwong PD, et al. Heterologous epitope-scaffold prime: boosting immuno-focuses B cell

responses to the HIV gp41 2F5 neutralization determinant. *PLoS One*. **2011**. 6(1): 1-12.

68. Gupta RK, Rost BE, Relyveld E, Siber GR. Adjuvant properties of aluminum and calcium compounds, in: M.F. Powell, M.J. Newman (Eds.). *Vaccine Design: the Subunit and Adjuvant Approach*, Plenum Press, New York. **1995**. 229–248.
69. Han B, Guo J, Abrahaley T, Qin L, Wang L, Zheng Y, Li B, Liu D, Yao H, Yang J, Li C, Xi Z, Yang X. *PLoS One*. Adverse effect of nano-silicon dioxide on lung function of rats with or without ovalbumin immunization. **2011**. 6: e17236.
70. Hawiger D, Inaba K, Dorsett Y, Guo K, Mahnke K, *et al*. Dendritic cells induce peripheral T cell unresponsiveness under steady state conditions *in vivo*. *J. Exp. Med.* 2001. 194:769–80.
71. Hautanen A, Gailit J, Mann DM, Ruoslahti E. Effects of modifications of the RGD sequence and its context on recognition by the fibronectin receptor. *J. Biol. Chem*. **1984b**. 264: 1437-42.
72. Hemelaar J, et al. Global and regional distributions of HIV-1 genetic subtypes and recombinants in 2004. *AIDS*. **2006**. 20: W13-W23.
73. Hemraz UD, El-Bakkari M, Yamazaki T, Cho JY, Beingessner RL and Fenniri H. "Chiromers: Conformation-driven mirror-image supramolecular chirality isomerism identified in a new class of helical rosette nanotubes," *Nanoscale*. **2014**.
74. Iijima, S. Helical microtubules of graphitic carbon. *Nature* (London). **1991**. 354: 56–58.
75. Iijima, S, Ichihashi, T. Single-shell carbon nanotubes of 1-nm diameter. *Nature*. **1993**. 363: 603-605.
76. Inoue K, Takano H, Yanagisawa R, Hirano S, Sakurai M, Shimada A, Yoshikawa T. Effects of airway exposure to nanoparticles on lung inflammation induced by bacterial endotoxin in mice. *Environ. Health Perspect*. 2006. 114: 1325–1330.
77. Inoue K, Yanagisawa R, Koike E, Nishikawa M, Takano H. Repeated

pulmonary exposure to single-walled carbon nanotubes exacerbates allergic inflammation of the airway: possible role of oxidative stress. *Free Radical Biol. Med*. **2010**. 48: 924–934.

78. Jaiswal JK, Simon SM. Optical monitoring of single cells using quantum dots. *Methods Mol. Biol*. **2007**. 374: 93–104.
79. Johnston MI and Fauci AS. HIV vaccine development-improving on natural immunity. *N. Engl. J. Med*. **2011**. 365: 873-875.
80. Journeay WS, Janardhan KS, Singh B. Expression and function of endothelial monocyte-activating polypeptide-II in acute lung inflammation. *Inflamm. Res*. **2007**. 56: 175–181.
81. Journeay WS, Suri SS, Moralez JG, Fenniri H, Singh B. Rosette nanotubes show low acute pulmonary toxicity in vivo. *Int. J. Nanomedicine*. **2008**. 3(3): 373–383.
82. Journeay WS, Suri SS, Moralez JG, Fenniri H, Singh B. Low inflammatory activation by self-assembling Rosette nanotubes in human Calu-3 pulmonary epithelial cells. *Small*. **2008**. 4(6): 817-23.
83. Journeay WS, Suri SS, Moralez JG, Fenniri H, Singh B. Macrophage Inflammatory Response to Self-Assembling Rosette Nanotubes. *Small*. **2009**. 5(12): 1446-52.
84. Jovanovic´ SP, Markovic´ ZM, Kleut DN, et al. A novel method for the functionalization of gamma-irradiated single wall carbon nanotubes with DNA. *Nanotechnology*. **2009**. 20(44): 445602.
85. Kaiser E, Colescott RL, Bossinger CD, Cook PI. Color test for detection of free terminal amino groups in the solid-phase synthesis of peptides. *Anal. Biochem*. **1970**. 34(2): 595-598.
86. Kaminski RW, Turbyfill KR, Oaks EV. Mucosal adjuvant properties of the Shigella invasin complex. *Infect. Immun*. **2006**. 74: 2856–2866.
87. Kam NW, Liu Z, Dai H. Carbon nanotubes as intracellular transporters for proteins and DNA: an investigation of the uptake mechanism and pathway. *Angew Chem. Int. Ed. Engl*. **2006**. 45(4): 577–581.

88. Kao J, Houck K, Fan Y, Haehnel I, Libutti SK, Kayton ML, Grikscheit T, Chabot J, Nowygrod R, Greenberg S, Kuang WJ, Leung DW, Hayward JR, Kisiel W, Heath M, Brett J, Stern DM. Characterization of a novel tumor-derived cytokine. Endothelial-monocyte activating polypeptide II. *J. Biol. Chem*. **1994**. 269: 25106–25119.
89. Kao J, Ryan J, Brett J, Chen J, Shen H, Fan Y, Godman G, Familletti PC, F. Wang, Pan YCE, Stern D, Clauss M. Endothelial monocyte-activating polypeptide II. A novel tumor-derived polypeptide that activates host-response mechanisms. *J. Biol. Chem*. **1992**. 267: 20239–20247.
90. Klippstein R, Pozo D. Nanotechnology-based manipulation of dendritic cells for enhanced immunotherapy strategies. *Nanomedicine*. **2010**. 6(4): 523-9.
91. Klein F, Mouquet H, Dosenovic P, Scheid JF, Scharf L, and Nussenzweig MC. *Science*. **2013**. 341: 1199-1204.
92. Kobayashi Y. Neutrophil infiltration and chemokines. *Crit. Rev. Immunol*. **2006**. 26: 307–316.
93. Korber BT, Foley B, Gaschen B, Kuiken C. Epidemiological and immunological implications of the global variability of HIV-1. In: Pantaleo G, Walker BD eds. *Retroviral Immunology: Immune Response and Restoration. New Jersey: Humana Press*. **2001**. 1-32.
94. Korber BT, Letvin NL, Haynes BF. T-cell vaccine strategies for human immunodeficiency virus, the virus with a thousand faces. *J. Virol*. **2009**. 83: 8300-8314.
95. Kumar H, Kawai T, Akira S. Toll-like receptors and innate immunity. *Biochem. Biophys. Res. Commun*. **2009**. 388: 621-5.
96. Kwong PD, Wyatt R, Robinson J, Sweet RW, Sodroski J, Hendrickson WA. Structure of an HIV gp120 envelope glycoprotein in complex with the CD4 receptor and a neutralizing human antibody. *Nature.* **1998**. 393: 648–659.
97. Kwong PD, Mascola JR, Nabel GJ. Rational design of vaccines to elicit broadly neutralizing antibodies to HIV-1. *Cold Spring Harb Perspect Med*. **2011**. 1(1): 007278.

98. Kuzyk A, *et al*. DNA-based self-assembly of chiral plasmonic nanostructures with tailored optical response. *Nature.* **2012**. 483: 311-314.

99. Lam CW, James JT, McCluskey R, Arepalli S, Hunter RL. A review of carbon nanotube toxicity and assessment of potential occupational and environmental health risks. *Crit. Rev. Toxicol*. **2006**. 36(3): 189–217.

100. Le MH, Suri SS, Rakotondradany F, Fenniri H, Singh B. Rosette nanotubes inhibit bovine neutrophil chemotaxis. *Vet. Res*. **2010**. 41(5): 75.

101. Levy Y. Preparation for antiretroviral interruption by boosting the immune system. *Curr. Opin. HIV. AIDS*. **2008**. 3: 118-123.

102. Lidke DS, Nagy P, Jovin TM, Arndt-Jovin DJ. Biotin-ligand complexes with streptavidin quantum dots for in vivo cell labeling of membrane receptors. *Methods Mol. Biol*. **2007**. 374: 69–79.

103. Lindblad EB. Aluminium adjuvants – in retrospect and prospect. *Vaccine*. **2004**. 22(27–28): 3658–3668.

104. Liu K, Iyoda T, Saternus M, Kimura Y, Inaba K, Steinman RM. Immune tolerance following delivery of dying cells to dendritic cells in situ. *J. Exp. Med.* 2002. 196:1091–7.

105. Li Y, Migueles SA, Welcher B, Svehla K, Phogat A, Louder MK, et al. Broad HIV neutralization mediated by CD4-binding site antibodies. *Nat. Med*. **2007**. 13: 1032-4.

106. Lombardi G, Vasquez Y, Lombardi G, Vasquez Y. Dendritic cells. *Handb. Exp. Pharmacol*. **2009**. 188:v-ix.

107. Look M, Bandyopadhyay A, Blum JS, Fahmy TM. Application diseases in the developing world. *Advanced Drug Delivery Reviews.* **2010**. 62 (4-5): 378–393.

108. Lozano R, Naghavi M, Foreman K, et al. Global and regional mortality from 235 causes of death for 20 age groups in 1990 and 2010: a systematic analysis for the Global Burden of Disease Study 2010. *Lancet*. **2012.** 380: 2095–128.

109. Madani SY, Tan A, Dwek M, Seifalian AM. Functionalization of single-walled carbon nanotubes and their binding to cancer cells. Int J *Nanomedicine*. **2012**. 7: 905–914.

110. Madl AK, Pinkerton KE. Health effects of inhaled engineered and incidental nanoparticles. *Crit. Rev. Toxicol*. **2009**. 39: 629–658.

111. Manna SK, Sarkar S, Barr J, et al. Single-walled carbon nanotube induces oxidative stress and activates nuclear transcription factor-kappaB in human keratinocytes. *Nano Lett*. **2005**. 5(9): 1676–1684.

112. Manolova V, Flace A, Bauer M, Schwarz K, Saudan P, Bachmann MF. Nanoparticles target distinct dendritic cell populations according to their size. *Eur. J. Immunol*. **2008**. 38:1404-13.

113. Marsh A, Silvestri M, and Lehn J-M. Self-complementary hydrogen bonding heterocycles designed for the enforced self-assembly into supramolecular macrocycles. *Chem. Commun*. **1996**. 1527-1528.

114. Mascal M, Hext NM, Warmuth R, Moore MH, and Turkenburg JP. Programming a Hydrogen-Bonding Code for the Specific Generation of a Supermacrocycle. *Angew. Chem. Int. Ed. Engl*. **1996**. 108(19), 2203-2206.

115. Meng J, Meng J, Duan J, et al. Carbon nanotubes conjugated to tumor lysate protein enhance the efficacy of an antitumor immunotherapy. *Small*. **2008**. 4(9): 1364–1370.

116. Metchnikoff E. Sur la lutta des cellules de l'organismes centre l'invasion des microbes. *Annales. Inst. Pasteur Paris*. **1887**. 1: 321.

117. McCullough KC, Summerfield A. Targeting the porcine immune system-particulate vaccines in the 21st century. *Developmental and Comparative Immunology*. **2009**. 33 (3): 394–409.

118. Merrifield RB. Solid phase peptide synthesis I: Synthesis of a tetrapeptide. *J. Am. Chem. Soc*. **1963**. 85: 2149-2154.

119. Miles LEM, Hales CN. Labeled antibodies and immunological assay systems. *Nature*. **1968**. 219: 186-9.

120. Modeling of RGDSK-TB RNTs was done by Dr. Takeshi Yamazaki.

121. Moralez JG, Raez J, Yamazaki T, Motkuri RK, Kovalenko A, Fenniri H. Helical rosette nanotubes with tunable stability and hierarchy. *J. Am. Chem. Soc*. **2005**. 127(23): 8307–8309.

122. Mo H, Stamatatos L, Ip JE, Barbas CF, Parren PW, Burton DR, Moore JP, Ho DD. Human immunodeficiency virus type mutants that escape neutralization by human monoclonal antibody IgG1b12. *J. Virol.* **1997**. 71: 6869–6874.

123. (a) Muir T, Morales E, Root J, Kumar I, Garcia B, Vellandi C, Jenigian D, Marsh T, Henderson E and Vesenka JJ. Scanning force microscopy studies of X-ray-induced double-strand breaks in plasmid DNA. *Vac. Sci. Technol. A*. **1998**. 16: 1172-1177. (b) DeRose JA and Revel JP. Studying the surface of soft materials (live cells) at high resolution by scanning probe microscopy: challenges faced. *Thin Solid Films*. **1998**. 331: 194-202. (c) Kasumov AY, Klinov DV, Roche PE, Gueron S and Bouchiat H. Thickness and low-temperature conductivity of DNA molecules. *Appl. Phys. Lett*. **2004**. 84: 1007-1009.

124. Munier CM, Andersen CR, Kelleher AD. HIV vaccines: progress to date. *Drugs*. **2011**. 5; 71(4): 387-414.

125. Muster T, Steindl F, Purtscher M, Trkola A, Klima A, Himmler G, Ruker F, Katinger H. A conserved neutralizing epitope on gp41 of human immunodeficiency virus type 1. *J. Virol.* **1993**. 67:6642–6647.

126. Muster T, Guinea R, Trkola A, Purtscher M, Klima A, Steindl F, Palese P, Katinger H. Cross-neutralizing activity against divergent human immunodeficiency virus type 1 isolates induced by the gp41 sequence ELDKWAS. *J. Virol.* **1994**. 68: 4031–4034.

127. National Institute of Allergy and Infectious Diseases, Understanding vaccines: what they are and how they work. http://www.niaid.nih.gov/ publications/vaccine/pdf/undvacc.pdf.

128. Ndung'u T, Weiss RA. On HIV diversity. *AIDS.* **2012**. 26: 1255-1260.

129. Nel A, Xia T, Mädler L, Li N. Toxic potential of materials at the nanolevel. *Science*. **2006**. 311(5761): 622–627.

130. Neutra MR, Kozlowski PA. Mucosal vaccines: the promise and the challenge. *Nat. Rev. Immunol*. **2006**. 6: 148–158.

131. Ogra PL, Faden H, Welliver RC, Vaccination strategies for mucosal immune responses. *Clin. Microbiol. Rev*. **2001**. 14: 430–445.

132. O'Hagan DT. Microparticles as vaccine delivery systems, in: V.E.J.C Schijns, D.T. O'Hagan (Eds.). Immunopotentiators in Modern Vaccines Academic Press, Burlington, MA. **2006**. 123–147.

133. O'Hagan DT, De Gregorio E. The path to a successful vaccine adjuvant-the long and winding road. *Drug Discovery Today*. **2009**. 14 (11-12): 541–551.

134. *Pan W, Kastin AJ, Banks WA, Zadina JE.* Effects of peptides: a cross-listing of peptides and their central actions published in the journal Peptides from 1994 through 1998. *Peptides*. *1999. 20*(9): *1127*-38.

135. Pantarotto D, Briand JP, Prato M, Bianco A. Translocation of bioactive peptides across cell membranes by carbon nanotubes. *Chem. Commun*. (Camb). **2004**. 1: 16–17.

136. Parren PWHI, Moore JP, Burton DR, Sattentau QJ. The neutralizing antibody response to HIV-1: viral evasion and escape from humoral immunity. *AIDS.* **1999**. (suppl A): S137-S162.

137. Perrie Y, Mohammed AR, Kirby DJ, McNeil SE, Bramwell VW. Vaccine adjuvant systems: enhancing the efficacy of sub-unit protein antigens. *International Journal of Pharmaceutics*. **2008**. 364 (2): 272–280.

138. Plotkin SL, Plotkin SA. A short history of vaccination, in: S.A. Plotkin, W.A. Orenstein (Eds.). *Vaccines*, WB Saunders Company, Philadelphia. **2004**. 1–15.

139. Pierschbacher MD, Ruoslahti E. The cell attachment activity of fibronectin can be duplicated by small fragments of the molecule. *Nature.* **1984a**. 309: 30-33.

140. Pierschbacher MD, Ruoslahti E. Variants of the cell recognition site of fibronectin that retain attachment-promoting activity. *Proc. Natl. Acad. Sci*. USA. **1984b**. 81: 5985-88.

141. Prato M, Kostarelos K, and Bianco A. Functionalized carbon nanotubes in drug design and delivery. *Acc. Chem. Res.* **2008**. 41(1): 60-8.

142. Pytela R, Suzuki S, Breuss J, Erle DJ and Sheppard D. Polymerase chain reaction cloning with degenerate primers: homology-based identification of adhesion molecules. *Methods Enzymol*. **1994**. 245: 420-51.

143. Rabinovich NR, McInnes P, Klein DL, Hall BF. Vaccine technologies: view to the future. *Science*. **1994**. 265: 1401–1404.

144. Ravichandran P, Baluchamy S, Sadanandan B, et al. Multiwalled carbon nanotubes activate NF-kappaB and AP-1 signaling pathways to induce apoptosis in rat lung epithelial cells. *Apoptosis*. **2010**. 15(12): 1507–1516.

145. Reddy ST, Swartz MA, Hubbell JA. Targeting dendritic cells with biomaterials: developing the next generation of vaccines. *Trends Immunol*. 2006. 27:573-9.

146. Reischl D, Zimmer A. Drug delivery of siRNA therapeutics: potentials and limits of nanosystems. *Nanomedicine*. **2009**. 5:8-20.

147. Rerks-Ngarm S, Pitisuttithum P, Nitayaphan S, Kaewkungwal J, Chiu J, Paris R, Premsri N, Namwat C, de Souza M, Adams E, et al. MOPH-TAVEG Investigators. *N. Engl. J. Med*. **2009**. 361: 2209-2220.

148. Rich EA, Panuska JR, Wallis RS, Wolf CB, Leonard ML, Ellner JJ. Dyscoordinate expression of tumor necrosis factor-alpha by human blood monocytes and alveolar macrophages. *Am. Rev. Respir. Dis*. **1989**. 139: 1010–1016.

149. Rigby PJ and Goldie RG. Confocal microscopy in biomedical research. *Croat. Med. J*. **1999**. 40(3): 346-52.

150. Roben P, Moore JP, Thali M, Sodroski J, Barbas CF, Burton DR. Recognition properties of a panel of human recombinant Fab fragments to the CD4 binding site of gp120 that show differing abilities to neutralize human immunodeficiency virus type 1. *J. Virol.* **1994**. 68:4821–4828.

151. Russell-Jones GJ. Oral vaccine delivery. *J. Control. Release*. **2000**. 65: 49–54.

152. Sánchez-Pomales G, Santiago-Rodríguez L, Cabrera CR. DNA-functionalized carbon nanotubes for biosensing applications. *J. Nanosci. Nanotechnol.* **2009**. 9(4): 2175–2188.

153. Sattentau QJ, Moore JP. Conformational changes induced in the human immunodeficiency virus envelope glycoprotein by soluble CD4 binding. *J. Exp. Med*. **1991**. 174:407–415.

154. Sattentau QJ, Moore JP, Vignaux F, Traincard F, Poignard P. Conformational changes induced in the envelope glycoproteins of the human and simian immunodeficiency viruses by soluble receptor binding. *J. Virol.* **1993**. 67: 7383–7393.

155. Sattentau QJ, Moore JP. Human immunodeficiency virus type neutralization is determined by epitope exposure on the gp120 oligomer. *J. Exp. Med.* **1995**. 182: 185–196.

156. Saunders KO, Rudicell RS and Nabel GJ. The design and evaluation of HIV-1 vaccines. *AIDS*. **2012**. 26: 1293-1302.

157. Schuurs AHWM, van Weemen BK. Enzyme-immunoassay: a powerful analytical tool [Review]. *J. Immunoassay*. **1980**. 1: 229-49.

158. Stamatatos L, Morris L, Burton DR, Mascola JR. Neutralizing antibodies generated during natural HIV infection: good news for an HIV vaccine? *Nat Med*. **2009**. 15(8): 866-70.

159. SEM, TEM and AFM imaging was done by Dr. Jae-Young Cho.

160. Sewald N, Jakubke H-D. Peptides: Chemistry and Biology, Second Edition. Wiley-VCH, Verlag GmbH & Co. KGaA. **2002**. Chapter1 (1-4).

161. Shen H, Ackerman AL, Cody V, et al. Enhanced and prolonged cross-presentation following endosomal escape of exogenous antigens encapsulated in biodegradable nanoparticles. *Immunology*. **2006**. 117(1): 78–88.

162. Sheng KC, Kalkanidis M, Pouniotis DS, Esparon S, Tang CK, Apostolopoulos V, et al. Delivery of antigen using a novel mannosylated dendrimer potentiates immunogenicity *in vitro* and *in vivo*. Eur. J. Immuno. **2008**. 38:424-36.

163. Srivastava I, Singh M. DNA vaccines: focus on increasing potency and efficacy. *Int. J. Pharm. Med*. **2005**. 19: 15–28.

164. Simon JK, Edelman R. Clinical evaluation of adjuvants, in: Schijns VEJC, O'Hagan DT (Eds.), *Immunopotentiators in Modern Vaccines*, Academic Press, Burlington, MA. **2006**. 319–342.

165. Smith AM, Dave S, Nie S, True L, Gao X (2006) Multicolor quantum dots for molecular diagnostics of cancer. *Expert Rev. Mol. Diagn*. 2006. 6: 231–244.

166. Steinman RM, Cohn ZA. Identification of a novel cell type in peripheral lymphoid organs of mice. I.Morphology,quantitation, tissue distribution. *J. Exp. Med*. **1973**. 137: 1142–62.

167. Steinman RM, Hawiger D, and Nussenzweig MC. Tolerogenic Dendritic cells. Annual Review of Immunology. **2003**. 21: 685- 711.

168. Steinman R. Dendritic cells and vaccines. Baylor University Medical Center Proceedings. **2008**. 21 (1): 3–8.

169. Suri SS, Mills S, Aulakh GK, Rakotondradany F, Fenniri H, Singh B. RGD-tagged helical rosette nanotubes aggravate acute lipopolysaccharide-induced lung inflammation. *Int. J. Nanomedicine*. **2011**. 6: 3113-23.

170. Suri SS, Rakotondradany F, Myles AJ, Fenniri H, Singh B. The role of RGD-tagged helical rosette nanotubes in the induction of inflammation and apoptosis in human lung adenocarcinoma cells through the P38 MAPK pathway. *Biomaterials*. **2009**. 30(17): 3084–3090.

171. Tacken PJ, de Vries IJ, Torensma R, Figdor CG. Dendritic-cell Immunotherapy: from ex vivo loading to in vivo targeting. *Nat. Rev. Immunol*. **2007**. 7 (10): 790-802.

172. Tasis D, Tagmatarchis N, Bianco A, Prato M. Chemistry of carbon nanotubes. *Chem. Rev.* **2006**. 106: 1105–1136.

173. Taylor BS, Sobieszcyk ME, McCutchan FE, Hammer SM. The challenge of HIV-1 subtype diversity. *N. Engl. J. Med*. **2008**. 358: 1590-1602.

174. Thali M, Moore JP, Furman C, Charles M, Ho DD, Robinson J, Sodroski J. Characterization of conserved human immunodeficiency virus type 1

gp120 neutralization epitopes exposed upon gp120- CD4 binding. *J. Virol.* **1993**. 67: 3978–3988.

175. UNAIDS. UNAIDS report on the global AIDS epidemic 2012. http://www.unaids.org/en/media/unaids/contentassets/documents/epidemiology/2012/gr2012/20121120_ UNAIDS_Global_Report_2012_en.pdf (accessed March 6, 2013).

176. Villa CH, Dao T, Ahearn I, et al. Single-walled carbon nanotubes deliver peptide antigen into dendritic cells and enhance IgG responses to tumor-associated antigens. *ACS Nano*. **2011**. 5(7): 5300–5311.

177. Wadhwa PD, Zielske SP, Roth JC, Ballas CB, Bowman JE, Gerson SL. Cancer gene therapy: scientific basis. *Annu. Rev. Med*. **2002**. 53: 437–452.

178. Walsh G. Biopharmaceuticals: Biochemistry and Biotechnology, John Wiley, New York, **1998**.

179. Walker LM, Simek MD, Priddy F, Gach JS, Wagner D, Zwick MB, et al. A limited number of antibody specificities mediate broad and potent serum neutralization in selected HIV infected individuals. *PLoS. Pathog*. **2010**. 6(8): 1-14.

180. Wang H, Wang J, Deng X, et al. Biodistribution of carbon single-wall carbon nanotubes in mice. *J. Nanosci. Nanotechnol*. **2004**. 4(8): 1019–1024.

181. Wang J, Thorson L, Stokes RW, Santosuosso M, Huygen K, Zganiacz A, Hitt M, Xing Z. Single mucosal, but not parenteral, immunization with recombinant adenoviral-based vaccine provides potent protection from pulmonary tuberculosis. *J. Immunol*. **2004**. 173: 6357–6365.

182. Wang X, Uto T, Akagi T, Akashi M, Baba M. Poly(gamma-glutamic acid) nanoparticles as an efficient antigen delivery and adjuvant system: potential for an AIDS vaccine. *J. Med. Virol.* 2008. 80:11-9.

183. Webster DE, Gahan ME, Strugnell RA, Wesselingh SL. Advances in oral vaccine delivery options: what is on the horizon? *Am. J. Drug Deliv*. **2003**. 1: 227–240

184. Wiesm¨uller K-H, Fleckenstein B, Jung G. Peptide vaccines and peptide libraries. *Biol. Chem. Hoppe-Seyler. 2001. 382: 571.*

185. World Health Organization. The global burden of disease: 2004 update, Geneva, Switzerland, **2008**.

186. Wu X, Yang ZY, Li Y, Hogerkorp CM, Schief WR, Seaman MS, et al. Rational design of envelope identifies broadly neutralizing human monoclonal antibodies to HIV. *Science*. **2010**. 329: 856-61.

187. Xiao Y, Lu Y and Chen YH. Epitope-vaccine as a new strategy against HIV-1 mutation. *Immunol. Lett*. **2001**. 77: 3-6.

188. Xiao Y, Dong XN and Chen YH. Neutralizing antibodies: mechanism of neutralization and protective activity against HIV-1. *Immunol. Res*. **2002**, 25: 193-200.

189. Yalow RS, Berson SA. Immunoassay of endogenous plasma insulin in man. *Clin. Invest*. **1960**. 39: 1157-75.

190. Young SL, Wilson M, Wilson S, Beagley KW, Ward V and Baird MA. Transcutaneous vaccination with virus-like particles. *Vaccine*. **2006**. 24(26): 5406-12.

191. Zagury, D, Bernard J, Cheynier R, Desportes I, Leonard R, Fouchard M, Reveil B, Ittele D, Lurhuma Z, Mbayo K, Wane J, Salaun J, Goussard B, Dechazal L, Burny A, Nara P and Gallo RC. A group-specific anamnestic immune reaction against HIV induced by a candidate vaccine against AIDS. *Nature* (London). **1988**. 332:728-731.

192. Zauner, W, Lingnau K, Mattner F, von Gabain A and Buschle M. Defined synthetic vaccines. *Biol. Chem.* Hoppe-Seyler **2001**. 382: 581

193. Zhang L, Rodriguez J, Raez J, Myles AJ, Fenniri H, Webster TJ. Biologically inspired rosette nanotubes and nanocrystalline hydroxyapatite hydrogel nanocomposites as improved bone substitutes. *Nanotechnology*. **2009**. 20(17): 175101.

194. Zhang L, Hemraz UD, Fenniri H, Webster TJ. Tuning cell adhesion on titanium with osteogenic rosette nanotubes. *J. Biomed. Mater. Res. A*. **2010**. 95(2): 550-63.

195. Zhou HY, Ohnuma Y, Takita H, Fujisawa R, Mizuno M, Kuboki Y. Effects of a bone lysine-rich 18 kDa protein on osteoblast-like MC3T3-E1 cells. *Biochem. Biophys. Res. Commun.* **1992**. 186(3): 1288-93.

196. Zhou T, Georgiev I, Wu X, Yang ZY, Dai K, Finzi A, et al. Structural basis for broad and potent neutralization of HIV by antibody VRC01. *Science*. **2010**. 329: 811-7.